A deterministic model of a neuromorphic nanoparticle network

Matthew D. Pike

A thesis submitted in partial fulfilment
of the requirements for the degree of
Master of Engineering
in
Electrical and Computer Engineering
at the
University of Canterbury,
Christchurch, New Zealand.

29 November 2019

ABSTRACT

A research group at the University of Canterbury are developing an experimental device that may have some statistical properties in common with biological neuronal networks. Measurements of the device's conductance have shown step change events, with evidence of correlation in the probability distribution of event-to-event intervals and also in the autocorrelation function of event times. A simulation of the device was previously developed using a probabilistic approach to modelling the internal activity. This probabilistic model was able to produce visually similar conductance behaviour but was unable to reproduce evidence of correlation.

The two main objectives of this Master's project were to improve the simulation to produce behaviour more like the real device and also show evidence of correlation, and to develop tools to aid analysis and visualisation of simulation behaviour.

The existing probabilistic switching model was investigated and it was confirmed that it does not produce evidence of correlation in conductance step change events. Two new probabilistic models were developed by first adding gradual rather than instantaneous switching, and then implementing switching probability dependent on electric field and current, rather than fixed probability. The new models were tested and found to be unable to produce evidence of correlation, despite their differences to the original probabilistic model.

A new switching model was developed using deterministic rules based on physical processes rather than probability. The deterministic model was successful in producing evidence of correlation, for a range of configuration parameters. The conductance behaviour of the deterministic simulation was consistent with the experimental device and showed evidence of correlation in both the probability distribution of event-to-event intervals, and also in the autocorrelation function of event times. The effects of the deterministic simulation parameters (such as voltage, and dependence on electric field strength and current) were explored over ranges of values. The behaviour for each simulation was recorded and plotted, mapping trends of behaviour. It was found that for the parameters controlling the electric field strength dependence and the current dependence, there is a small range of ratios of these parameters that produce the desired behaviour. The insight gained from this mapping can be used to produce simulations that behave in a qualitatively similar fashion to the experimental device, which is a

significant achievement.

Tools were developed to aid in analysis and assessment of simulation behaviour. A script written in MATLAB analyses and plots the behaviour and statistics of simulated or experimentally measured data. Tools like this one were crucial for assessing the performance of the simulation and comparing it to the experimental device. Other scripts written in Python extract internal details of the simulated device to plot visualisations of the internal structure and conditions, or histograms of event distribution with respect to electric field and current producing those events.

CONTENTS

ACKNOWLEDGEMENTS

My supervisors (Prof. Phil Bones, Prof. Simon Brown, Dr. Steve Weddell) have been very helpful to me in keeping me on track and in discussing my ideas with them. They have been very patient with me when I had problems both personal and technical. Their guidance was very much appreciated.

My research colleague Shota Shirai has been a great help to me by sharing some of his MATLAB functions, and helping me to debug some problems.

Assoc. Prof. Matthew D. Arnold, of the School of Mathematical and Physical Sciences at the University of Technology Sydney, has been a great help to me by helping me solve some difficult software problems and by executing numerous simulations for me quickly when I lacked key results.

The whole neuromorphic materials research team lead by Prof. Simon Brown has been a great help to me by talking with me about concepts of how switching occurs in the device, how we get meaning from the statistics of the measurement, and giving me their opinion on my figures and ideas.

My dear partner kept me sane and well-fed throughout the long (and seemingly always extending) duration of my Master's work. I am forever grateful for her balance of patience and insistence that I finish.

PREFACE

The nanotechnology research group lead by Prof. Simon Brown at the University of Canterbury (UC) has a subgroup focused on researching possible neuromorphic, critical, and/or otherwise computationally useful properties of a percolated network-on-chip device that they have been developing over several years. To further understanding of the internal structure, functional model, and network related properties of the device, a simulation program was developed to produce simulated boards containing conductive networks with non-linear switching elements that are intended to behave similarly to the internal switching elements of the experimental device.

The simulation program was first developed in 2015 by James Carr and Simon Brown, building on previous modelling work during the previous decade by J. Schmelzer Jr., A. Sattar, Shawn Fostner, and Simon Brown. The simulation was then further developed by Aaron Stockdill in 2016 and 2017, and by Matthew Arnold in 2017. I joined the research group in 2018 for my Master's degree and continued developing the program.

I wrote this thesis as a part of the requirements of my Master's degree, obviously, but also as a means to document and describe the contributions I have made to the simulation program used by the neuromorphic materials research team. The intention is that my work will make the simulation useful for making predictions about the experimental device. As you will read in this thesis, I was able to make the simulation more closely reproduce experimental behaviour.

One of the benefits of the simulation program is being able to investigate the *internal* distribution of currents, voltages, and conductances in a percolated network – this is not possible with the experimental device. It is hoped that the simulation can be used to validate a theoretical model of the device properties by producing results in the simulation that are arguably similar to the external measurements from the real device.

NOTATION

Acronyms and symbols used in this thesis:

V - voltage

d - effective gap length in a switching gap

E - electric field strength

I - current

E_T - electric field strength threshold

I_T - current threshold

E_R - electric field strength switching dependence range

I_R - current switching dependence range

S_R - step range

G_{tunnel} - Conductance of a tunnel

A - parameter in tunnel conductance equation

β - parameter in tunnel conductance equation

G - conductance

G_{on} - Conductance of a newly formed filament

d_{max} - largest gap size allowed in simulation

ΔG - Size of change in conductance

Δd - Size of change in effective gap length

Δw - Size of change in filament width

IEI - inter-event interval

PDF - probability distribution function

ACF - autocorrelation function

P_{up} - probability of switching up (from tunnel to filament)

P_{down} - probability of switching down (from filament to tunnel)

Chapter 1

INTRODUCTION

1.1 MOTIVATION – THE LURE OF NEUROMORPHIC HARDWARE

Computers today are capable of performing precise calculations quickly and efficiently, but with few exceptions the human brain still far outperforms computers in tasks of pattern recognition and complex planning – and it does so using a fraction of the power consumed by a computer. Computers using machine learning methods have succeeded in certain challenging pattern recognition and planning tasks, even surpassing humans in performance, but with significant power consumption requirements. One notable case of a computer surpassing human ability in a difficult problem is the computer program AlphaGo beating the top-ranking professional player of the game Go [1]. While the power consumption of the human player's brain is only about 20 W [2], the power consumption of AlphaGo has been stated as about 5000 W [3] – a difference of two orders of magnitude. Achieving a similar computing ability with equally low power consumption is highly desirable.

Typically, machine learning methods are implemented entirely in software, but a review of recent research into reservoir computing (a subfield of machine learning research) has shown that it is possible to use many different types of hardware in place of some key components of the methods [4]. One type of hardware called 'neuromorphic' aims to achieve high energy efficiency by mimicking the brain [5]. Recent research has shown evidence of neuromorphic behaviour in percolating [6, 7] nanoparticle films [8]. The Master's project builds on that research, so the experimental device studied in that research is discussed further in Section 1.1.1.

1.1.1 The experimental device

Work has been done researching possible computationally useful properties of a percolated nanoparticle film device [8], referred to henceforth as the **device**. It is hoped that the device can eventually be used in computing applications to perform machine learning computations.

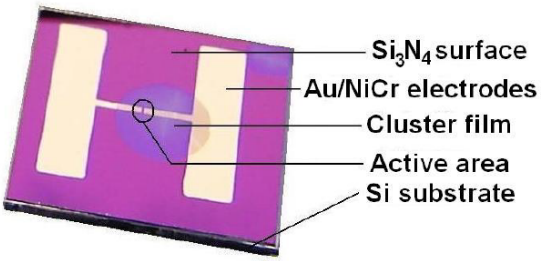

Figure 1.1 A photograph of a fabricated experimental device on a 10 mm × 10 mm Si wafer, with a Si_3N_4 surface. The prefabricated Au/NiCr electrodes are separated by a 100 µm wide gap, where tin (Sn) nanoparticle clusters are deposited (the active area).
After Mallinson. [9].

The device, shown in Figure 1.1, consists of an insulating substrate with two parallel electrodes connected by a tin (Sn) nanoparticle film, formed by deposition. Nanoparticles are deposited randomly, forming connections when overlapping or closely adjacent. Since the nanoparticles are deposited randomly, there is a specific probability that connections made between the nanoparticles will form a complete path between the two electrodes. Site and continuum percolation theory [6] predict that for an infinite area there is a critical deposition threshold in terms of the percentage of the area covered. When the percentage of the area covered is below the threshold the probability of a complete path is 0, and when it is above the threshold the probability is 1. For a finite system such as the nanoparticle film on the device, the threshold is not so sharply defined, rather the probability is expected to increase steeply at the critical threshold, but not immediately reach unity [7].

The device manufacturing process [10, 11] is now briefly described. Two Au/NiCr electrodes are lithographically printed onto the silicon nitride (Si_3N_4) surface of a Si substrate, and then the substrate is placed into a temperature and pressure controlled sputter deposition chamber [12]. A small voltage is applied across the substrate electrodes, and the resulting current is measured in order to determine the conductance. The active area of 100 µm × 300 µm [11] between the electrodes receives a deposition of nanoparticles of tin with mean diameter ∼8.5 nm[11, 13], while the conductance is continuously monitored. Once the conductance begins to increase and reaches a predetermined point, the stream of particles is shut off. At this point, the surface coverage of tin particles on the substrate is close to the critical percolation threshold $p_c \approx 0.68$ [10]: the nanoparticles on the substrate have clustered together and the network of connections between clusters nearly forms a complete bridge between the two electrodes. This condition is optimal for observing the switching behaviour in the conductance of the device [10].

After deposition, a voltage is applied across the electrodes and the current is measured over time to determine changes in conductance. Step changes in the conductance

are understood to be due to nanoscale filament connections forming and breaking in gaps between tin particles on the device [10]. Filaments[14] provide higher conductance, while in their absence, quantum tunnelling effects [15, Chapter 6] allow much lower conductance in the tunnel gaps [10]. The statistics of the timing and size of observed changes are brain-like and are discussed in Section 1.1.2.

It is not practical to directly probe the internal state of the device because of its small scale, the rate at which the state changes, and because of the need to have the device inside a controlled chamber during experiments. It is only practical to determine the state of the device via measurements made at the external electrodes. To explore theoretical models of the internal structure, function, and network related properties of the device, a simulation [8, 16] of the device was developed. The simulation uses conductive networks with non-linear switching elements, which are intended to behave similarly to the internal switching elements of the experimental device.

One of the benefits of simulating the device is being able to investigate the resulting structure of the internal connections, and the distribution of currents, voltages, and conductances in the percolated network. Another benefit is that numerous simulations can be run in parallel and repeated with small changes, allowing much faster investigation of changing conditions than can be achieved with experiments. It is hoped that the simulation will validate theoretical models of the device properties by producing results that are similar to the measurements of the real device, and allow investigation of the computational capability of these properties via simulation. The simulation will also potentially allow crude prediction of the effect of different device conditions and guide design of future devices.

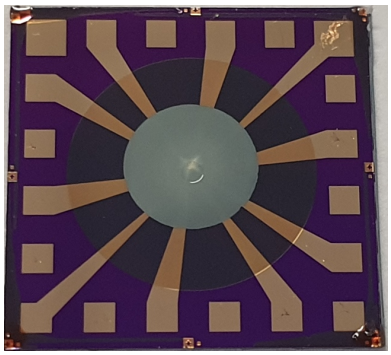

Figure 1.2 A photograph of a fabricated experimental device using the multiple electrode design.

It is recognised that performing useful computations will require devices with multiple electrodes. A recent variation of the device design uses multiple electrodes equally spaced on the perimeter of the substrate, with tracks tapering to a point within the target deposition area at the centre of the wafer. An example of this design is shown in Figure 1.2. It is hoped that this variant will allow information about the locations of the internal switching events to be extracted from the external measurements at the

electrodes, or that the properties of measurements on the multiple electrodes will be useful for reservoir computing.

1.1.2 Observed properties of the experimental device

During experiments with voltage applied, stepwise conductance changes have been observed [10]. Figure 1.3 shows a measurement of device conductance over time while a voltage is applied, as well as the measurement-to-measurement changes in that conductance over time. These measurements are recorded in terms of the conductance quantum G_0, defined as $G_0 = 2e^2/h$, where e is the charge of an electron, and h is Planck's constant. Previous work demonstrated that, for much smaller gaps between electrodes than in the experimental device [10], measured conductance is quantised to integer multiples of the conductance quantum, like a single atomic switch [17]. It is expected that observing perfectly quantised steps in total device conductance will be rare, as the internal structure of the device is a complex hierarchical network of series and parallel quantised conductance elements [18], rather than a single atomic switch. Nonetheless, G_0 is a convenient unit for conductance measurements of the device as it provides a relevant magnitude as a reference.

Events are defined as any step changes in conductance, in practice limited to those that are large enough to distinguish them from measurement noise. Investigating the statistics of these events has revealed significant properties of the device. These findings are discussed here in order to highlight the observed properties of the experimental device which are desired features in the simulation.

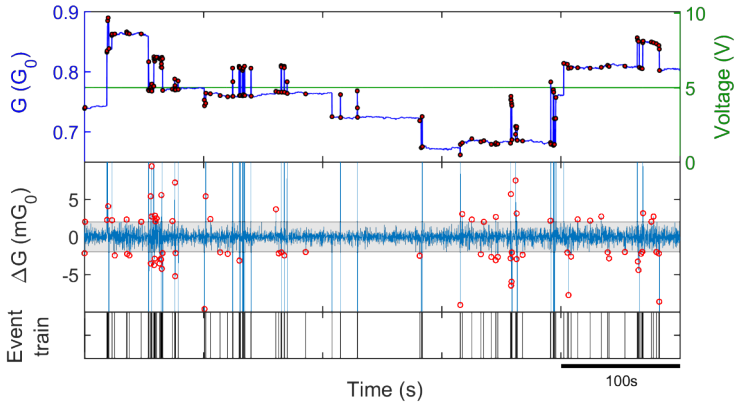

Figure 1.3 The top panel shows the conductance (G) switching response of the device in response to a constant voltage with a fixed amplitude of 5 V, for a period of approximately 500 seconds. Both small and large changes in G occur. Changes above a threshold are marked in red as switching events. The middle panel shows ΔG, with the switching events above the threshold (grey zone) marked in red. Note that the magnitude and rate of the conductance changes are non-uniform. The bottom panel displays the events as a binary series. (Units of the quantum of conductance, $G_0 = 2e^2/h$, have been used for convenience).
After Shirai et al. [18].

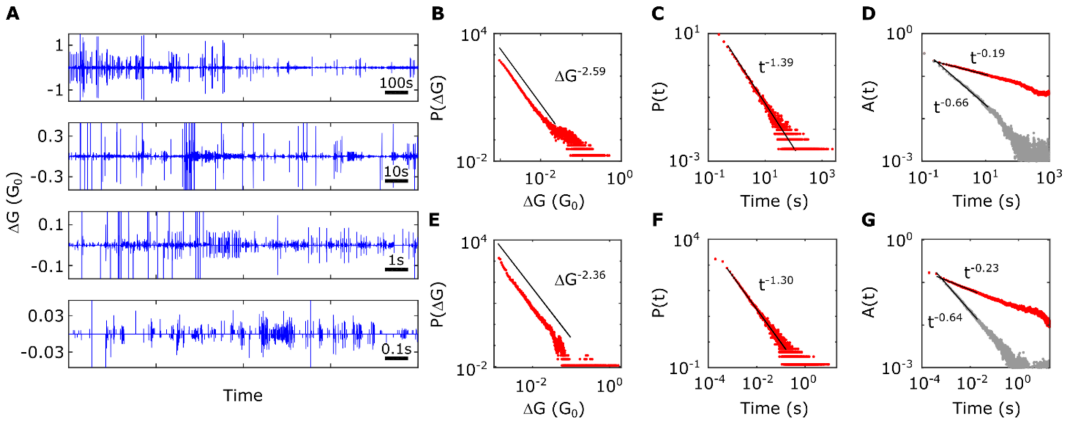

Figure 1.4 The total device conductance exhibits complex patterns of switching events that range over several orders of magnitude, and are similarly distributed temporally at multiple time scales.
(A) The top panel shows data from 2400 s of recorded conductance changes, while the three below it show subsets of 10, 100, and 1000 times shorter periods with 3, 9, and 27 times magnification in the vertical scale respectively. The vertical scale uses units of $G_0 = 2e^2/h$, the quantum of conductance. The data shown in B, C, D (sample I) are obtained with a relatively slow sampling rate of 5 Hz and the data shown in E, F, G (sample II) are measured 1000 times faster, i.e., at 5 kHz – (See Materials and Methods of Mallinson et al. [19] for further details).
(B, E) The probability density functions (PDF) for changes in total network conductance, P(ΔG), due to switching activity. They show that the probability distribution of ΔG is heavy-tailed, and that ΔG ranges over several orders of magnitude.
(C, F) The PDFs for inter-event intervals showing that the inter-event intervals follow power-law distributions, suggesting the existence of correlations between the events.
(D, G) Log-log plots of the autocorrelation function (ACF) of the switching event times (red), and after shuffling the inter-event intervals (grey). The ACF decays over several decades as a power-law, suggesting long-range temporal correlation between events. Any temporal correlation is destroyed by the shuffling, resulting in a significant increase in slope of the ACF providing strong evidence of temporal correlation between non-shuffled events.
After Mallinson et al. [19].

Measured changes in the device conductance (**ΔG**) range over several orders of magnitude. This is shown in the four panels of Figure 1.4 (A) which show complex ΔG patterns at several different magnitudes and time scales [19]. The device not only shows a range of magnitudes of ΔG but also a heavy tailed probability distribution of ΔG with a shape that is consistent with a power law over several orders of magnitude. This is shown in the probability density function (**PDF**) log-log plots in Figure 1.4 (B, E) by the straight line fits over many orders of magnitude, combined with the lack of exponential drop-off in the tail (right-hand limit). The heavy tailed probability distribution of ΔG, consistent with the findings of Shirai et al. [18], indicates that (given identical switching elements) the internal structure of the device is a highly branched and fractal network. The heavy tailed distribution is also consistent with spatial self-similarity in percolating structures [19]. This is desirable in neuromorphic hardware because it has been shown that such networks can have better performance in solving challenging reservoir computing problems than random structures [20].

While the device is under constant voltage DC stimulus, the times between consecutive ΔG events, termed inter-event intervals (**IEIs**), have been shown to have a

power-law probability distribution [18]. This is demonstrated by the straight line fits in the IEI PDF plots shown in Figure 1.4 (C) for sampling at 5 Hz, and Figure 1.4 (F) for sampling at 5 kHz. This behaviour implies scale-free dynamics, and is consistent with temporally correlated non-Poisson processes [21]. The auto-correlation function (**ACF**) of the event times has been shown to decay slowly as a power-law over several decades. This is demonstrated in the ACF log-log plots shown in Figure 1.4 (D) for 5 Hz sampling and Figure 1.4 (G) for 5 kHz sampling. The slow decay (shallow slope) suggests long-range temporal correlation in the device behaviour, but can also arise due to renewal processes [22]. Shuffling the IEIs destroys correlation between events [21]. In Figure 1.4 (D,G), the slope of the ACF for the shuffled IEIs can be seen to be considerably steeper than that for the non-shuffled IEIs, providing strong evidence of long-range temporal correlation in the non-shuffled IEIs [19, 21]. The exponents of the power-law fits of the non-shuffled IEIs in the ACF plots for two different sampling rates are almost identical ($\beta \sim 0.2$) [19]. This is strong evidence of temporal self-similarity [19, 23], consistent with the qualitatively similar patterns of event timing shown at different time scales in Figure 1.4 (A).

1.1.3 General model of the device

In this subsection, a model of the device is described to provide context for the tools discussed in Chapter 2. As mentioned above in Section 1.1.1, the device consists of an area with two electrodes connected by a percolated network of tin nanoparticles. Nanoparticles which overlap conduct strongly through Ohmic connections, while quantum tunnelling across small gaps between non-overlapping nanoparticles forms alternative low conductance pathways for current. Filaments can grow in the small gaps between particles: a fully grown filament introduces an Ohmic connection, but can break (forming a gap again) if sufficient current is passed through it.

The device is modelled in software as a 2D area, referred to henceforth as a **board**, covered in randomly placed and uniformly sized discs which represent individual tin nanoparticles, referred to henceforth as **particles**. The area is defined by specifying **board dimensions**: width and height, in units of particle diameters. The particles are placed on the board until the desired **coverage**, or filled fraction of the board area, is reached. The locations are repeatably determined according to a choice of **random seed**. Particles which overlap are treated collectively as a single **group** or cluster of particles. Particles which are not overlapping or in contact, but which are sufficiently close together, are considered **connected** by a switching junction. Each **switching junction** is a conducting element with a conductance that changes during the simulation according to the rules of the switching model used. Any particles or groups touching the left or right vertical boundaries of the board are considered **inputs** or **outputs** respectively – these boundaries represent the two **electrodes** of the device.

The connections made by the junctions, between groups on the board and from groups to the electrodes, collectively form a conductance network. Any group connected to only one other group is pruned by being relabelled as part of that other group. Any group not connected to any other group is labelled as **isolated** and is then ignored during network calculations. Repeating the pruning and isolating process until no more changes are made results in a network in which there are no dead-end inter-group connections and all non-isolated groups contribute to the conductance between the electrodes. There is an exception: if three or more groups form a loop without connecting to the inputs and outputs, the pruning process will overlook them despite them being isolated from the rest of the network. These 'floating' loops do not provide meaningful paths for current to flow and so this unimportant oversight in the algorithm can be safely ignored. This minor error could be remedied in future by using a graph traversal algorithm to test whether each non-isolated group can reach both the input and output electrodes through the network of connections.

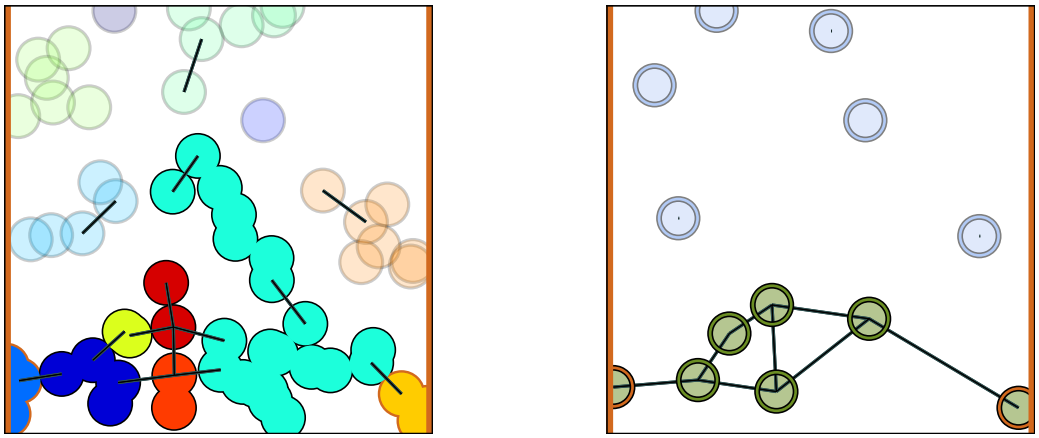

(a) Particle view (b) Network view

Figure 1.5 Two views of a specific example of a board. The coverage and size has been set low for simplicity. Junctions are shown with dark lines. Isolated groups are shown by transparency and light grey edges of the circles. Electrodes locations are indicated by the orange bars on the left and right edges. Non-isolated groups touching the electrodes are drawn with orange outer edges.
(a) Each node represents a particle. Groups of particles have randomly assigned colours.
(b) Each node now represents a particle group and is positioned at the cluster centroid. Isolated groups are light blue. Non-isolated groups are green.

Figure 1.5 shows an example board in terms of its particles and its groups. In the particle view shown in Figure 1.5a, the particles are coloured according to their group, and the groups are randomly assigned a colour. Particles belonging to isolated groups are rendered transparent with grey edges. The switching junctions between particles are shown with a dark line. The electrodes are coloured orange, and the outer edges of non-isolated particles touching an electrode (the inputs and outputs) are coloured to match. In the network view shown in Figure 1.5b, the network nodes correspond to

particle groups and the network edges correspond to the junctions between those groups. The network nodes are positioned at the centroids of the particle groups they represent and drawn as rings with transparent centres. The parallel junctions between pairs of groups are drawn as single dark lines. The isolated groups are coloured pale blue and the non-isolated groups are coloured green. The electrode boundaries are indicated by the vertical orange lines on the left and right edges, and the non-isolated groups that have particles in contact with the electrodes have their outer edge coloured to match the electrode.

After the algorithm has constructed a board according to the process described above, a user specified voltage is applied across the electrodes of the network. The simulated input electric potential is applied to the inputs (optionally a unique potential for each input), while the outputs are set to ground potential (zero). The resulting potentials of the groups and the resulting currents of the conductance network are computed. The chosen switching model is then used to determine changes to apply to each of the switching junctions – usually based on the electric fields and currents calculated as present in the junctions. This process of calculating potentials and currents, and updating switches, is called a single **time-step**. The simulation applies user-defined voltages to the network for a specified number of time-steps, usually a fixed DC voltage for tens of thousands of time-steps. Extracted measurements are recorded into an output file for each time-step.

It is worth noting that each set of values for board dimensions, coverage, and random seed, repeatably produces a unique board with a unique dynamical conductance network that has a characteristic behaviour. Some simulated boards (again, unique to their combination of random seed and board parameters) are known to have trivial conductance networks; for the simulations investigated in the Master's project, boards for which non-trivial networks had been confirmed were used. Examples of trivial conductance networks are: a single group bridging the electrodes; no path between the electrodes; and a single path between the electrodes.

As mentioned above, two particles sufficiently close together form a switching junction. 'Sufficiently close' here means within a maximum gap distance $\boldsymbol{d_{max}}$, defined below. In the original switching model, the junctions have two static conductance states – one low and one high [8]. The low conductance or **open** state is the default state, and it is included in the model because conductive surfaces very close together demonstrate a low conductance through the small gap between them, due to tunnelling. The tunnelling conductance is modelled here as

$$G_{tunnel}(d) = Ae^{-\beta d} \ , \tag{1.1}$$

where $\mathbf{d}$ is the gap length (in units of particle diameter), $\mathbf{A}$ is 1 and $\boldsymbol{\beta}$ is 100 [8, 10, 24, 25]. It is worth noting here that the maximum gap distance d_{max} mentioned above is defined

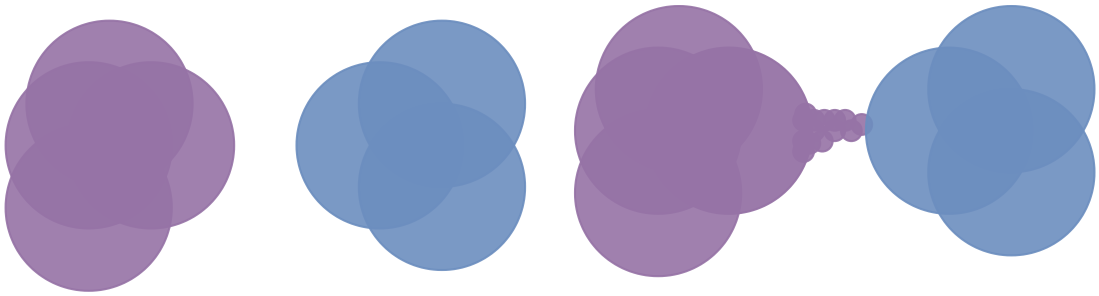

(a) Adjacent particles with a quantum tunnelling conductance in the gap

(b) Adjacent particles with an Ohmic conductance through a filament that has grown in the gap.

Figure 1.6 A simple illustration of a switching junction as a gap or filament.

as the gap length at which the tunnelling conductance given in Equation (1.1) equals 1×10^{-15} (a negligible value), for which the values of A and β used gives $d_{max} = 0.3454$ particle diameters in length.

The high conductance or **closed** state is based on the growth of filaments. The applied voltage forms an electric field in the gap, and if the field applied to two very close tin surfaces is sufficiently strong, then a filament will start to form [10, 14, 26]. If the filament completes the bridge between particles, then the small tunnelling conductance is replaced by the significantly larger Ohmic conductance of the filament. This is modelled here as a fixed conductance, G_{on}, that is larger than the maximum of the tunnelling conductance – 10 for the default filament conductance, as compared to 1 for the tunnelling conductance. Figure 1.6 shows simple illustrations of a switching junction as a gap and as a filament. This concludes the basic description of how the device is modelled in the simulation. The rules for how the switches transition between states, and variants on the conductance models, depend on the switching model used. The existing version, before the Master's project, was the probabilistic switching model described in the next section.

1.1.4 The base model simulation

The **base model**, described here briefly, is the version of the probabilistic switching model used in the simulation before the Master's project was commenced. The modifications to this probabilistic switching model and development of a new deterministic model achieved by the author are presented in Chapter 3 and Chapter 4, respectively. In the base model, the changes to the switching elements at each time-step are governed by the model developed by Fostner and Brown [8]. If the electric field ($\mathbf{E}$) in an open switching junction is above the specified electric field threshold ($\boldsymbol{E_T}$), then there is a fixed specified probability for that open switch to switch up in conductance ($\boldsymbol{P_{up}}$), closing the gap by forming a filament or closed switching junction. In practice the switching junction simply increases its conductance to G_{on}. Similarly, if a closed switching element has a

current (**I**) above the specified current threshold ($\boldsymbol{I_T}$), then there is a fixed specified probability for that closed switch to switch down in conductance ($\boldsymbol{P_{down}}$), removing the filament and reopening the gap. In practice the switching junction simply decreases its conductance back down to the value calculated from its gap length and the exponential model of tunnelling conductance, as in Equation (1.1).

In summary, the key features of the base simulation model are:

- Each switching element has two possible static states: 'on' (filament) with a conductance G_{on}, or 'off' (tunnelling gap) with a conductance G_{tunnel}.
- G_{on} is a fixed number shared by all filaments. G_{tunnel} is calculated individually for each tunnel gap based on gap length.
- At each time-step, switching from 'off' (tunnel gap) to 'on' (filament) occurs with probability P_{up} provided $E > E_T$.
- At each time-step, switching from 'on' (filament) to 'off' (tunnel gap) occurs with probability P_{down} provided $I > I_T$.

1.2 OBJECTIVES

The objectives of the Master's project are discussed here briefly, using the terminology and background information covered above.

1.2.1 Improve the match between model and experimental results

Simulating the device using a hypothesised model can provide some validation of that model – if the simulation produces behaviour similar to that of the measured device, then the functional model used may be valid. If the model validly represents the dynamics of the network, then it may provide further insight into how these dynamics arise and how they can be utilised. As discussed in Section 1.1.2, important properties have been observed in the device. The primary objective of the Master's work is to make improvements to the simulation that allow these experimentally observed properties to be demonstrated in simulations of the device. To summarise, those properties are:

- ΔG measurements ranging over several orders of magnitude.
- IEIs that follow a power law probability distribution.
- ACF of event times for shuffled and non-shuffled IEIs providing strong evidence of temporal correlation in the events.

Few of these are observed in the simulated board while using the existing probabilistic switching model (described briefly in Section 1.1.4, and in more detail in Chapter 3), which suggests that the model needs improvement in order to reproduce the behaviour of the device. The simulated ΔG ranges over several orders of magnitude while using virtually identical switching junctions, suggesting that the network structure in the board is already similar to that in the device. Based on this, the network generation model used by the simulation to produce the conductance network may be valid and so making improvements to the switching model is the focus of the Master's project. The effect of modifying aspects of the base model is explored to create new switching models and improve overall board behaviour, and a new deterministic version is presented as the main achievement of the Master's project. In comparing results for new switching model candidates, the performance of each candidate is represented by particular results that show behaviour judged most similar to the experimental data (out of the results of all parameter sets explored for that switching model). These representative results are referred to as the **best match** results of each model.

1.2.2 Develop tools to better comprehend simulation results

As it is simulated, the board can be inspected in great detail. External measurements are generated by the program, but these do not provide a sense of the internal behaviour. A suite of tools are needed to reveal and analyse the percolated switching network inside the board. Among the existing tools, two tools developed by Aaron Stockdill [27] in 2017 provide a visual representation of the simulated board as an area covered in particles, or as an area containing a graph of the electrical conductance network in the board. These tools, in addition to data extraction tools built into the simulation, are discussed further in Sections 2.1.1 to 2.1.3.

As part of the Master's project, the board viewing tools were further developed into new versions. The particle view showing potentials has been modified to have improved colour schemes. The network view has been developed into a tool to visualise the magnitude of current throughout the board using a log-scale blue-to-red colour code. In both new views, event locations are highlighted and colour coded for switch-up or switch-down events, and key simulation parameters are recorded on one side of the figure. The new board viewing tool is discussed in Section 2.3. New scripts were developed to automate identification of time-steps with switching events, and plotting of the board views. New Python modules collect data such as currents, electric fields, gap lengths, and conductances. One important new script makes histograms of the current and electric fields on switching junctions, to help understand the distributions of currents and electric fields that result in switching. This histogram producing script is discussed in Section 2.4. Modifications to data extraction tools built into the simulation are discussed in Section 2.5.

1.3 THESIS STRUCTURE

Pre-existing tools for analysing the simulation (found among the provided project files) are described and discussed in Chapter 2. A subset of these tools were improved and adapted for use in assessing the effects of modifications to the simulation, in addition to two completely new tools, one for internal measurements and one for external. These tools (pre-existing and new) are discussed before exploring modifications to the simulation because one of the tools is used extensively in assessing behaviour.

The initial probabilistic model described in Section 1.1.4 was further developed through several major modifications. The major modifications to the base model are discussed in Chapter 3, mostly in chronological order as in some cases the results of one modification inspired work on another.

The modifications made to the probabilistic model were used as inspiration for a deterministic model. This model has very promising behaviour and became the primary focus of the Master's work. The model development is discussed in Chapter 4. Extensive exploration of parameter space (the space of possible model parameter values) was performed to map the region that produces desirable simulation results, discussed in Chapter 5. This thesis concludes in Chapter 6 with a brief discussion of achievements, objectives, critique, and future work.

Chapter 2

TOOLS FOR THE SIMULATION

The Master's project used and developed MATLAB and Python tools in the form of scripts that either process measurement data of the type produced by both experiment and simulation, or extract information about the internal behaviour of the simulated networks from recorded simulation states, called 'statefiles'.

It is important to cover these tools before considering analysis of the simulation, as the tools were used to produce many of the figures discussed in later chapters. Some tools were inherited when the Master's project began and have since been built upon – these existing tools are discussed, followed by those developed by the author.

2.1 INTRODUCTION

The primary data gathered from the percolated particle network device in experiments are measurements of conductance over time. These are calculated from voltage and current samples. The length of the dataset gathered is typically in the thousands or millions of samples. Tools are necessary for calculating and visualising properties of these data, and similar data extracted from simulations.

The MATLAB 6-panel plotter tool, discussed in detail in Section 2.2, analyses measured conductance data (from either a simulation or an experiment). It then produces a figure with 6 different plots that each show different information about the measured conductance and the underlying statistics. These figures, termed '6-panel plots', allow visual comparison of the simulation and experimental behaviour, and have become a valuable tool in interpreting results.

There is hope that if the external behaviour of the simulated network is similar to the device, then the accessible internal behaviour of the simulated network may be similar to the inaccessible internal behaviour of the network on the physical device. Several tools existed at the beginning of the Master's project, some for analysis of external measurements and some for extracting and analysing the internal behaviour of the board. These existing tools are discussed briefly in Sections 2.1.1 to 2.1.3, and were used as a starting point for development of two new board viewing tools, discussed in

Section 2.3. Section 2.4 presents a new tool which extracts and plots the current and electric field in switching junctions as histograms.

2.1.1 Existing tools – particle and network board viewers

Several pre-existing tools deserve mentioning, as they contributed to the tools developed by the author. Two board viewer tools which show the simulated board either as an area populated with particles, or as a network of connections, are discussed here.

The particle viewer tool produces a visualisation of the board at the particle level. Each particle is drawn as a circle, either rendered in grey-scale to indicate potential (if the potentials are known, as is the case when a saved simulation statefile has been loaded) or coloured according to their groups, with randomly chosen colours. The switching junctions between the particles are drawn as dark grey rectangles. The particle potentials board view can be used for judging the sizes and distribution of groups of particles, and for observing the changes in distribution of potentials across the board over time. Example particle board views are shown in Figure 2.1a and Figure 2.1b with colouring according to potentials and groups, respectively.

The network viewer tool produces a visualisation of the board at the group level, showing the groups and their connections. Each group is drawn as a single coloured circle positioned at the centroid of all of its particles, and the parallel switching junctions connecting neighbouring groups are drawn as lines. This forms a network plot of nodes (groups) and edges (parallel switching junctions). Optionally, the edges are coloured red if any of their parallel switch connections are in the filament state – thus showing which parts of the network are 'on'. The network board view can be used for observing the structure of the conductance network and the locations of filaments. An example network board view is shown in Figure 2.1c.

2.1.2 Existing tools – switching locations viewer

The switching event locations board viewer produces a visualisation of the board at the particle level, but highlights locations of events rather than the potentials. Each switching junction is coloured green if any switching events are recorded in that junction during an entire simulation. An example switching locations view is shown in Figure 2.2.

The switching event locations board view provides a visual indication of where the switching activity is concentrated on the board, which gives information about the distribution of the switching activity – if all the activity is in a small area of the board, then the board activity may be trivial and not sufficiently spatially distributed to produce non-trivial conductance switching behaviour. An example of trivial activity is the majority of switching events occurring in only one junction. If a board only shows

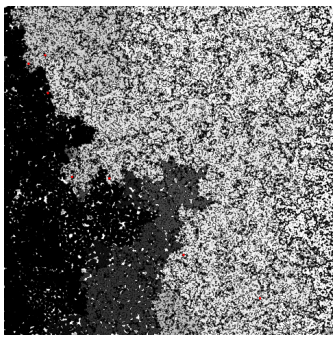

(a) An example particle potentials board view produced by the initial tool version. The particles are rendered in greyscale for the range of potentials distributed across the board.

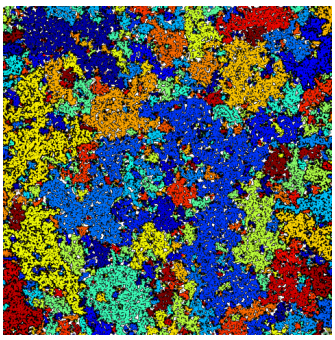

(b) An example particle groups board view produced by the initial tool version. The particles are coloured randomly according to the groups that particles belong to.

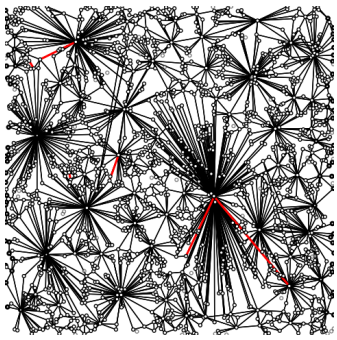

(c) An example network board view produced by the initial tool version. The network edges are coloured according to the conductance type – filament or tunnel gap.

Figure 2.1 Examples of the three main board view types initially available.

switching on a small number of conducting pathways, then the resulting statistics of the output measurements may not be diverse enough to demonstrate the statistical behaviour of the device that the board is intended to replicate. Any board known to have trivial switching activity is excluded from further simulations, by no longer using the set of random seed, board dimensions, and coverage values that produce that particular board.

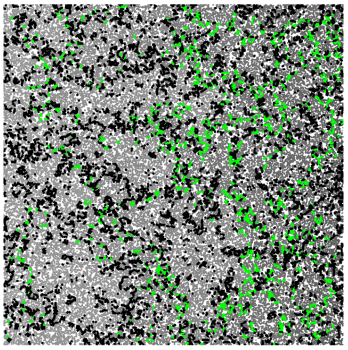

Figure 2.2 An example switching event locations board view produced by the initial tool version. The board is rendered in greyscale, with switching junctions coloured green if they switched during a specified time window or black if they did not.

2.1.3 Existing tools – simulation output tools

The simulation program includes several built-in tools for extracting different types of data. Three of them are called ‘datfiles’, ‘dump’, and ‘special’. ‘Datfiles’ causes the simulation to record a wide range of external measurements, similar to those accessible

from the device. This provides the measurement data used extensively in the thesis. 'Dump' causes the simulation to save snapshots of the internal board state at every time-step. These saved simulation statefiles are used to allow analysis of internal conditions throughout a recorded simulation. 'Special' records power, current, and switching event information for every switching junction in a board. This is used by several scripts that were included with the pre-existing source code, but, due to poor documentation, the purpose and proper use of many of these scripts was not determined during the Master's project.

2.2 MATLAB SCRIPT FOR PLOTTING MEASUREMENTS IN PANEL FIGURES

External measurements of boards or devices were analysed and then plotted using a script written in MATLAB. The building blocks of this script came from a pre-existing suite of functions developed by Shota Shirai, a colleague in the research group. Features of the script were added and developed gradually over the course of the Master's project. The figures produced by the script consist of six small plots arranged in a grid, with numerous annotations providing additional information. These figures, referred to as '6-panel plots', are explained in detail here.

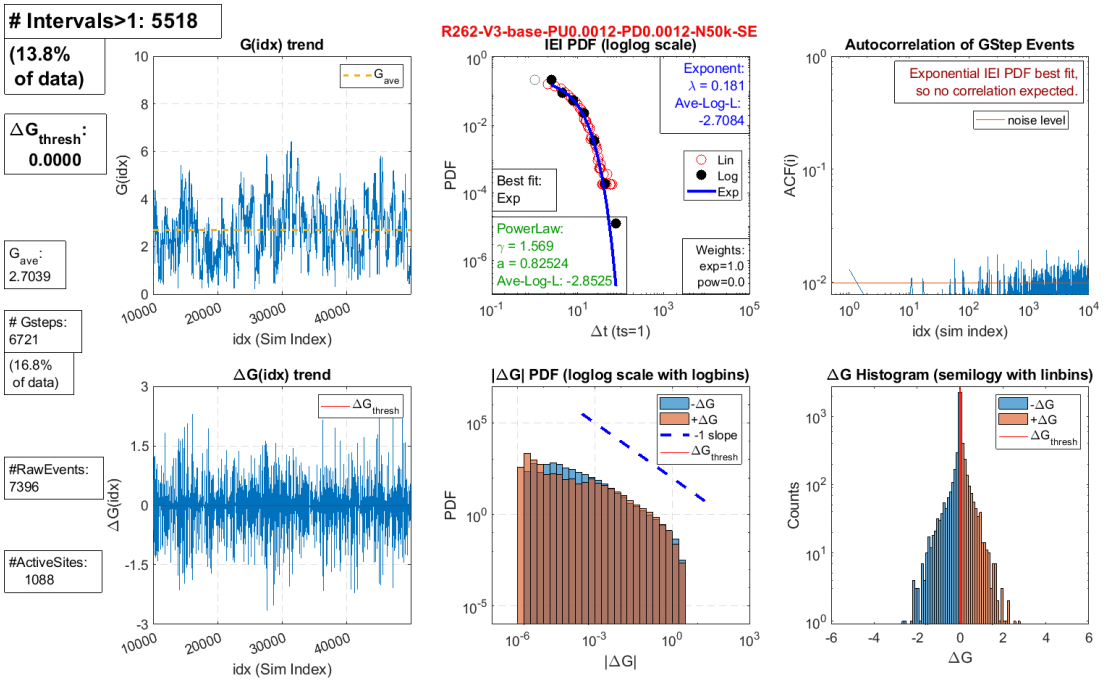

Figure 2.3 A typical figure produced by the 6-panel plot MATLAB tool.

An example 6-panel plot figure is shown in Figure 2.3. The elements are listed and described in this section. On the left edge of the figure are eight annotation boxes. These annotations are listed and described in Table 2.1.

Table 2.1 The eight annotations that appear on the left-hand edge of the 6-panel plot are listed and described here.

# Intervals>1: 5518 (13.8% of data)	**# Intervals>1**: This states the number of inter-event intervals in the data analysed that were longer than one time-step. The minimum length in time-steps can be changed to other values if necessary. This only affects the IEI analysis. **(% of data)**: This is the % of the time-steps analysed that were the beginning of intervals greater than one time-step in duration.
ΔG_{thresh}: 0.0000	ΔG_{thresh}: This is the minimum change in G used in analysis to detect step change events in G. For the simulations, it was possible to have events reported explicitly by the program or have conductance only change as a result of events (making any change indicate an event). For experimental data, a non-zero threshold is required in order to exclude changes due to noise.
G_{ave}: 2.7039	G_{ave}: This is the average G for the set of data analysed.
# Gsteps: 6721 (16.8% of data)	**# Gsteps**: This is the number of events detected by observing the discrete conductance changes, or the number of time-steps that had a change in G greater than the threshold. **(% of data)**: This is the % of the time-steps analysed that had a change in G greater than the threshold. This indicates the event density of the data, which is a key indicator of overall activity rate in the simulation – if the data density is too high (above 20%), then the quality of the interval statistics is negatively impacted.

(Table continues on next page)

(Continuation of Table 2.1)

#RawEvents: 7396	**#RawEvents**: This is the total number of events explicitly reported by the simulation. Unlike the event count detected by observing discrete conductance changes, this count includes all events that occur on the same time-step. This annotation is only produced when analysing results of simulations.
#ActiveSites: 1088	**#ActiveSites**: This is the total number of switching junctions that switched during an entire simulation. Unlike other values shown in the 6-panel plots, this value is pre-calculated and so it cannot account for skipped data. This annotation is only produced when analysing results of simulations that have recorded this information.

(End of Table)

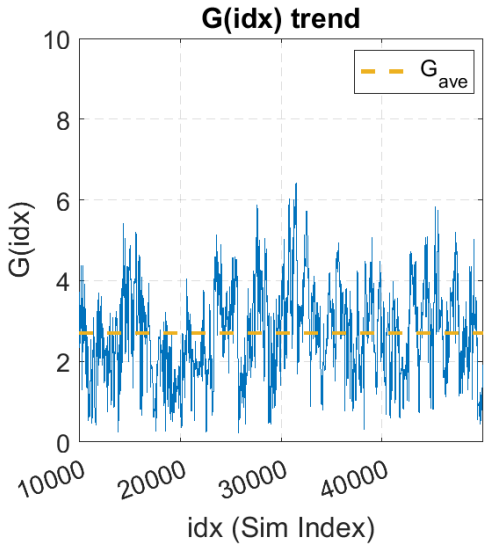

Figure 2.4 6-panel plot, conductance subplot.

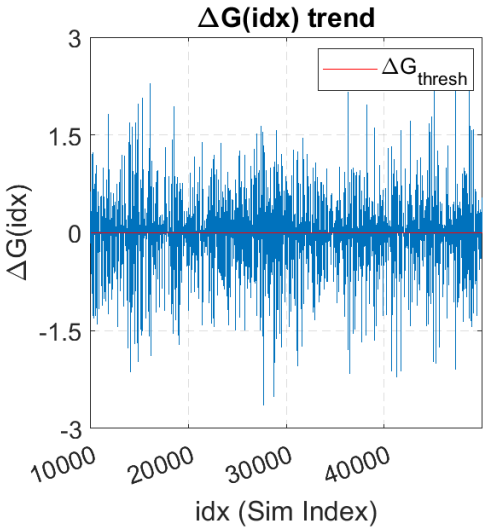

Figure 2.5 6-panel plot, change in conductance subplot.

The subplot in the top left of the 6-panel plot (and in Figure 2.4) shows the conductance over time for the simulation. The blue trend is the conductance, in units of G_0 for experimental data and arbitrary units for simulation data. The dashed yellow line indicates the average value of G for the data analysed. Note that the first 10 000 time-steps of simulation data are routinely skipped, as a crude measure to exclude

the majority of the initial transient events that occur in a simulated board while it approaches steady state activity. Long simulations (more than 100 000 time-steps) are reliably indicative of long-term behaviour, but are not often generated due to computing constraints, so simulations considered in this thesis are typically 50 000 time-steps in duration.

The subplot in the bottom left of the 6-panel plot (and in Figure 2.5) shows the change in conductance over time for the simulation. The blue trend is the difference in G between consecutive time-steps. The red line, if present, is the threshold for event detection, ΔG_{thresh}.

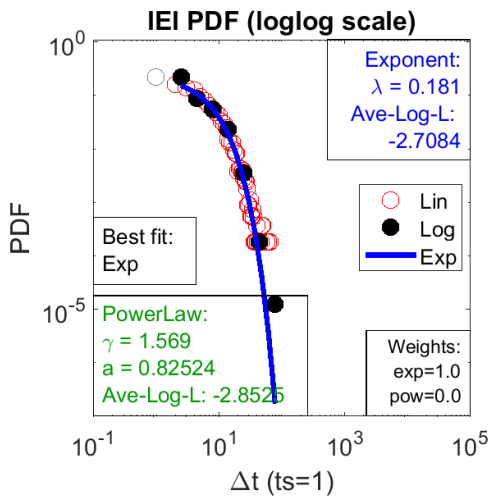

Figure 2.6 6-panel plot, IEI PDF subplot.

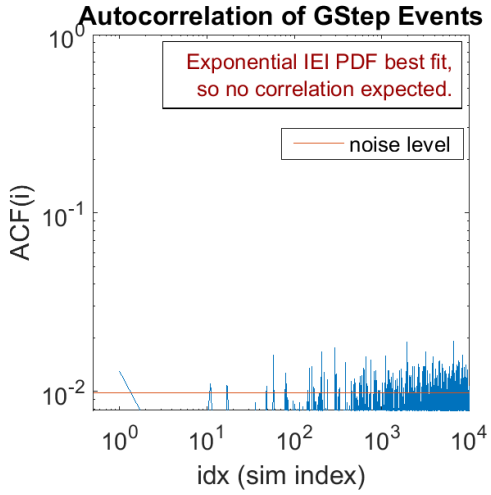

Figure 2.7 6-panel plot, event autocorrelation subplot.

The subplot in the top middle of the 6-panel plot (and in Figure 2.6) shows the probability density function of the inter-event intervals for the simulation, on log-log scale axes. Recall that events are defined as step changes in conductance and inter-event intervals are the number of simulation time-steps between two events (Section 1.1.2). The IEI data is shown both in linearly spaced bins (red circles) and in logarithmically spaced bins (black dots). The intervals below the minimum duration in time-steps are shown in linearly spaced bins (grey circles) and are not included in the model fitting process. The IEI data is processed by maximum likelihood estimation (MLE) to find parameters for a best fit using an exponential law model and a power law model. The Akaike information criterion (AIC) [28] is then used to judge which of the two models is a better fit for the data. The best fitting model is then declared in the 'Best fit:' annotation on the middle left of the plot, and is plotted along with the data – blue for exponential law model ('exp') or green for power law model ('pow'). The calculated AIC weights are shown in the 'Weights' annotation in the bottom right of the plot – these weights add to 1.0, and typically the weight of the best fitting model is 1.0. The parameters calculated for the models are displayed in the annotations at the top right

(exponential) and the bottom left (power). Typically, the data trend curves downwards for an exponential law and maintains a straight downward slope for a power law.

The subplot in the top right of the 6-panel plot (and in Figure 2.7) shows the autocorrelation function of the event occurrence time series. To produce this plot, each time-step in the simulation is encoded as '1' for an event or '0' for no event, creating a binary time-series. Then, the autocorrelation of this binary time series is calculated for a range of time lag values. The ideal response is a linear trend above the noise, with a shallow slope, suggesting long-term correlation between events. If the best fitting model for the IEI data is the exponential law model, an annotation is included in the top right to warn that correlation should not be expected in this data. Based on the range of time-steps considered, the noise level is estimated as $1.96/\sqrt{timerange}$, where *timerange* is the number of time-steps analysed (typically 40 000). This approximates the 97.5% quantile of a standard normal distribution. This noise level is indicated by the red line in Figure 2.7. Noise can show above this line, but it is reasonable to assume that activity below this line does not indicate any correlation between the events.

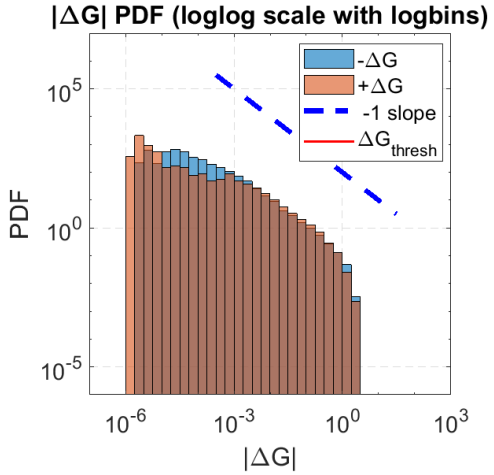

Figure 2.8 6-panel plot, log-log axes, log-binned PDF normalised histogram of change in conductance subplot.

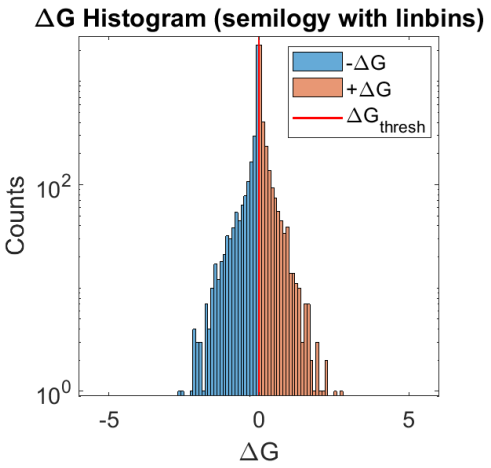

Figure 2.9 6-panel plot, log-scale y-axis, linear-binned histogram of change in conductance subplot.

The subplot in the bottom middle of the 6-panel plot (and in Figure 2.8) shows a histogram of the magnitude of up and down changes in conductance, shown in log-log scale, with logarithmically sized histogram bins. If the ΔG_{thresh} is non-zero, it is shown as a vertical red line. The down event (-ΔG) data is shown in transparent blue, and the up event (+ΔG) data is shown in transparent orange. If the events are power law distributed in ΔG magnitude then they will demonstrate a straight line trend. If the ΔG magnitudes of the events are equally distributed across the orders of magnitude, then this plot will show a slope of -1. A dashed blue line shows a slope of -1 as a tool for visual comparison.

The subplot in the bottom right of the 6-panel plot (and in Figure 2.9) shows a

histogram of the up and down changes in conductance, shown in log-linear scale. The histogram bins are of fixed sized (as opposed to logarithmically sized as in previous plots here). The down event (-ΔG) data is shown in blue, and the up event (+ΔG) data is shown in orange. The ΔG_{thresh} is shown as vertical red lines for positive and negative values.

Numerous metrics, such as the average conductance, are calculated in the process of producing these 6-panel plots. These metrics are recorded into a comma-separated-value file after processing the data of each simulation. This allows plotting of the trend in model behaviour over many simulations, to test the effect of varying the value of a given parameter.

2.3 PYTHON SCRIPT FOR BOARD VIEW OF POTENTIALS AND CURRENTS

A script was written in Python to produce figures visualising the saved states of simulated boards as group network maps showing current, and as particle maps showing potentials. The building blocks of this script came from existing Python scripts that display the board particle plot of potentials in greyscale, and that display the board group network map with filaments highlighted (Section 2.1.1). The new board views both use new colour scales and have additional markings to indicate locations of switching events. The meanings of the colours and markings are indicated with a colour bar and a legend. The new views also both include text annotations which note the following: simulation parameters which give context to the plot, the state (or time-step) number being viewed, and the total conductance of the board. One of the two new views shows a map of particles and their potentials, and the other other shows a map of groups and currents flowing between the groups.

In the new board view showing a map of particle potentials, the potentials of the particles are shown using a blue-scale instead of grey-scale, and the particles that are in input or output groups are highlighted with orange. For board states with recent switching events, the location and type of switching event are shown using colour-coded rings and dots. The change in total conductance preceding the state shown (PrevDeltaG) is printed at the top. An example board particle potential map is shown in Figure 2.10a.

In the new board view showing a map of groups and connections, the intensity of current is shown using a custom blue-to-red colour scale, and using a range of network edge thicknesses. The colour scale is logarithmic, to clearly show the strongest current paths. Any currents of negligible magnitude are given a pale blue colour (not shown in the colour bar) to allow these connections to be visually ignored. For board states with recent switching events, the network connections where the events were located are highlighted with colour coded borders. An example board conductance network with intensity of currents is shown in Figure 2.10b.

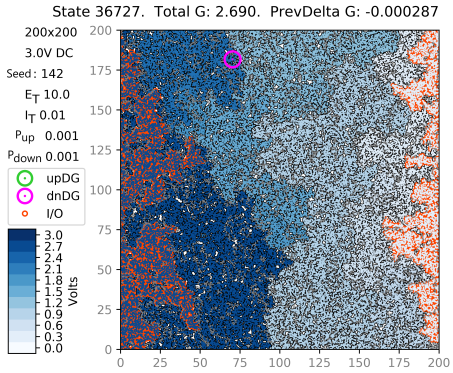

(a) An example output of the new particle potentials viewer, with switching events highlighted.

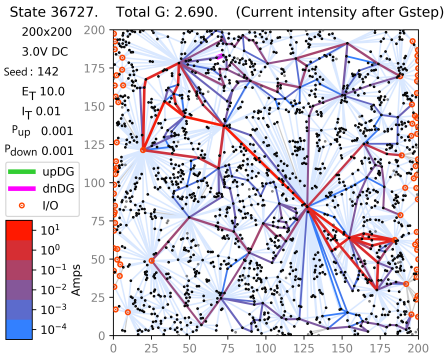

(b) An example output of the new conductance network with current intensity viewer, with switching events highlighted.

Figure 2.10 Examples of the new versions of the two main board view types initially available.

2.4 SWITCH ENERGY HISTOGRAM SCRIPT

A new Python script, termed the 'switch energy histogram' script, was written to produce histograms of the electric field and current (energy) in all switching junctions, over a range of simulation time-steps in which switching events occurred. To supplement this script, two new Python modules were written to provide methods for collecting information from the simulation. One focuses on collecting data from the external measurements recorded by the simulation. The other focuses on collecting data from loaded copies of simulation boards and states, allowing access to the internal state of the simulation at any time-step.

Investigating the distribution of electric fields and currents in the network when switching events occur aids model development by showing what conditions lead to switching events. If the values of electric field strengths and currents are unexpected, histograms of the distributions may highlight possible errors in the model (for example, events should not occur below E_T or I_T), or may provide other insight into the internal behaviour of the network.

To produce the histograms, the script reads all saved simulation states within a specified time-step range, accumulating counts of electric fields and currents present on all switching junctions at time-steps in which any switching event occurs. The electric field strengths during switch-up events and the currents during switch-down events are plotted in one histogram each, showing the total counts of tunnels or filament for each electric field strength or current value, respectively.

An example of switch event histograms for switch-down currents and an example for switch-up electric fields can been seen in Figure 2.11a and in Figure 2.11b, respectively. The counts of all switching junctions and of triggered junctions are shown separately. This gives an impression of the overall distribution, and of the subset corresponding to

events. The highest current that produced switch-down events, and the highest electric field strength that produced switch-up events can be seen, as well as the distribution from highest to lowest. In this example, the distribution of counts for triggered junctions appears to follow the curve of the distribution of counts for all junctions. Note that the relevant switching thresholds are marked, and that the counts for switching junctions only appear above those thresholds. An annotation in the top left shows the number of raw up or down events, and the number of Gsteps (step changes in measured G). Note that multiple raw events may contribute to a single externally measured Gstep, so the sum of the up and down counts may exceed the number of Gsteps. The annotation also shows activity percentage, i.e., the percentage of time-steps with Gsteps.

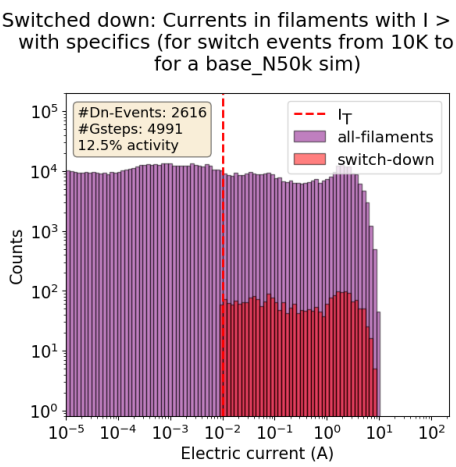

(a) A histogram of currents in filaments, switching and not.

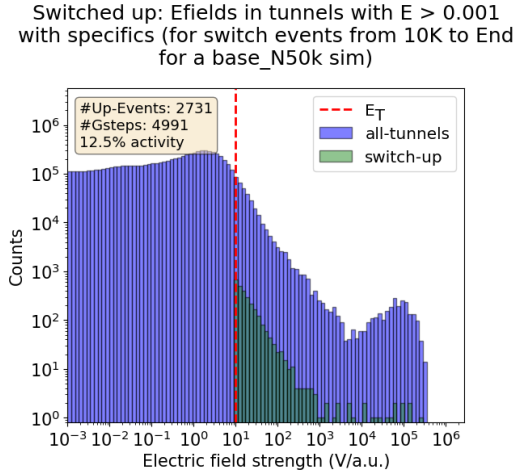

(b) A histogram of electric fields in tunnel gaps, switching and not.

Figure 2.11 Examples of the switching event histograms.

2.5 MODIFICATION OF BUILT-IN SIMULATION OUTPUT TOOLS

The built-in output tools of the simulation (Section 2.1.3) were further developed as necessary during the Master's project. The 'datfiles' tool, which records measured data at every time-step, and the 'dump' tool, which saves statefiles at every time-step, were combined into a new tool called 'combined'. This allows statefiles and external results to be collected after running a simulation only once, rather than twice.

The recorded external measurements (applied voltage, input currents, output currents) did not allow investigation of the contribution of a board's individual switching junctions. There was interest in answering questions like 'how many junctions were active during the simulation?', 'how many times did each junction switch?', and 'how many events occurred on the same time-step?'. These questions can be answered by analysing statefiles, but that approach requires collection of the statefiles (which take a great

deal of storage space) and then analysis of the statefiles (which can take a considerable amount of processing time). To answer these questions routinely, and with minimal cost in time or storage, the simulation output tools 'datfiles' and 'combined' were both modified to record which junctions switched at every time-step during simulations. At each time-step with an event, all junctions were recorded in binary as either switched or unchanged. This binary string was then run-length encoded, for compact storage, and saved to a file. The recorded switching information enabled analysis of events in terms of which specific junctions switched and how much the total conductance was changed as a result of the switching of each junction.

Chapter 3

PROBABILISTIC SWITCHING MODELS

The purpose of the simulation is to reproduce behaviour observed in the experimental data, in order to understand the experimental percolating network device. That goal is subdivided into the objectives listed in Section 1.2.1. This chapter explores the behaviour shown by simulations using three different probabilistic switching models: the base model (Section 1.1.4) originally developed by Fostner and Brown [8], and two new probabilistic models.

In Section 3.1, the base model is discussed and, by comparing representative results with experimental data, it is shown that this model does not meet the requirements of the objectives. In Section 3.2, a new model that uses multiple rather than single time-step switching is discussed and explored, and representative results are compared with experimental data and with the base model results. Section 3.3 discusses and explores a second new model that uses switching probabilities dependent on electric field strength and current (rather than fixed probabilities), and then compares the behaviour with experimental data and results from the other two models.

The conclusion of this chapter (Section 3.4) is that probabilistic switching seems to be inherently unable to reproduce the experimental data IEI distribution and correlations between switching events. In an effort to reproduce the aspects of the experimental data, a new model without probabilistic switching (a deterministic model) is discussed and explored in Chapter 4.

3.1 INTRODUCTION

Section 3.1.1 presents a representative set of results from a simulation using the base model, where the simulation parameters have been chosen to generate G(idx) data similar to experimental G(t) data. The simulation data and experimental data are compared and discussed. The results from the base model are also compared for two different choices of switching probabilities. Then, in Section 3.1.2, the two new models covered in Sections 3.2 and 3.3 are named and briefly described.

3.1.1 Base model observations

As discussed in Chapter 1, one of the ultimate goals is to use the simulation to predict experimental results. This will not be possible until the simulation can produce results that match known experiment results, based on a specific set of criteria. In testing different models and parameter choices, the simulation behaviour is compared with the experimental data according to three criteria (Section 1.2.1):

- ΔG values ranging over several orders of magnitude,
- an IEI distribution that is linear on a log-log plot, consistent with an underlying power-law distribution,
- evidence of correlation between switching event times.

Once the behaviour shown in simulation data meets the criteria, it can then be concluded that the switching model used can reproduce the behaviour of the primary switching processes at work in the experimental device.

It was known prior to this Master's project that the base model does not meet the above criteria. This section shows that the base model is capable of generating G(idx) data that is similar in number of events and in magnitude distribution to the experimental data, but also shows that the generated events have IEI distributions that are not linear on a log-log plot, and do not show any evidence of correlation between event times. Since this does not meet the criteria, new models need to be developed and tested. In order to assess whether new models perform better than the base model in terms of the criteria outlined above, a representative example of simulation data generated using the base model is needed. This 'baseline' example allows side-by-side comparison of plotted results from new models with the base model, to determine whether any of the new models are closer to meeting the criteria than the base model.

Recall that Section 1.1.3 gives a description of the general model of the device, i.e., how all the particles are arranged and connected with each other, and how the network state is updated. In particular, recall that a single instance of calculating all potentials and currents, and updating all switches in the network, is called a time-step. The probabilities of switching (P_{up} and P_{down}) are fixed in the base model, and each switching event occurs within a single time-step (Section 1.1.4).

The base model was used with a particular set of parameters to produce the baseline example results. The probabilities and other parameters used for generating the baseline example are listed in Table 3.1. The data extracted from the baseline simulation was processed by the tool described in Section 2.2, to produce the six plots showing the simulation behaviour in Figure 3.1. For comparison with the baseline simulation, a representative example of experimental data is shown in Figure 3.2.

Table 3.1 The simulation parameters used to generate the baseline results in Figure 3.1. The meaning of each parameter is explained in Section 1.1.3 and Section 1.1.4, and they are listed in Appendix A.

Voltage(DC)	P_{up}	G_{on}	Random Seed	d_{max}
3.0 V	0.0006	10	262	0.3454
E_T	P_{down}	A	Coverage	Timespan
10.0	0.0020	1.0	0.65	50000
I_T	Size	β		
0.01	200 x 200	100		

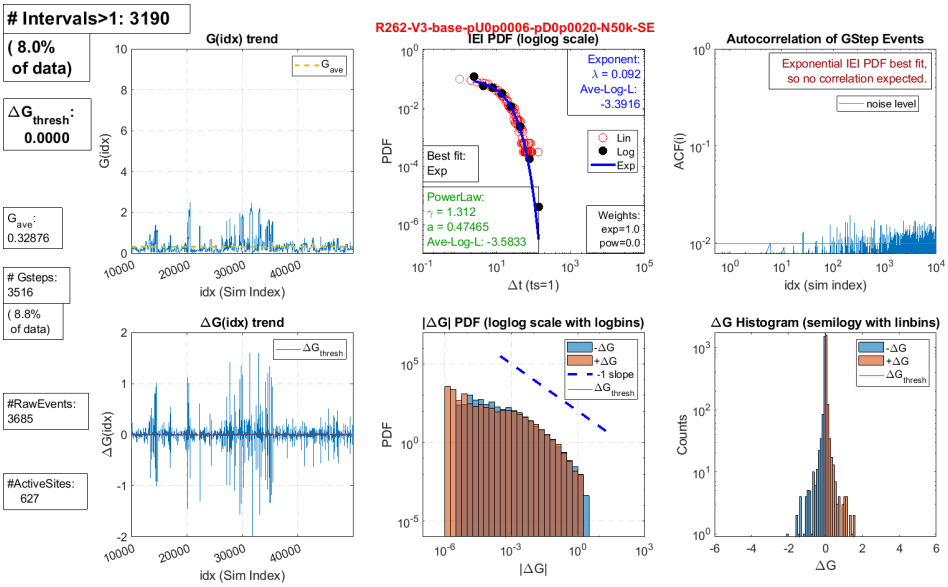

Figure 3.1 A six-panel plot showing representative analysis results of the closest match possible to the experimental data using the base model simulation. Note the curved appearance of the trend in the IEI plot, and the lack of a clear trend in the autocorrelation plot. These results in particular are for analysis of a simulation using the parameters listed in Table 3.1.

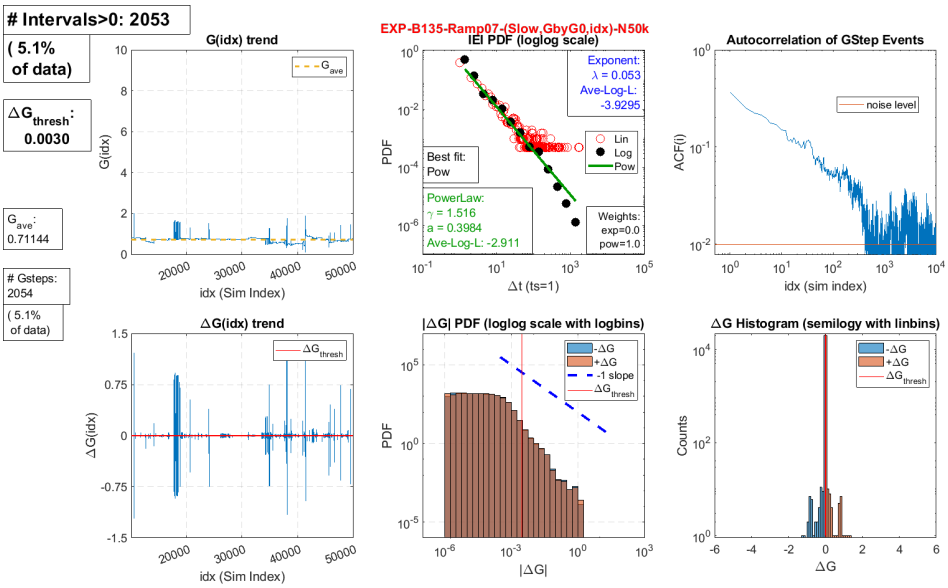

Figure 3.2 Key analysis results of an experimental dataset (not simulated) shown in a six-panel plot generated in MATLAB. Note the linear appearance of the trend in the IEI plot, and the clear trend over several decades in the autocorrelation plot.

There are some significant differences between the probabilistic simulation behaviour shown in Figure 3.1 and the experimental behaviour shown in Figure 3.2. Two clear and important differences are in the IEI and the ACF plots (top-middle and top-right plots of each figure, respectively). The experimental IEI data is best fitted with a power law distribution whereas the baseline simulation IEI data is best fitted with an exponential law distribution. This best fit was determined by using maximum likelihood estimation (MLE) to determine the parameters of an exponential model and of a power model, and then using the Akaike information criterion (AIC) [28] to choose between the two models (Section 2.2). In the ACF plots, there is a clear and strong trend above the noise for over three decades in the experimental data that does not appear in the simulation data.

A wide range of parameter choices for the base model have been explored during the Master's project, and none produced results that demonstrated all of the properties observed in the experimental results. The behaviour was explored for parameter choices including but not limited to:

- probabilities between 0.0001 and 0.5000,
- voltages between 1 and 10 V,
- three magnitudes of the current and electric field strength threshold,
- board coverages from 0.50 to 0.69,
- and ten different random seeds.

Despite not meeting the criteria, these baseline results resemble the experimental results best out of all parameter choices explored. To allow more detailed scrutiny, each of the six subplots from the baseline results are compared with the corresponding subplots from the experimental results. These comparisons appear in Figures 3.3 to 3.8 inclusive.

The base model can be made to generate G(idx) data that appear qualitatively similar to that of the experimental results, as shown in Figure 3.3 where both simulation and experiment G(idx) data appear to repeatedly spike upwards in bursts from a minimum G value. This is done by choosing the magnitude and ratio of the switching probabilities, P_{up} and P_{down}, such that the number of switching events is less than 10% of the number of time-steps and the overall conductance remains low.

The appearance of the ΔG behaviour of the base model has limited similarity to that of the experimental, as shown in the comparison of the two in Figure 3.4. Both have a range of large and small changes, but the base model lacks the clustering of large changes. The base model appears to have changes of all size occurring randomly – as expected from a simple probabilistic model.

The difference between the IEI distributions of the base model and of the experimental results is apparent – one appears curved and one appears linear. As demonstrated

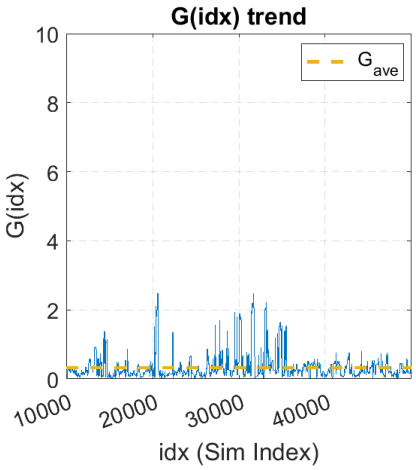

(a) Subplot from the baseline results.

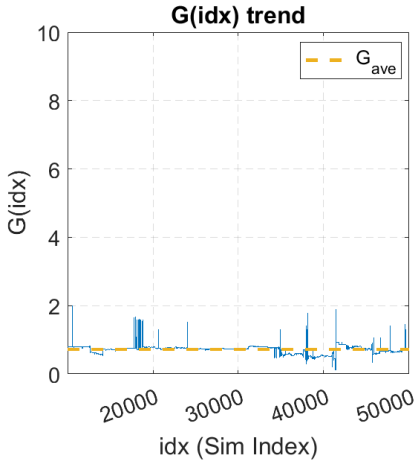

(b) Subplot from the example experimental results.

Figure 3.3 Comparison of the conductance trends for the baseline results with the example experimental results.

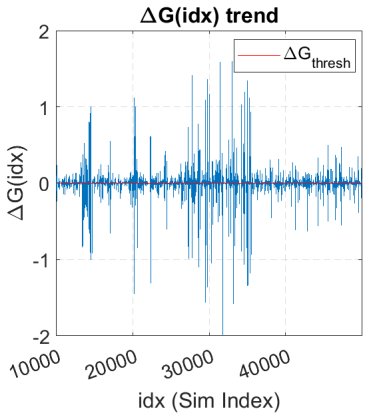

(a) Subplot from the baseline results.

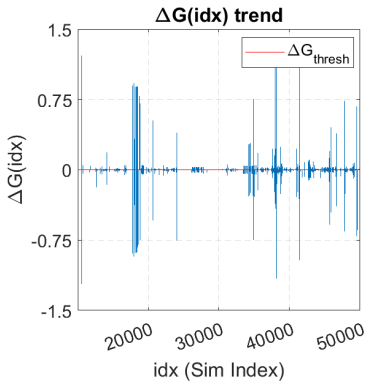

(b) Subplot from the example experimental results.

Figure 3.4 Comparison of the conductance change trends of the baseline results and the example experimental data.

in Figure 3.5, the base model produces IEIs that are distributed in a manner consistent with an exponential law distribution, while the experimental results are consistent with a power law distribution over several decades. These distributions are indicated by the best fit models included in the IEI plots.

When comparing the base model simulation results with the experimental results, there is a clear difference in the existence of correlation between events. As shown in Figure 3.6, the base model shows no evidence of correlation that can be reliably distinguished from random noise, whereas the experimental results show evidence of correlation that decays slowly over several decades of lag (Δt).

As shown in Figure 3.7, both the base model and experimental results show a

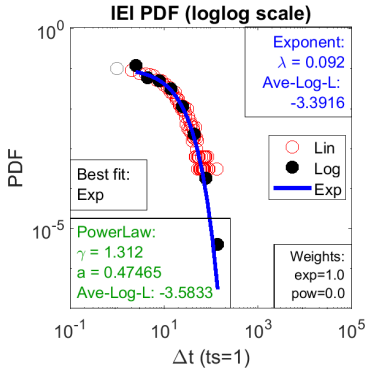

(a) Subplot from the baseline results.

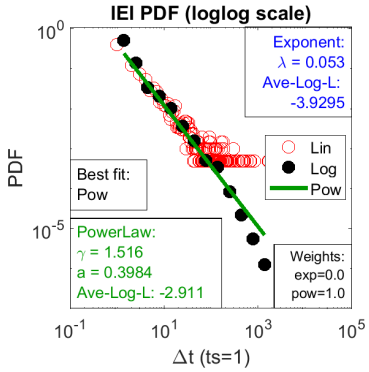

(b) Subplot from the example experimental results.

Figure 3.5 Comparison of the IEI plots for the baseline results with the example experimental results.

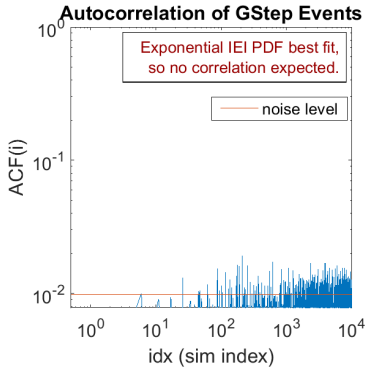

(a) Subplot from the baseline results.

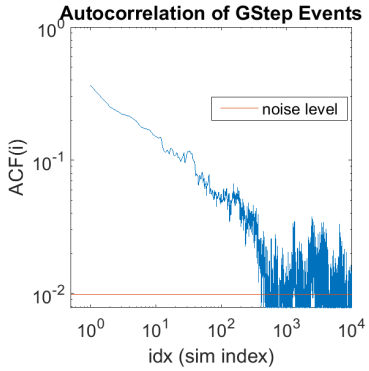

(b) Subplot from the example experimental results.

Figure 3.6 Comparison of the ACF log-log plots for the baseline results with the example experimental results.

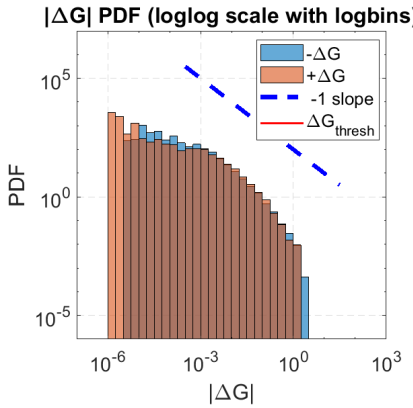

(a) Subplot from the baseline results.

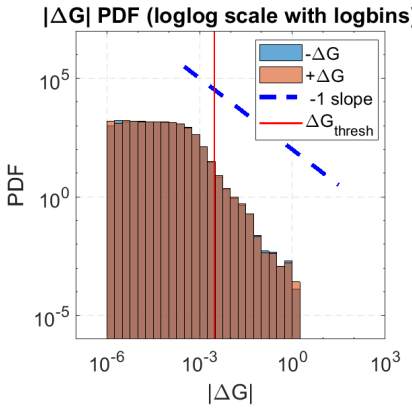

(b) Subplot from the example experimental results.

Figure 3.7 Comparison of the log-log histogram of $|\Delta G|$ for the baseline results with the example experimental results.

range of magnitudes of ΔG. The slopes of the $|\Delta G|$ PDF histograms differ slightly – the base model shows a less steep decay for increases in ΔG when compared with the experimental data. There is also a difference in the left-hand limits of the data. The experimental data shows a flat section, while the base model simulation results show a gentle curve. This is assumed to be due to the limitations of measurements in the experimental case.

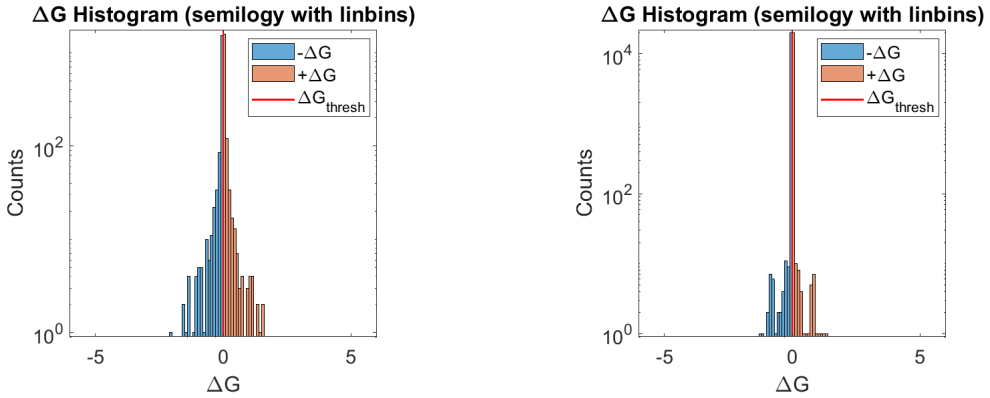

(a) Subplot from the baseline results.

(b) Subplot from the example experimental results.

Figure 3.8 Comparison of the log-lin histogram of ΔG for the baseline results with the example experimental results.

As shown in Figure 3.8, when assessing the distribution of ΔG on a linear scale there does not appear to be any notable difference between the results of simulation and experiment.

It was noted while testing different parameter values that the base model IEI and ACF results were not very sensitive to the choice of probabilities in the simulation. To demonstrate this, Figure 3.9 compares the G(idx), IEI, and ACF baseline results with those of another base model example generated using a different choice of P_{up} and P_{down}.

The baseline results show G(idx) data that is visually similar to that of the experimental data in the sense that there are groups of spikes and the G(idx) tends to spike upwards from an overall minimum. In contrast, the second base model example (generated using a different choice of P_{up} and P_{down}), shows much higher G(idx) that appears to be spiking rapidly about a moving average. Note that despite the drastic difference in G(idx), there is little difference in the IEI and ACF plots of the two base model examples.

Observations of the behaviour of the base model examples discussed here confirmed that the switching behaviour produced by the base model does not meet all of the objectives. Specifically, the base model does not produce IEI data that is consistent with an underlying power-law distribution, nor does analysis of the switching events show any evidence of correlation, so the base model simulation is not a good match to the

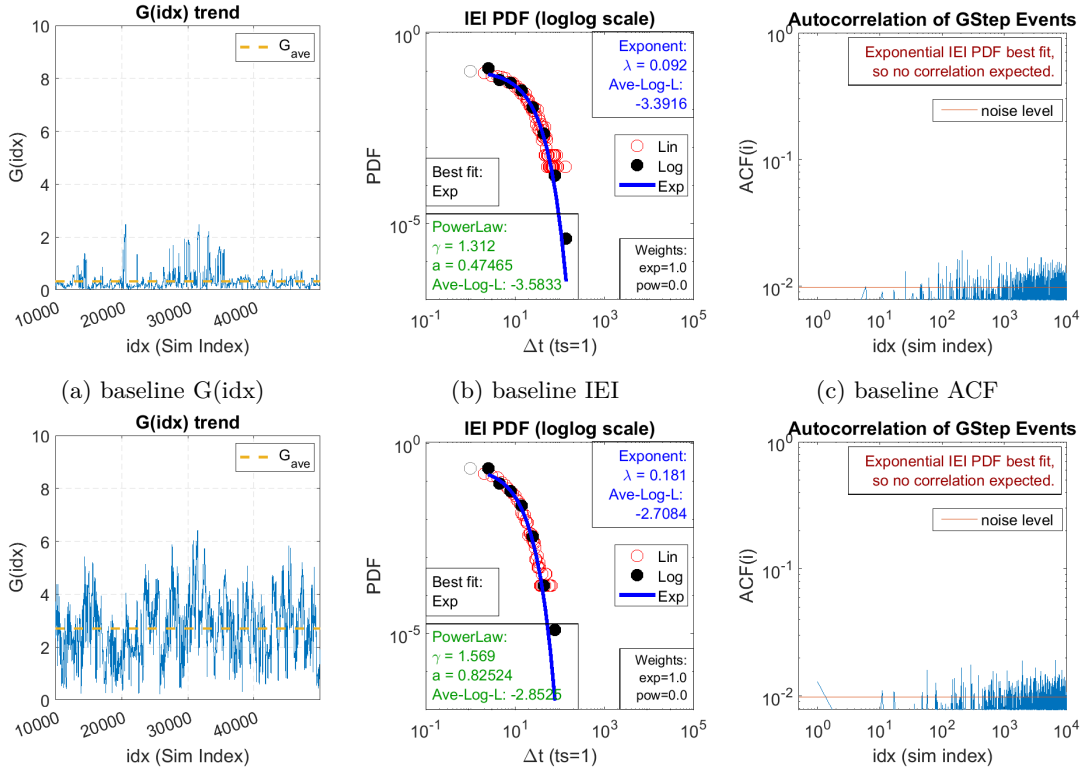

(a) baseline G(idx)

(b) baseline IEI

(c) baseline ACF

(d) another base model example, G(idx)

(e) another base model example, IEI

(f) another base model example, ACF

Figure 3.9 Comparison of G, IEI, and ACF behaviour of the baseline example and another example using the base model. As noted in the subfigure captions, the first row shows the behaviour for the baseline example data while the second row shows the behaviour for a different base model example model. The only difference in the parameters used was the probabilities – baseline used P_{up} of 0.06% and P_{down} of 0.20%, whereas the other base model example used 0.12% for both. Note that while the G(idx) plots are markedly different, the IEI plots are quite similar in shape and neither of the ACF plots show significant activity above the noise.

experimental device. New switching models needed to be developed in order to improve the match of the simulation to the experimental device. Two properties of the base model that may be limiting the success of the simulation in matching the experimental results are a) that switching events are triggered *probabilistically* for switches that meet the relevant threshold, and b) that conductance changes are *instantaneous* between the filament and tunnel gap states once triggered. These properties are included for the sake of simplification, but are unphysical, and it is conjectured that replacing these with more realistic properties may allow some of the experimentally observed behaviours to emerge in the simulation.

3.1.2 Simulation modifications, in brief

The next two sections of this chapter explore two major modifications of the base model that aim to introduce correlation between switching events. These modifications are briefly described here.

The first modification, considered in Section 3.2, tests the effect of making the switching process take place gradually, over multiple time-steps. Recall that in the base model, switching is instantaneous, i.e., it takes one time-step. The hypothesis was that correlation may emerge if the changes in conductances are delayed multiple time-steps, to allow switching processes to begin while others are in progress. The gradual changes in conductance are motivated by observations of experimental device conductance changes that are continuous as a function of time before some events.

The second modification, considered in Section 3.3, tests the effect of making the switching probability for each junction dependent on the electric field strength and current in that junction. Recall that in the base model, the switching probabilities are fixed. The hypothesis was that dependent probability would allow changes of voltage and current caused by one switching event to cause further switching events, thereby producing measurable correlation. This was also explored in combination with the multiple time-step switching modification.

3.2 MULTISTEP SWITCHING

The multistep switching model explored in this section was made by modifying the base model switching process to take multiple time-steps, gradually changing conductance a small amount on each time step before the large change at completion. This increase in time taken for changes in switch conductance is the key difference between this model and the base model. The motivation and hypothesis are discussed in Section 3.2.1. In Section 3.2.2, the physical concepts supporting the model are discussed, followed by the details of implementation. Finally, Section 3.2.3 presents results of simulations using the multistep model that demonstrate that it is not an improvement over the base model in terms of imitating the behaviour observed in experimental data.

3.2.1 Motivation for change

The observed statistics of measurements simulated using the base model indicate that there is no correlation between switching events (Section 3.1.1). For correlation to exist, it is believed that switching events must influence the likelihood of additional events.

The base switching model implements switching events as single time-step processes. Switches in the (open) tunnel gap state may switch to the (closed) filament state on any simulation time-step while their electric field is above the electric field threshold. Similarly, switches in the closed state may switch to the open state on any time-step while their current is above the current threshold. Open switches connected in parallel share voltage, so once a switch closes the voltage across that gap (and all parallel switch gaps) is significantly reduced due to the increase in switch conductance and the consequent voltage redistribution throughout the board network. Analogously, closed switches in series (particularly those in single file) share the same current, so multiple closed switches in series may experience a significant decrease in current when one switch opens.

Delaying the execution of triggered switching events would delay changes in the electric fields and currents. Extending the switching process over multiple time-steps may allow additional parallel connected open switches to trigger their closing processes, and similarly may allow additional series connected closed switches to trigger their opening processes. The hypothesis was that this might lead to observable temporal correlations between switching events. Conductance of the experimental device has been observed to increase slightly before some switching up events, and decrease slightly before some switching down events. It was thought that these gradual changes in conductance may contribute to producing correlated events.

3.2.2 Physical concepts and implementation details

The general model of switching junctions uses tunnelling conductance when open, and a filament conductance when closed (Section 1.1.3). It is reasonable to surmise that in a physical switching junction there are intermediate states between open and closed, and that a filament passes through various stages of growth. As a filament grows, the effective gap length decreases, and so the conductance due to tunnelling increases. This description is consistent with the device switching behaviour observed by Bose et al. [11]: a gradual increase in conductance before a sudden increase.

For the case of decreasing conductance, it is reasonable to surmise that in a physical switching junction there are intermediate states between closed and open, and that a filament gradually becomes thinner. This thinning process can be attributed to electromigration, consistent with observations of electromigration in nanowires [29, 30]. As a filament becomes thinner, its conductance decreases slightly. This description is consistent with observations of increasing resistance as a result of thinning filaments [31], and can explain observations of gradual decreases in experimental device conductance observed before switching down events. To incorporate these concepts of growing and thinning filaments, the multistep switching model extends the switching process over several time-steps, with gradual changes in conductance during the switching up and switching down processes.

The base switch model updates conductance whenever a switch is triggered, and does not update any other properties of the switch. In this multistep modification, a new switch variable – $\boldsymbol{Length_{mod}}$ – records reduction of effective gap length due to partial filament growth in the gap of an open switch. Similarly, the same variable is used again to track filament thinning in closed switches. A second new simulation parameter, $\boldsymbol{S_R}$ (short for Step-Range), specifies a fixed number of time-steps to complete the gradual switching process of triggered switches.

The gradual switching process is implemented as follows. Fully open switches in the multistep model have a $Length_{mod}$ of 0.0, indicating that there is no filament growth in the gap. As an open switch transitions to the closed state, the growing filament is modelled, at each time-step i, by increasing $Length_{mod}$ according to

$$Length_{mod}(i) = Length_{mod}(i-1) + \frac{Length}{S_R} \quad , \tag{3.1}$$

such that after S_R time-steps the switch has $Length_{mod} = Length$, indicating that the filament has grown to completely bridge the gap. During the filament growth process, the tunnel gap conductance is updated at each time-step i using the conductance Equation 1.1 and the effective tunnel distance (gap length) of

$$Tunnel_{distance}(i) = Length - Length_{mod}(i) \quad . \tag{3.2}$$

This makes the conductance of the gap increase gradually as the effective tunnel distance decreases. Once the filament is complete, the conductance is set according to the filament conductance set by the parameter G_{on}. An example of the changing conductance of a closing switch is shown in Figure 3.10a for three different values of S_R and for $G_{on} = 10$.

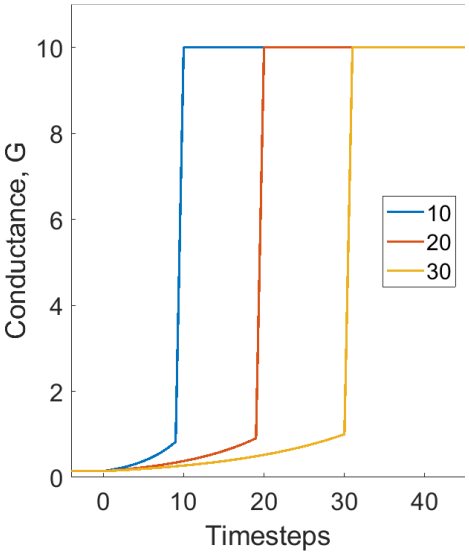

(a) The increasing tunnelling conductance of a gap containing a growing filament, until a step change due to completion.

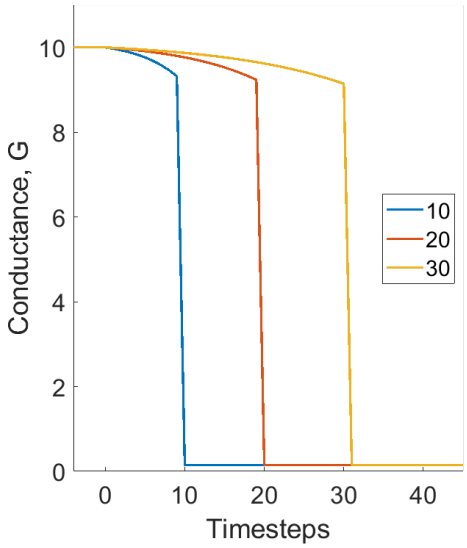

(b) The decreasing Ohmic conductance due to a filament thinning (due to electromigration caused by excessive current), until a step change due to filament breakage.

Figure 3.10 Conductance change over time in a multistep switching model. Shown for three different choices of S_R (number of time-steps per switching transition).

For a closed switch transitioning to the open state, the process is similar. $Length_{mod}$ is used again to track the process as described above for a growing filament, but using a negative $Length_{mod}$ to indicate that it is tracking a filament that is thinning in diameter rather than growing in length. Here $Length_{mod} = -Length$ initially, and increases to 0.0 in S_R time-steps as per Equation (3.1). While the filament is thinning, the gradually decreasing conductance is calculated using

$$G_{filament}(i) = G_{on} + G_{tunnel}(Length) - G_{tunnel}(|Length_{mod}(i)|) \quad . \tag{3.3}$$

Note that since $Length_{mod}(0) = -Length$, Equation (3.3) gives $G_{filament}(0) = G_{on}$, as intended for a complete filament. Once the filament is thinned to 0 diameter ($Length_{mod} \geq 0.0$), it is considered broken and the conductance is set as a tunnel in an empty gap, with $Length_{mod}$ reset to 0.0. This is an oversimplification – the filament is modelled here as completely removed once broken, whereas experimental filaments breaking due to electromigration have been shown to only lose a fraction of the filament length [29, 30]. An example of the changing conductance of an opening switch in the multistep model is shown in Figure 3.10b for three values of S_R and for $G_{on} = 10$.

3.2.3 Results

The results obtained with the multistep model are summarised below. Figure 3.11 shows the multistep model for S_R=5 time-steps. When a switch closes (Figure 3.11a), the conductance increases gradually before increasing sharply to its final state. When a switch opens (Figure 3.11b), the conductance decreases gradually before decreasing sharply to its final state. The switching up and switching down processes both take 5 time-steps to complete, showing that the model works as intended.

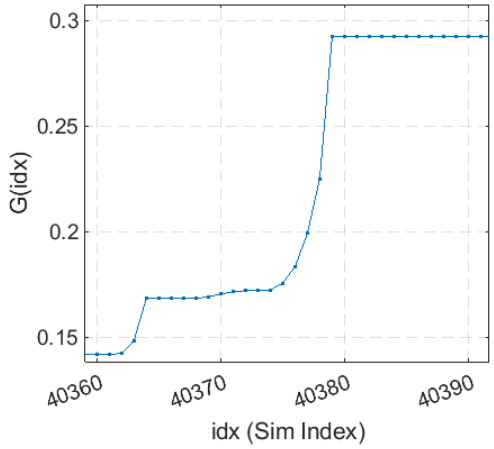

(a) Modelled increasing tunnelling conductance of a gap containing a growing filament, until a step change due to completion.

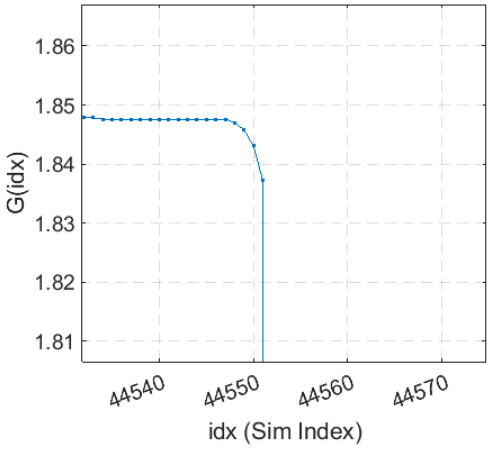

(b) Modelled decreasing Ohmic conductance due to a filament thinning (due to electromigration caused by excessive current), until a step change due to filament breakage.

Figure 3.11 Total conductance changing over time demonstrated in the multistep switching model, for 5-step switching. When a filament is growing as in (a), the conductance increases in gradually increasing increments until a sharp change at completion. When a filament is thinning as in (b), the conductance decreases in gradually increasing increments until a sharp change at completion. This is the expected behaviour; this shows that the switching model works as intended.

The model parameters that produced a conductance trend that is most similar to the experimental measurements were P_{up} 0.06% and P_{down} 0.20%. These results, shown in Figure 3.12, are an example of the closest resemblance to the experimental data achieved using the multistep model, and are referred to as the 'best match' results (Section 1.2.1) of the multistep model. These results show that the effect of the multiple-step switching process with no other changes applied is to extend the time for switching equally for all switches. This does not change the IEI distribution, nor does it cause correlation between switching events. Thus, the 6-panel plot in Figure 3.12 does not show the key characteristic behaviour observed in the experimental device, and therefore the multistep model is not an improvement on the base model.

The plots in Figure 3.13 show the IEI behaviour for 1-step, 2-step, 5-step, and 10-step switching processes in the multistep model while keeping all other simulation parameters unchanged. It is obvious that even the 10-step process does not have a significant effect on the IEI distribution, other than to slightly reduce the number

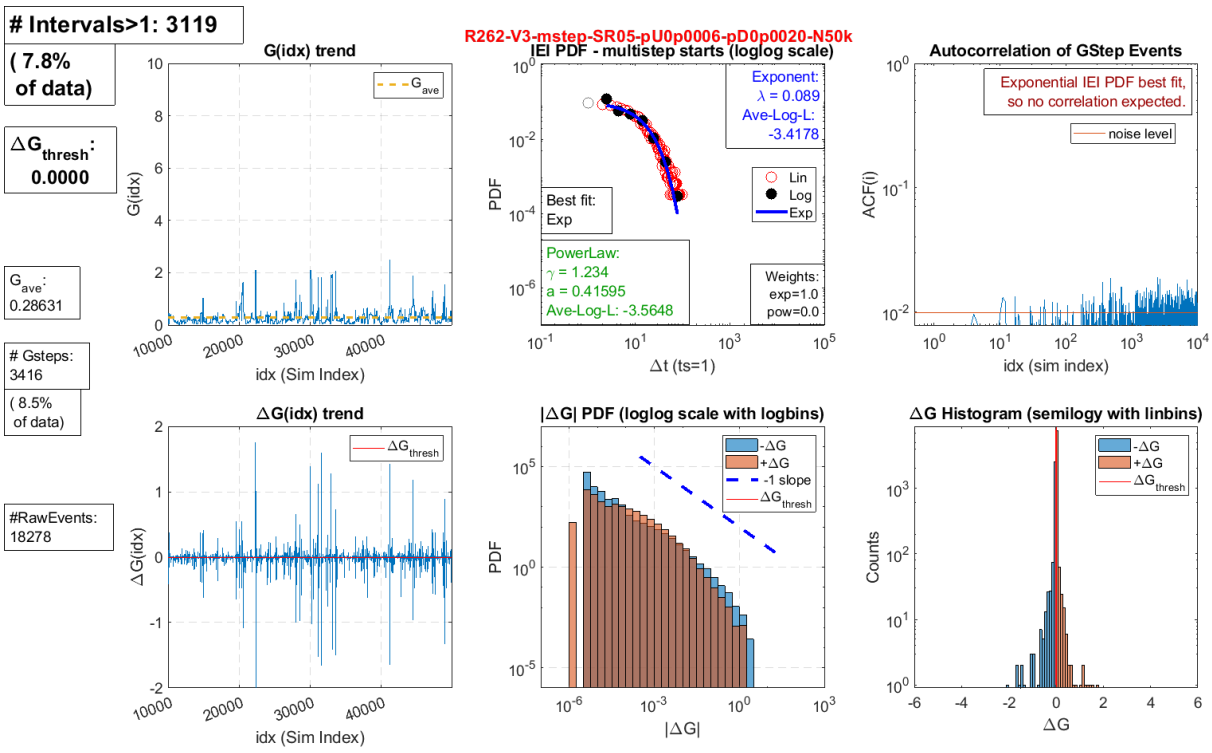

Figure 3.12 A six-panel plot showing results of the multistep model that were most similar to the experiment, for: 5-step switching; P_{up} 0.06%; P_{down} 0.20%. Note the curved appearance of the trend in the IEI plot, and the lack of trend in the autocorrelation – it does not show improvement over the base model.

of times that switching events happen in the simulation. The insensitivity of the IEI behaviour can be explained by the following argument. The switches that have electric field or current exceeding the corresponding thresholds on each time-step can be thought of as being a set of candidates for switching. While any switch is in the process of switching, it is excluded from the set of candidates. Since the model uses fixed probabilities for switching, switching on average occurs on a fixed percentage of the set of candidates. Since the multistep model effectively reduces the set of candidates by delaying switching, the overall effect of multistep switching is that the number of switching events is reduced. Next, in Section 3.3, the addition of electric field and current dependent switching probability to the base and multistep models is explored.

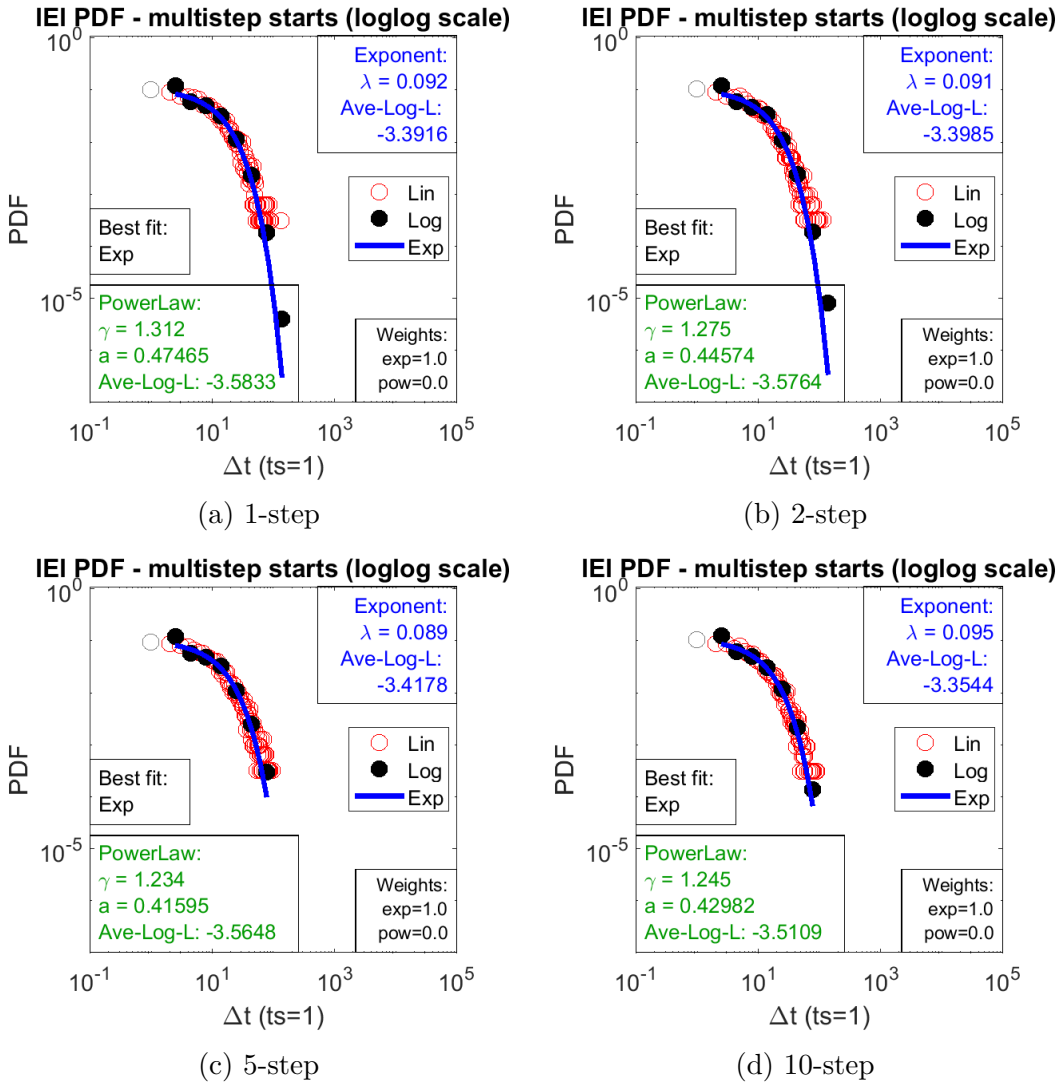

Figure 3.13 IEI PDF loglog plots of one simulation repeated for 4 different choices of number of time-steps per switching process. 1-step switching behaves identically to the base switching model. The simulations used seed 262, 3 V, 0.06% switch up probability and 0.20% switch down probability.

3.3 ELECTRIC FIELD AND CURRENT DEPENDENT SWITCHING PROBABILITY

Recall that in the base model (described in Sections 1.1.4 and 3.1.1), the probability of a switching up event is independent of the extent by which the electric field across a junction exceeds the electric field threshold. The same applies for the probability of a switching down event, in terms of the current. In contrast, in the model described in this section, the probability of switching is no longer constant but instead varies according to the electric field and current.

The probability of a switching junction in the tunnel gap state switching up into the filament state is now determined by the extent that its electric field exceeds the electric field threshold, linearly increasing up to a maximum probability of 0.50. Similarly, the probability of a switching junction in the filament state switching down into the tunnel gap state is now determined by the extent that its current exceeds the current threshold, linearly increasing up to a maximum probability of 0.50.

Section 3.3.1 covers why electric field and current dependent probability (**EI-dependent P**) was explored. Section 3.3.2 provides details of the implementation and physical concepts. Finally, Section 3.3.3 discusses the results of some simulations using the EI-dependent P switching model.

3.3.1 Motivation for developing this model

One of the goals of the simulation is to demonstrate similar statistics in the simulated switching events to those observed in the experimental device (Section 1.2.1), including the distribution of IEIs, which show a power law behaviour over several decades (Section 1.1.2), indicating the presence of correlations between the events.

The results of simulations using the base model and the multistep model both show IEI behaviour that is consistent with an exponential law distribution. This indicates that there is no correlation between the switching events in those models, and is consistent with the behaviour of independent random events [21].

Switching events are changes in conductance, which necessarily also change the current and electric field distribution on the simulated board. Based on this, it was conjectured that making the probability of events depend on the currents and electric fields may yield some correlation between events, and may also result in IEI behaviour more consistent with a power law distribution. This is the hypothesis underpinning this new switching model.

3.3.2 Physical concepts and implementation details

The core concept of the EI-dependent P model is varying the switching probabilities dynamically with changes in network conditions caused by previous switching events. This is achieved by making the probabilities depend on the electric field strength for tunnel gaps switching up, and depend on the current for filaments switching down. This is justified by considering how electric field strength and current may influence physical filament growth and thinning.

If a gap has sufficiently high electric field strength to grow a filament, it seems reasonable that an increased electric field would result in more rapid filament growth. This is consistent with findings of Yang et al. [14] that show the growth rate of filaments can increase with electric field. Similarly, if a filament has sufficient current to slowly thin until breakage [29, 30], it seems reasonable that increased current would result in more rapid filament thinning. These increased rates of growth and destruction are represented in this model using increased probabilities of switching up and down.

For each switching junction, the probability of switching is calculated based on the current or electric field. The 'switching up' probability ($P_{up}(E)$) of each switching junction that is in the tunnel gap state is calculated using the electric field, according to Equation (3.4). The relationship of the switching up probability with respect to the electric field is shown in Figure 3.14, where a general case is shown with a linear scale horizontal axis to emphasise that the probability varies linearly in the ramp region. The relationship is also shown in Figure 3.15 for an example with a logarithmic scale horizontal axis to emphasise that E_R (short for electric field range) is typically chosen to be several orders of magnitude higher than E_T.

$$P_{up}(E) = \begin{cases} 0.0, & \text{if } E < E_T \\ P_{up,base} + (E - E_T)\frac{(0.5 - P_{up,base})}{E_R}, & \text{if } E_T \leq E \leq E_T + E_R \\ 0.5, & \text{if } E \geq E_T + E_R \\ P_{up,base}, & \text{if } E_R = 0 \text{ (special case),} \\ & \text{and } E \geq E_T \end{cases} \tag{3.4}$$

The 'switching down' probability ($P_{down}(I)$) of each switching junction that is in the filament state is calculated using the current, according to Equation (3.5). The relationship of the switching down probability with respect to the current is shown in Figure 3.16 where a general case is shown with a linear scale horizontal axis to emphasise that the probability varies linearly in the ramp region. The relationship is also shown in Figure 3.17 for an example with a logarithmic scale horizontal axis to emphasise that I_R (short for current range) is typically chosen to be several orders of

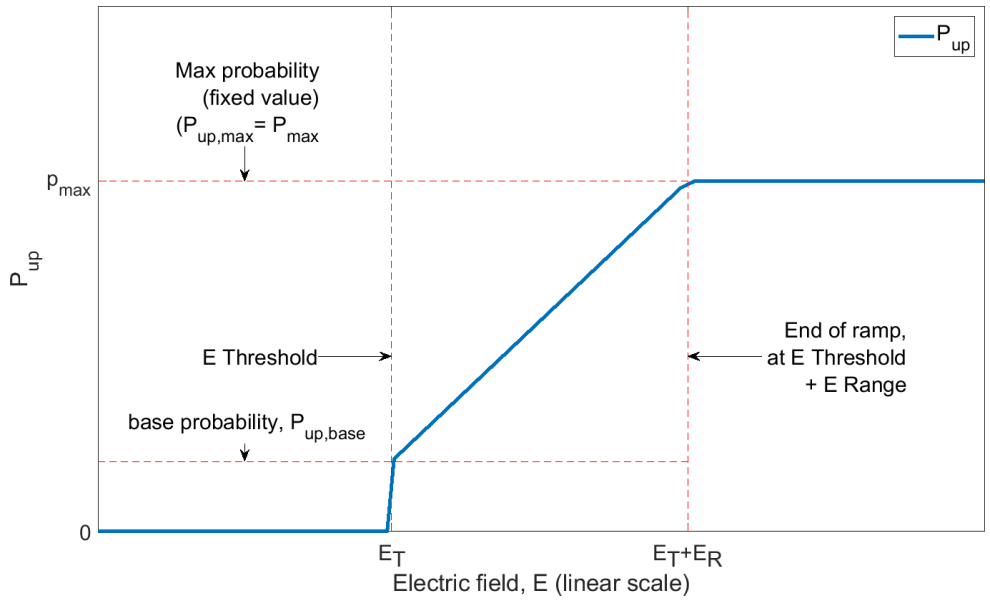

Figure 3.14 A cartoon of the general form of the relationship of the switch up probability (from tunnel gap up to filament) to electric field.

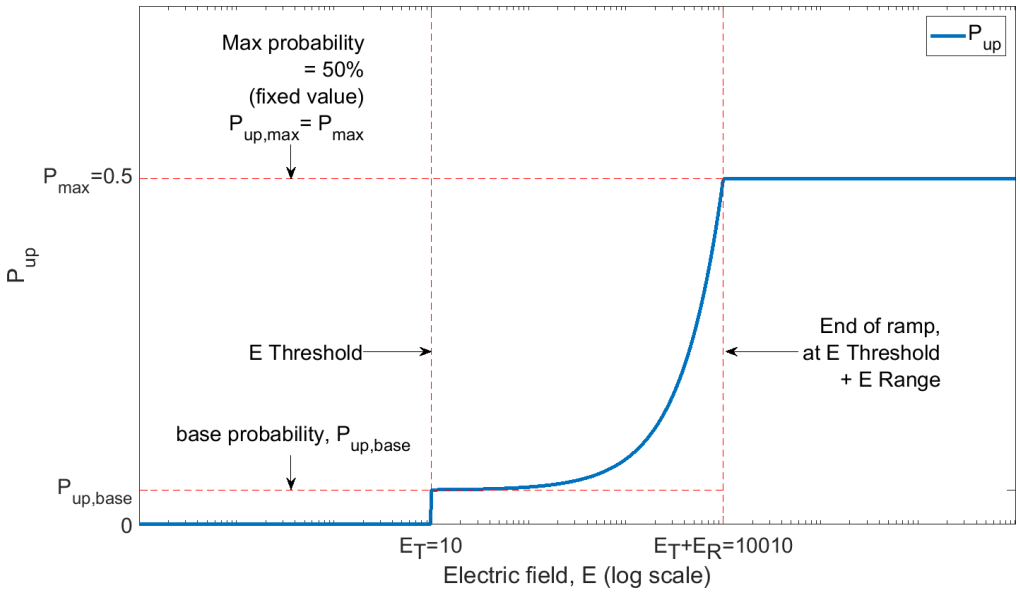

Figure 3.15 A plot of switch up probability (from tunnel gap up to filament) relative to electric field. Note that the probability increases linearly with electric field.

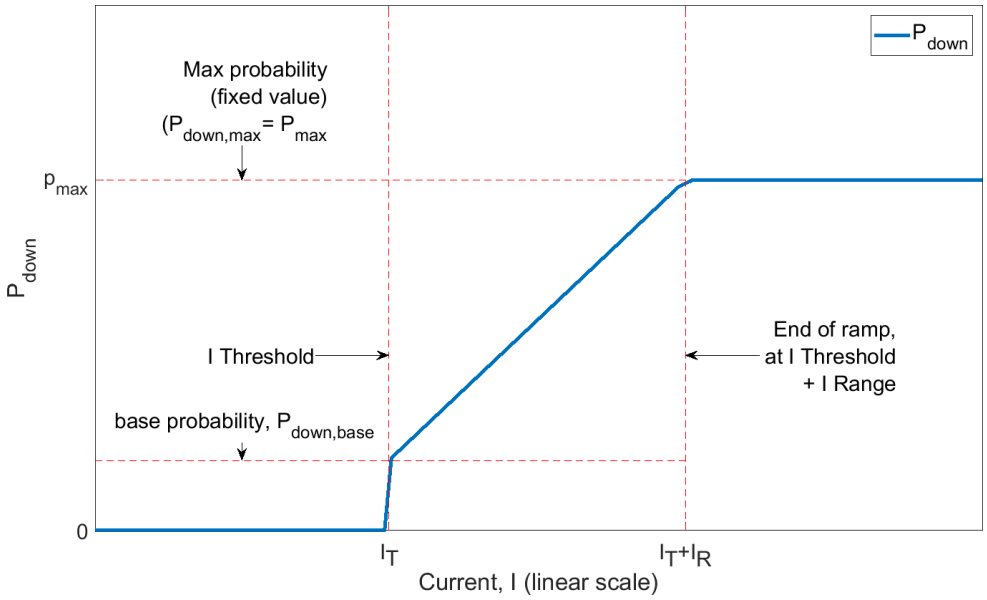

Figure 3.16 A cartoon of the general form of the relationship of the switch down probability (from filament down to tunnel gap) to current.

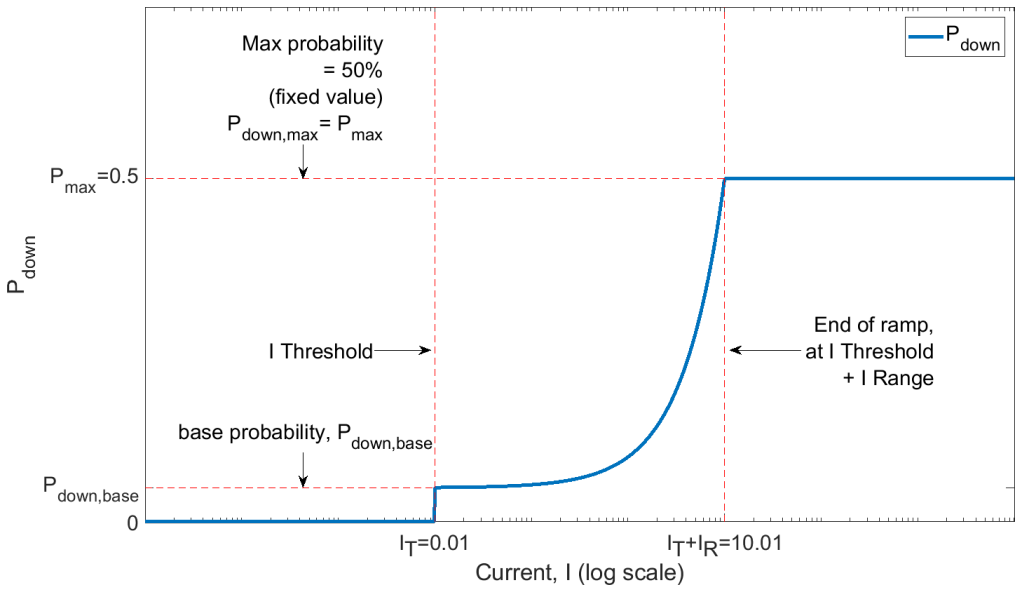

Figure 3.17 A plot of switch down probability (from filament down to tunnel gap) relative to current. Note that the probability increases linearly with current.

magnitude higher than I_T.

$$P_{down}(I) = \begin{cases} 0.0, & \text{if } I < I_T \\ P_{down,base} + (I - I_T)\frac{(0.5 - P_{down,base})}{I_R}, & \text{if } I_T \leq I \leq I_T + I_R \\ 0.5, & \text{if } I \geq I_T + I_R \\ P_{down,base}, & \text{if } I_R = 0 \text{ (special case),} \\ & \text{and } I \geq I_T \end{cases} \tag{3.5}$$

The probability varies in the same way for switching up or down. The probability is zero below the threshold, steps up to a base value at the threshold, ramps up linearly until the probability reaches a maximum value. Including the base probability value allows this model to mimic the base model, in terms of the probability of switching at the threshold.

As described above, the probability of switching increases linearly as a ramp, shown in Figures 3.14 and 3.16. The slope of the ramp is defined in Equations (3.4) and (3.5), as $\frac{P_{up,base}}{E_R}$ for the switching up probability and $\frac{P_{down,base}}{I_R}$ for the switching down probability. The exception to that is when the denominator (E_R or I_R) is 0, in which case the slope is 0 and the probability is constant and equal to the base probability value.

The maximum probability for switching up or switching down is set to 0.50. This means that the minimum possible expected switching time for any switch is two time-steps. This was considered appropriate since the simulation time is limited to discrete values.

3.3.3 Results

The behaviour of the electric field and current dependent probability model is summarised with a few example simulations shown and discussed below.

Example results of closest resemblance to the experimental data, when using the EI-Dependent model, are shown in Figure 3.18. These 'best match' results (Section 1.2.1) were produced by selecting simulation parameters that produced a G(idx) trend that is similar to the experimental measurements in terms of the number of step change events and the general shape. The base model baseline example (Figure 3.1) was used as a template for selecting these parameters. The effect of the electric field and current dependence is to increase the switching probabilities, so the base switching probabilities were reduced to half, thereby reducing the switching activity. Specifically, $P_{up,base}$ and $P_{down,base}$ were set to 0.03% and 0.10%, respectively.

The electric field and current dependence parameters, E_R and I_R, were set such that the reduction in base probabilities was compensated for. The effects of these

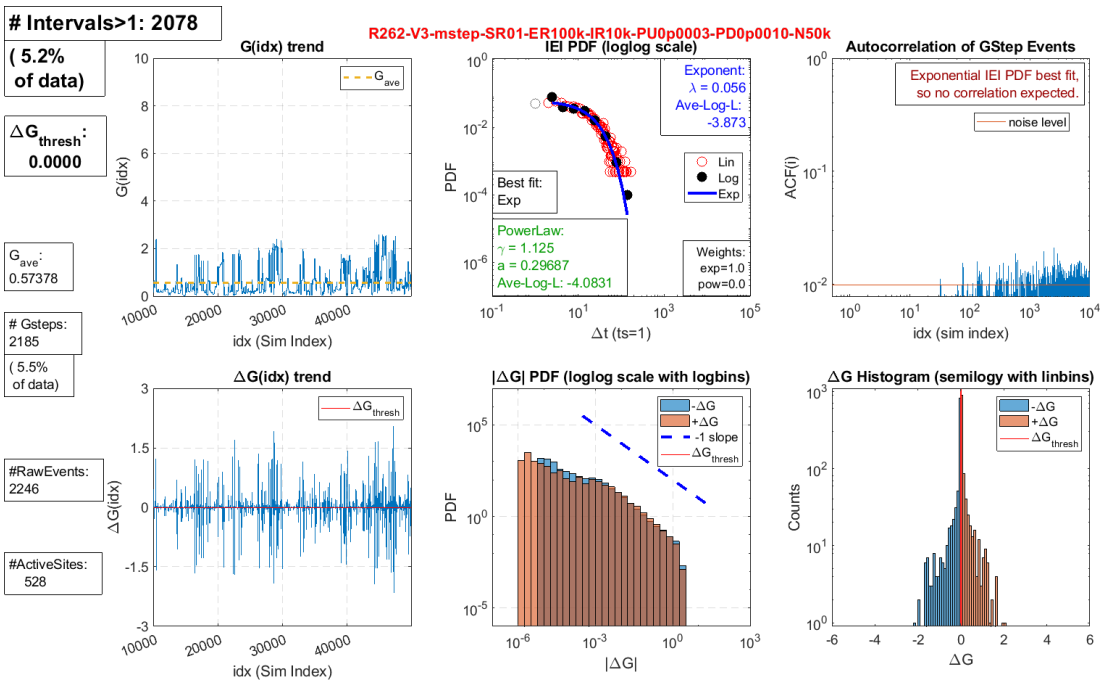

Figure 3.18 A six-panel plot showing the analysis results of the best match EI-Dependent P simulation. These results were produced using lower switching probabilities than in the best match base model results, and using weak dependence parameters in the electric field and current dependent probability model.

parameters are inversely proportional to their value, so large values were necessary to avoid increasing the probabilities by too much. Lowering E_R tends to increase the conductance and lowering I_R tends to decrease the conductance, so the ratio of the two parameters was set such that the conductance trend was similar to that of the experimental measurements. Specifically, E_R and I_R were set to 100k and 10k, respectively. These statements about the effects of E_R and I_R are supported by examples below, and overall, it was found that there is very little difference between the electric field and current dependent model behaviour and that of the base model. This conclusion is supported by further examples below.

As mentioned earlier in this section, and as explained in the implementation section, E_R and I_R act inversely on the effective up and down switching rates respectively, so larger values of E_R and I_R result in lower rates. This is demonstrated here with three examples of changes relative to the simulation producing the behaviour shown in Figure 3.18: the effect of a decrease in E_R; the effect of a decrease in I_R; and finally, the effect of a decrease in both E_R and I_R.

Decreasing E_R increases the dependence of the switching up probability on the electric field strength. It effectively increases the number of switching up events that occur during a simulation, and hence increases the expected conductance and number of events. An example of this effect is demonstrated in the comparison of G(idx) trends in Figure 3.19, where Figure 3.19a shows the best matching behaviour, and Figure 3.19b

shows the effect of E_R set to half as much. The full 6-panel plot of the simulation with reduced E_R is in Appendix B, in Figure B.2.

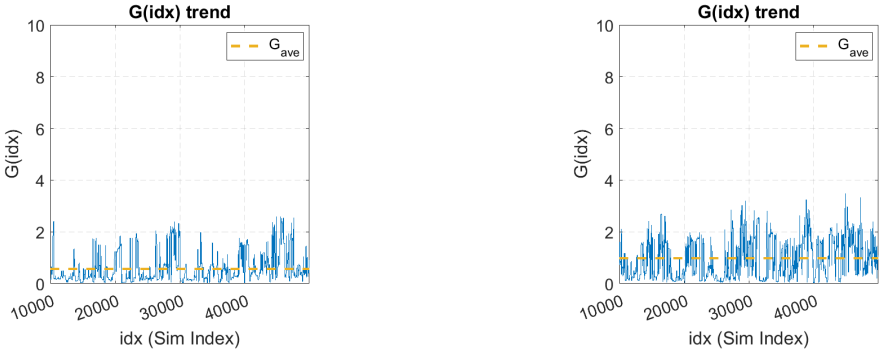

(a) Result best matching experiment.

(b) Result when E_R is reduced to half.

Figure 3.19 Comparison of the G(idx) trend plots for the best match EI-dependent probability model results with the results when using E_R reduced by half. The mean conductance increased from 0.57 to 0.97, and the number of step changes in G increased from 2185 to 2875. The maximum G(idx) increased from ∼2.5 to ∼3.5.

Decreasing I_R increases the dependence of the switching down probability on the current. It effectively increases the number of switching down events that occur during a simulation, and hence decreases the expected conductance but increases the number of events. An example of this effect is demonstrated in the comparison of G(idx) trends in Figure 3.20, where Figure 3.20a shows the best matching behaviour, and Figure 3.20b shows the effect of I_R set to one tenth as much. The full 6-panel plot of the simulation with reduced I_R is in Appendix B, in Figure B.3.

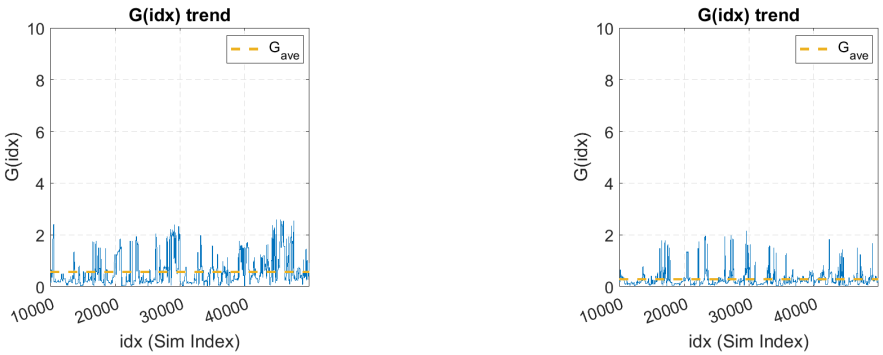

(a) Result best matching experiment.

(b) Result when I_R is reduced to a tenth.

Figure 3.20 Comparison of the G(idx) trend plots for the best match EI-dependent probability model results with the results when using I_R reduced to one tenth. The mean conductance decreased from 0.57 to 0.28, and the number of step changes in G increased from 2185 to 2234. The maximum G(idx) decreased from ∼2.5 to ∼2.0.

Decreasing both E_R and I_R increases the dependence of the switching up probability on electric field, and the dependence of the switching down probability on current. It effectively increases the number of switching up events and the number of switching down events that occur during a simulation. The overall effect on the expected conductance

depends on the extent that each have been decreased, since the effects of E_R and I_R counteract in this regard. For example, setting E_R to one half and I_R to one tenth of the values used in Figure 3.18 resulted in minimal change in overall G(idx) while increasing the number of switching events that occurred. Plots of this data are in Appendix B, in Figure B.4 and Figure B.5.

To test that the model was increasing the switching probability, a simulation was run with $P_{up,base} = 0$ and $P_{down,base} = 0$. This simulation showed switching activity. The occurrence of switching despite 0% base switching probability is not sufficient to prove that the model works entirely as intended, but it does show that the probability of switching increases from the set base values with the electric field and current. The results of that simulation are shown in Figure B.6.

The electric field and current dependent model includes the features of the multi-step model, so it is possible to test the effect of switching processes that change conductance gradually over multiple time-steps while also varying the switching probabilities with the changes in electric fields and currents that result from those switching processes. An example of this is shown in the six-panel plot figure in Figure 3.21. In this figure, the IEI behaviour appears to follow an exponential law, and there is no evidence of correlation. This result suggests that even multi-step switching combined with electric field and current dependent switching probabilities is not sufficient to change the inherent lack of correlation between switching events seen in the behaviour of the base model simulation.

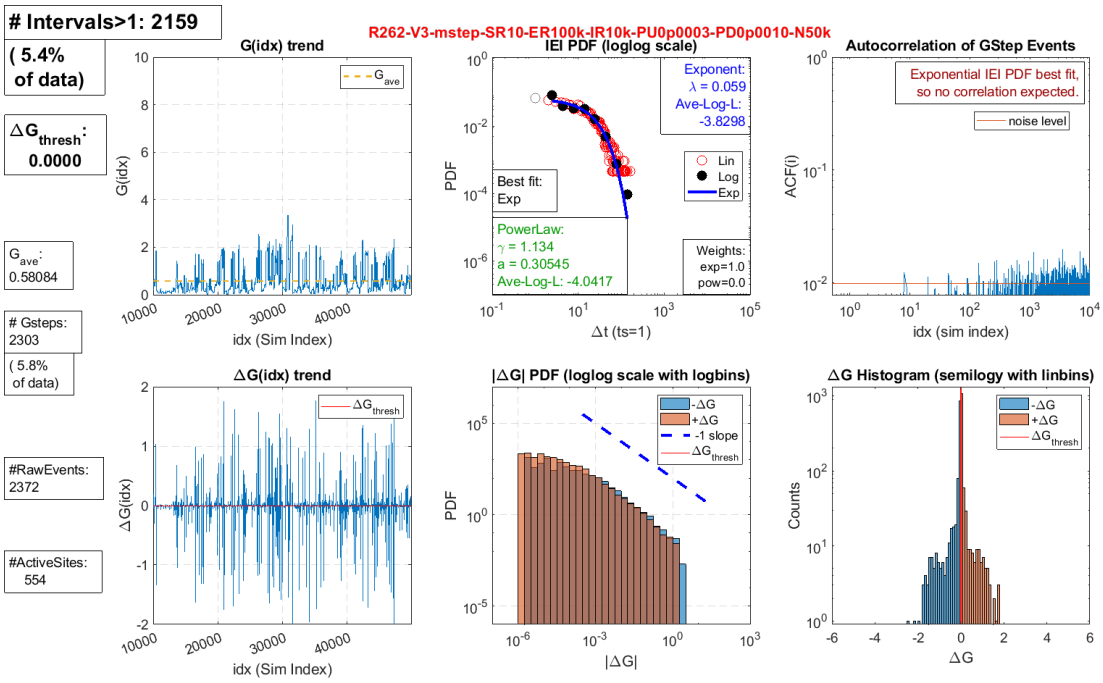

Figure 3.21 Six-panel plot results of the EI-dependent P model, with multistep switching included. E_R and I_R were set to the same values as for the best match results of this model (shown in Figure 3.18), the base probabilities $P_{up,base}$ and $P_{down,base}$ were set to 0.03% and 0.10%, and the duration of switching was set to 10 time-steps.

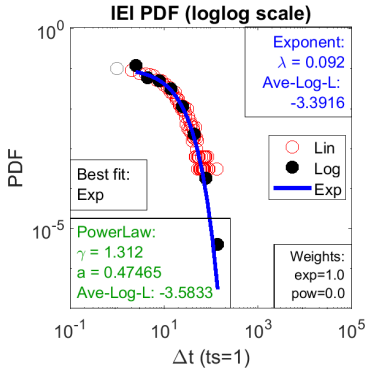

(a) IEI PDF plot from the best match base model results, for P_{up} and P_{down} of 0.06% and 0.20%.

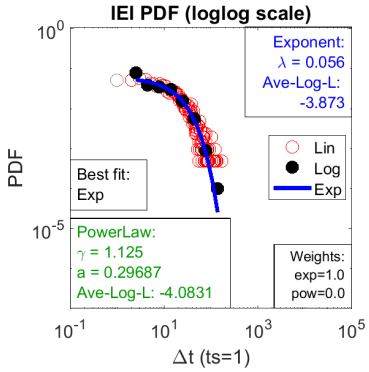

(b) IEI PDF plot from the best match EI-dependent P model results, for P_{up} and P_{down} of 0.03% and 0.10% and for E_R and I_R of 100k and 10k.

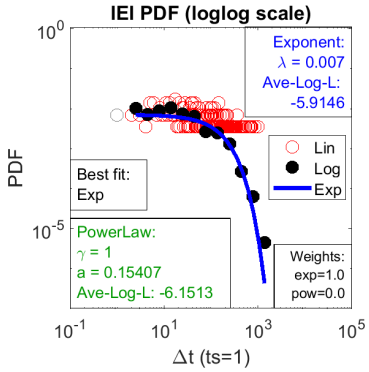

(c) IEI PDF plot from EI-dependent P model results for zero base probability, for E_R and I_R of 100k and 10k.

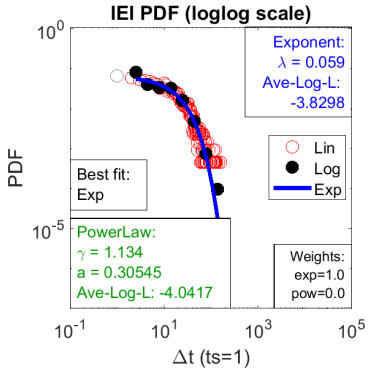

(d) IEI PDF plot from EI-dependent P model results for inclusion of 10-step switching, for P_{up} and P_{down} of 0.03% and 0.10% and for E_R and I_R of 100k and 10k.

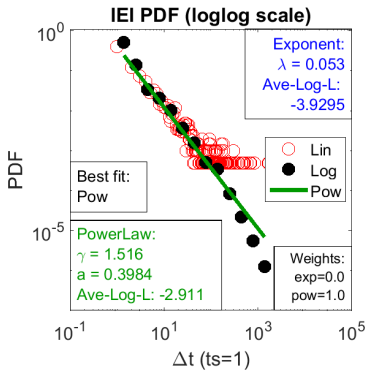

(e) IEI PDF plot from the example experimental results, shown in full in Figure 3.2.

Figure 3.22 Comparison of the IEI plots attained for the best match base model results, three different EI-dependent P model results, and the example experimental results. The EI-dependent P model results show the behaviour for non-zero base probability, zero base probability, and 10-step switching for non-zero base probability – quite different cases.

Finally, in Figure 3.22, the IEI plots from the results are shown together for comparison. There is negligible difference in IEI distribution between the base model and the EI-dependent P model, in terms of the consistent curved visual appearance in the IEI plots. In contrast, the visual appearance of experimental behaviour in the IEI plot is linear. The base and the EI-dependent P models both produce IEIs are that distributed in a manner consistent with an exponential law, while the experimental results are clearly consistent with a power law distribution. Based on comparisons of the experimental results, those of the base model, and those of the EI-dependent P model, it can be concluded that the EI-dependent P model does not produce behaviour that is satisfactorily similar to that of the experimental device. Furthermore, it can be concluded that the combined introduction of multiple time-step switching and variable probability has not resulted in any significant change in behaviour. In particular, the distribution of IEIs for the example EI-dependent P results shown in Figure 3.22b is qualitatively different to that of the experimental results in Figure 3.22e, and is similar to that of the base model shown in Figure 3.22a.

3.4 CONCLUSION

Analysis of the switching events in the simulations using probabilistic models shows no evidence of correlation. The development of new models without probabilistic switching was considered necessary, based on the results of this chapter. This development is presented in Chapter 4.

Chapter 4

DETERMINISTIC SWITCHING MODEL

The simulation using the base version probabilistic switching model showed some similarity in behaviour to that of the experimental device, but lacked key statistical properties - in particular, the simulated behaviour lacked a power law distribution of switching events and it also lacked correlation between switching events. The base model switching behaviour exhibits exponential decay in the IEI distributions, showing that events were uncorrelated, and is consistent with independent events [21]. This behaviour persisted in the new models presented in Chapter 3, showing that the changes made to the switching model were not sufficient to introduce correlations with probabilistic switching.

In pursuit of a simulation more representative of the device, the switching model was modified to be deterministic rather than probabilistic. The modifications made, and the resulting switching model, are discussed in this chapter. The general design of the model is discussed in Section 4.1. The concepts motivating this model are discussed further in Section 4.2, the details of the implementation are discussed in Section 4.3, and the resulting behaviour is presented in Section 4.4. In Section 4.5 a variant of the deterministic model is developed and presented along with results particular to that variant. In Section 4.6, the chapter is concluded.

4.1 INTRODUCTION

The probabilistic model used random probability to distribute events in time and space across the complex simulated network, to account for the stochastic nature of experimentally observed switching, and to account for different switching times in each tunnel gap given different local environments [8]. The best available theoretical model of the filament/tunnel gap switching phenomenon is not probabilistic. Given this, and given that thus far the probabilistic approach has not produced the sought-after behaviour, it is therefore logical to explore modelling the switching phenomenon as a deterministic process. The decision was made to remove probability from the switching model, and implement deterministic rules to govern the behaviour of the switching

junctions.

The design of the deterministic switching model was inspired by evidence of electric field dependent gradual filament growth [11], and also by observations made by the research group (to be submitted for publication) which show evidence of both growing and thinning filaments in the experimental device. In the new deterministic model, any tunnel gap with an electric field above the electric field threshold begins transitioning to a filament. The rate at which the transitioning progresses varies with the magnitude of electric field in that gap. Switching up occurs when the filament is completed (as depicted in Figure 4.1).

Once a filament is formed, if its current is above the current threshold it begins transitioning back to a tunnel gap. The rate at which a transitioning filament progresses varies with the magnitude of current in the filament. Switching down occurs when the filament is thinned completely (as depicted in Figure 4.2).

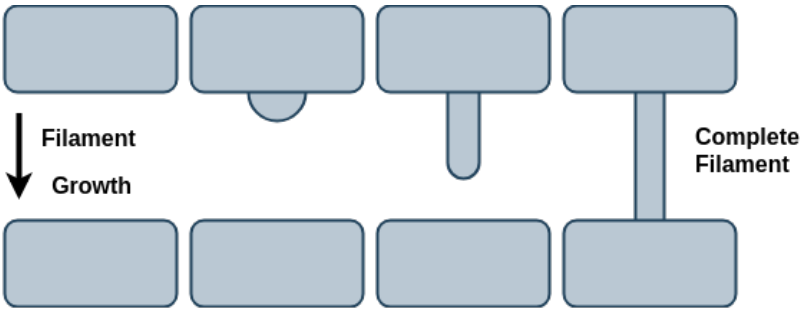

Figure 4.1 A representation of a filament growing longer in a gap, due to an electric field.

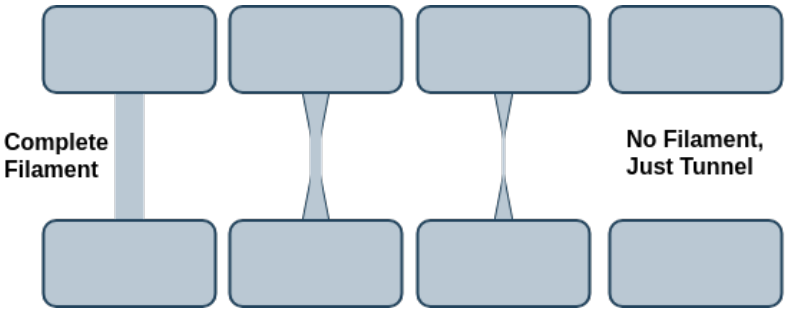

Figure 4.2 A representation of a completed filament thinning, due to current in the filament.

4.2 PHYSICAL CONCEPTS

The switching junctions have two distinct states, one with high conductance and one with low conductance, corresponding to the high conductance of an Ohmic filament and the low conductance of a tunnel gap, respectively. These will be referred to here as the **filament** and **tunnel gap** states. Transitions between the two states can be explained by considering observations of nanoscale filament phenomena. It is known

that nanoscale filaments can form in nanoscale gaps [14, 32]. It is also known that filaments can break [10, 30, 31, 33]. When filaments break, small gaps are produced. A small gap exhibits a low conductance due to tunnelling, which depends on the gap distance [15]. New experimental data (to be submitted for publication) show evidence of gradual (rather than instantaneous) changes between filament and tunnel gap states of elements in the experimental device. To allow for gradual changes, intermediate states of filament growth and breakage have been accounted for in the model.

Filament growth can be explained by electric field induced surface diffusion [34] or electric field induced evaporation [35]. A sufficiently strong electric field is required for any filament growth to occur [11, 34]. This is accounted for in the model by the electric field strength threshold, E_T. Stronger electric fields result in faster filament growth [14]. This gives the justification to make the filament growth rate increase with electric field strength in the deterministic model.

Electromigration is thought to be the dominant mechanism driving filament thinning and current driven atomic wire breaking [10, 26, 30, 31, 33]. The electromigration rate increases linearly with current density once a threshold current density has been met [36], which results in filament decay and eventual breakage. The deterministic model uses current and the current threshold, I_T, to account for the current density and threshold current density in this process. Research has shown that a nanofilament can thin and then break at a single point [30, 31]. For simplicity, the model uses the simplified approach of modelling complete filament removal, rather than modelling a constriction and breakage of a single point of the filament. The switching junction is thus able to behave the same during subsequent growing and thinning cycles, given the same conditions.

The multi-step model explored in Section 3.2 implemented growth and thinning of filaments using temporary modification of filament lengths. This variable filament length feature is used in the deterministic model to allow the switching junctions to partially transition in each time-step (as depicted for growing filaments in Figure 4.1 and as depicted for thinning filaments in Figure 4.2). Implementing partial switching per time-step is necessary for modelling slow and fast switching processes distinctly, as it allows individual switching junctions to transition over a different number of time-steps.

The electric field and current dependent probability model explored in Section 3.3 varied the probability of switching with the electric field and current in the switching junctions. This dependence is used in the deterministic model to locally determine the electromigration and filament growth rates. This allows the junctions to influence each other directly by changing the rates of growth/thinning on switching junctions that are in the process of switching.

4.3 IMPLEMENTATION DETAILS

While in the tunnel gap state, switching junctions each have a characteristic natural gap length, *Length*. This is the distance spanning the empty gap when no filament growth is present. As the filament grows, the effective gap length is gradually reduced from *Length* to zero . Once the effective gap length reaches zero, the switching junction enters the filament state.

In the filament state, the filament width is initially considered to be 1.0, and this width value is gradually reduced to zero as the filament thins on each time-step. Once the filament width reaches zero, the switching junction enters the tunnel gap state.

The rates of filament growth and filament thinning depend on the conditions of each switching junction. The incremental filament growth (gain in filament length) per time-step of a switching junction in the tunnel gap state is dependent on the strength of the electric field, E, in that switching junction gap. It also depends on the electric field threshold E_T, and on the electric field sensitivity range parameter E_R. For each time-step i, the change in effective gap length, Δd_i, for a switching junction in the gap state is calculated using

$$\Delta d_i = \begin{cases} (d_{max})^{\frac{(E_i - E_T)}{E_R}}, & \text{if } E_T \leq E_i \leq (E_T + E_R) \\ d_{max}, & \text{if } E_i > (E_T + E_R) \\ 0, & \text{otherwise} \end{cases} , \tag{4.1}$$

where d_{max} is the maximum allowable gap length for the model, first introduced in Section 1.1.3.

The remaining gap length in a tunnel gap is then updated according to

$$d_i = \begin{cases} Length & \text{if } i = 0 \\ d_{i-1} - \Delta d_i & \text{if } \Delta d_i < d_{i-1} \\ 0, & \text{otherwise} \end{cases} . \tag{4.2}$$

The electric field strength dependence of deterministic filament growth per time-step, as per Equation (4.1), is shown in Figure 4.3 for three values of E_R, and in Figure 4.4 for three values of E_T.

For a switching junction in the filament state, the incremental filament thinning (loss of filament width), per time-step, is dependent on the current, I, in that filament. It also depends on the current threshold I_T, and on the current sensitivity range parameter I_R. The variable w_i is introduced to represent the remaining filament width at time-step i. For each time-step i, the change in filament width, Δw_i, for a switching junction in

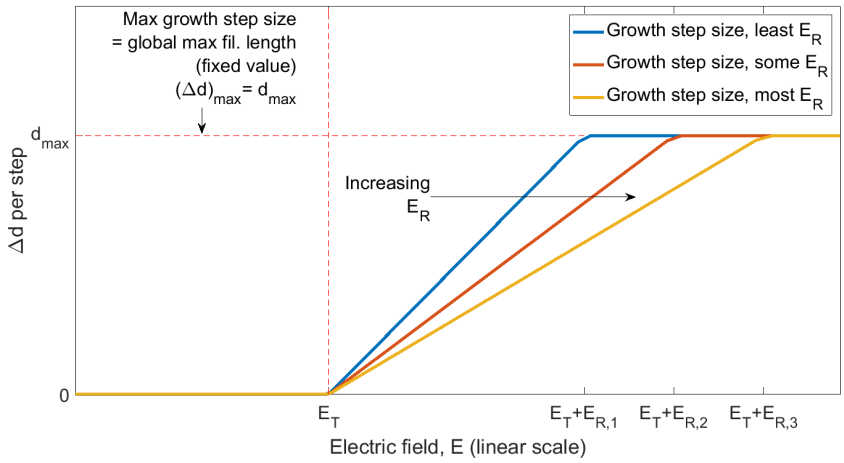

Figure 4.3 Deterministic growth per step due to E, for different E_R.

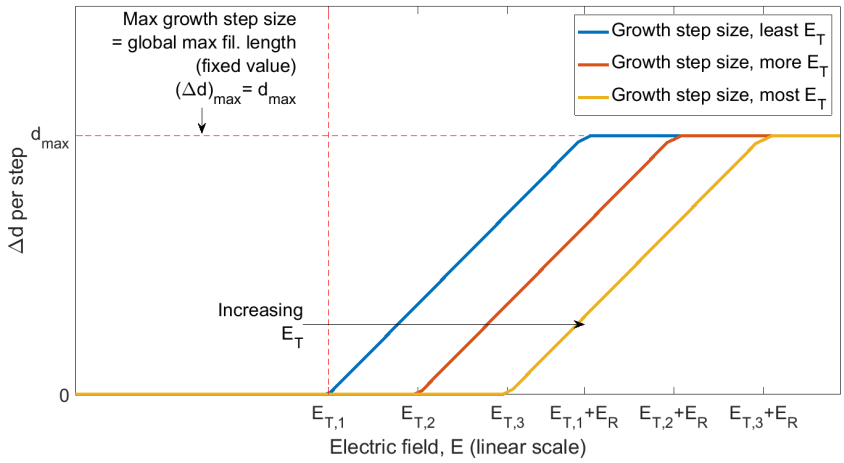

Figure 4.4 Deterministic growth per step due to E, for different E_T.

the filament state is calculated using

$$\Delta w_i = \begin{cases} (\Delta w_{\max})\frac{(I_i - I_T)}{I_R}, & \text{if } I_T \leq I_i \leq (I_T + I_R) \\ w_{max}, & \text{if } I_i > (I_T + I_R) \\ 0, & \text{otherwise} \end{cases}, \tag{4.3}$$

where Δw_{max} is defined as equal to the maximum allowable filament width for the model, 1.0.

The remaining filament width is then updated according to Equation (4.4). Once the remaining filament width reaches zero, the switching junction enters the tunnel gap state, with the gap length set to the characteristic natural *Length* of the gap once more.

$$w_i = \begin{cases} w_{max} & \text{if } i = 0 \\ w_{i-1} - \Delta w_i & \text{if } \Delta w_i < w_{i-1} \\ 0, & \text{otherwise} \end{cases} \tag{4.4}$$

The current dependence of deterministic filament thinning per time-step, as per Equation (4.3), is shown in Figure 4.5 for three values of I_R, and in Figure 4.6 for three values of I_T.

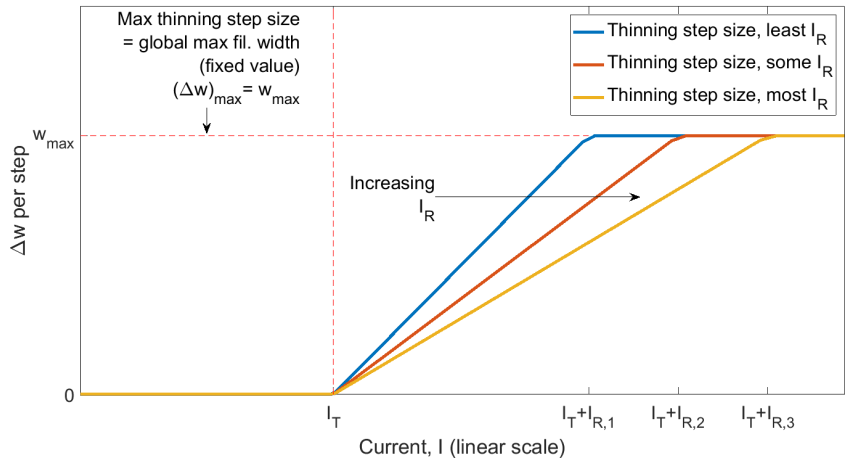

Figure 4.5 Deterministic thinning per step due to I, for different I_R.

There are two versions of the switching junction conductance model used in the deterministic switching model. The first version, based the original conductance model (Section 1.1.3), uses the filament state conductance $G_{filament} = G_{on}$, and the tunnel gap state conductance $G_{tunnel} = Ae^{-\beta d}$ with d set to *Length*.

The second version uses **creeping conductance**. Creeping conductance is defined here as a modelled conductance that changes gradually before switching up or down, as it does in the multistep model presented in Section 3.2. **Creep-up** refers to the conductance of a tunnel gap increasing as the gap length is reduced by a filament

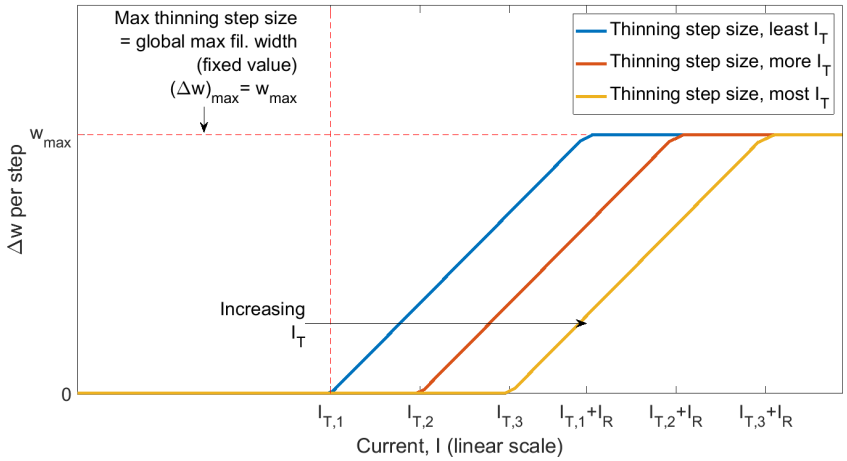

Figure 4.6 Deterministic thinning per step due to I, for different I_T.

growing in the gap. **Creep-down** refers to the conductance of a filament reducing as a filament thins during current induced decay. For simplicity, the version *without* creeping conductance has been the primary focus while investigating the behaviour of the deterministic model.

When in use, the creep-up conductance is calculated (as for tunnelling) using

$$G_{tunnel}(d_i) = Ae^{-\beta d_i} \quad , \tag{4.5}$$

where d_i is the changing effective gap distance as found in Equation (4.2).

When in use, the creep-down conductance is calculated by subtracting conductance loss ($G_{loss}(w_i)$) from the initial filament conductance (G_{on}) as shown in Equations (4.6) and (4.7), where w_i is the filament width as per Equation (4.4).

$$G_{filament}(w_i) = G_{on} - G_{loss}(w_i) \tag{4.6}$$

$$G_{loss}(w_i) = A\Big(e^{-\beta d_0} - e^{-\beta d_0(w_i/w_0)}\Big) \tag{4.7}$$

The conductance loss component (G_{loss}) of the creep-down conductance model is designed to increase exponentially with decreasing filament width, in a similar manner to the creep-up conductance. This is achieved by using the tunnel conductance model in Equation (1.1), for the initial gap distance ($d_0 = Length$) scaled by the filament width, w_i, at each time-step: $-Ae^{-\beta d_0(w_i/w_0)}$. This is offset by $Ae^{-\beta d_0}$ to ensure that $G_{loss}(w_0) = 0$. The overall effect of this conductance loss model is that during thinning the filament conductance decreases exponentially with decreasing filament width.

Examples of creeping conductances of a single switching junction, for a range of constant voltages, are shown below in Figure 4.7a and Figure 4.7b for creep-up and creep-down respectively. These figures demonstrate the behaviour described above: the

conductance of the switching junction increases exponentially (or creeps up) before completing the transition from tunnel gap to filament, and decreases exponentially (or creeps down) before completing the transition from filament to tunnel gap.

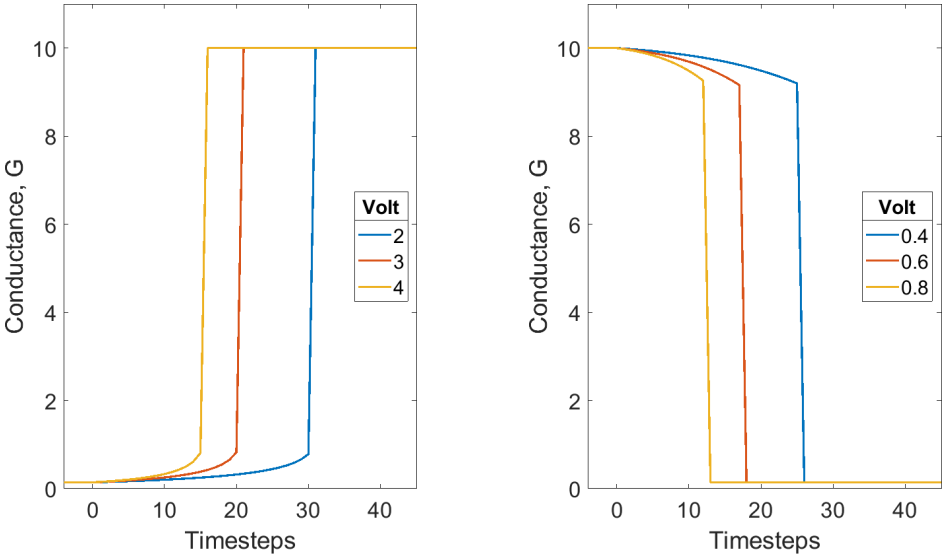

(a) A set of conductances during creep-up. (b) A set of conductances during creep-down.

Figure 4.7 Conductance creeping up and creeping down for an individual switching junction while (a) in the tunnel gap state, growing a filament in its gap and while (b) in the filament state, thinning a completed filament. The behaviour is shown for different voltages, indicated in the legend, applied directly to a single switching junction.

4.4 RESULTS

4.4.1 Results – no-creep conductance

In this section, the behaviour of the deterministic model, *without* creeping conductance included, is demonstrated with a few key examples. There is a small difference in the analysis of data for these examples, compared with Chapter 3. It was observed that, for many boards, this model shows an unusually high number of IEIs of 2 or 3 time-steps in duration. This resulted in outliers in the IEI data for some simulations, so only intervals greater than 3 time-steps were included in fitting models to the IEI data, to achieve consistent results. The points excluded from fitting are shown in the IEI plots as grey circles.

Figure 4.8 shows that the deterministic model can demonstrate conductance switching behaviour with a distribution of IEIs that appears linear in the IEI-PDF plot and is better fitted with a power law model than with an exponential law model. The simulation results also show some evidence of autocorrelation of the event times, as indicated by the response slowly decaying over several decades with a linear appearance. This is a significant improvement over the observed behaviour in all of the probabilistic

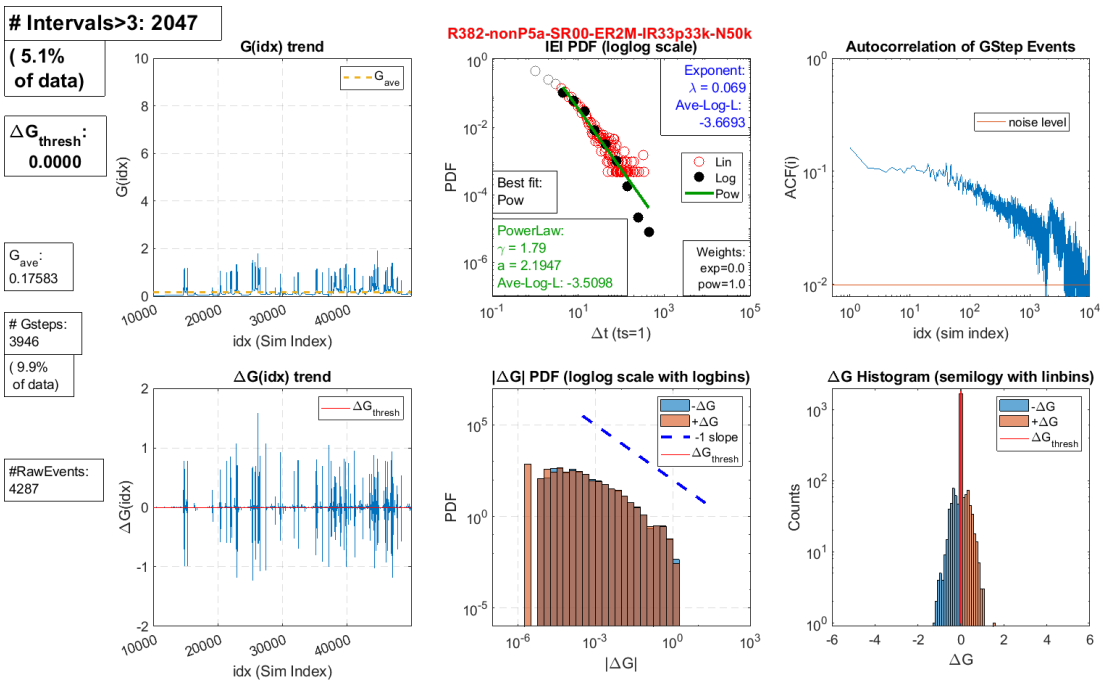

Figure 4.8 A six-panel plot showing analysis results of the best match deterministic model simulation (without creeping conductance). The relevant parameter values were: E_R 2M, I_R 33.33k, and random seed 382. Note the linear appearance of the IEI-PDF result, and the autocorrelation above the noise bound for several decades. This is significant improvement over the probabilistic models, which all had autocorrelation at or below the noise bound and curved IEI-PDF results.

models investigated in the Master's project.

As shown in Figure 4.9, increasing I_R (compared to the simulation with results shown in Figure 4.8) results in the simulated network exhibiting a higher mean conductance (G_{ave}) as well as higher instantaneous conductance. This is because increasing I_R inhibits switching down events, allowing the switching junctions to remain in the high conductance state longer and consequently results in a higher total network conductance. This increase in conductance appears to reach a new equilibrium: the higher conductance results in more current, which in turn encourages switching down events, thus counteracting the higher conductance. The increase in conductance is most visible after time-step 40 000 in Figure 4.9, at which point the lower bound of G(idx) has risen above the previous minimum.

The IEI-PDF in Figure 4.9 appears relatively linear, but the left-hand side of the autocorrelation trend has dropped in comparison with that shown in Figure 4.8. This result is typical of what is observed when parameter values are changed such that the lower bound of the conductance trend rises above the minimum; the observation applies to a greater extent in the next example.

As shown in Figure 4.10, decreasing E_R (compared to the simulation with results shown in Figure 4.9) results in the simulated network exhibiting a higher mean conductance, as well as higher instantaneous conductance. This is because increasing E_R

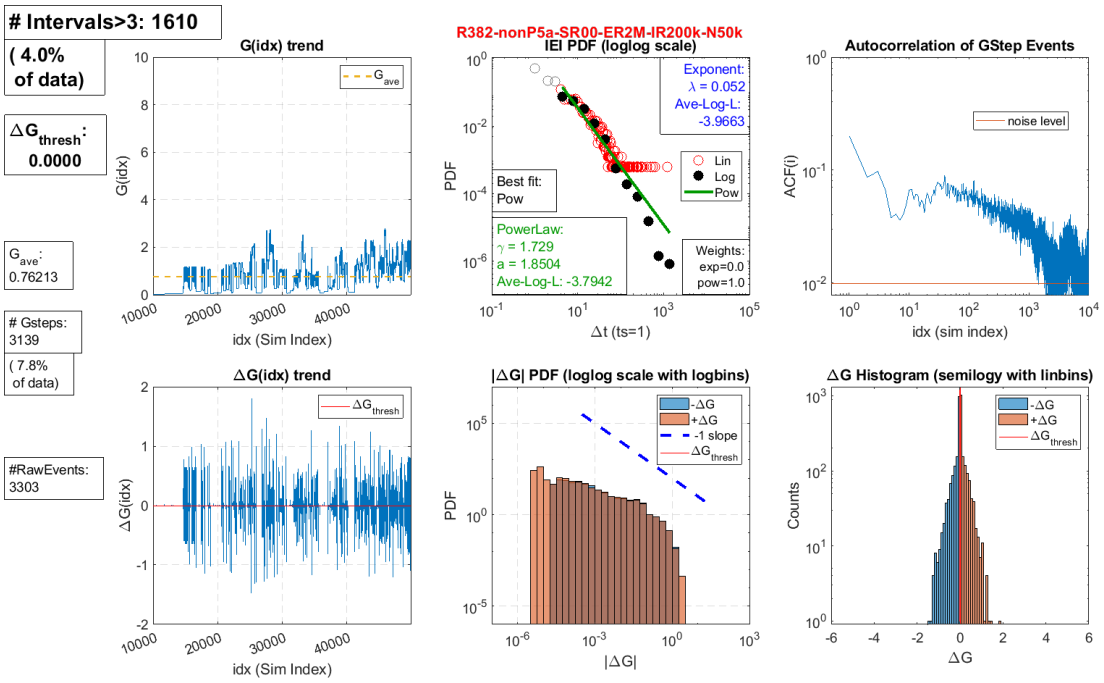

Figure 4.9 Here the I_R parameter is higher than for the simulation with results shown in Figure 4.8. Note that the result is an increased mean conductance. This is due to I_R inhibiting switching down events.

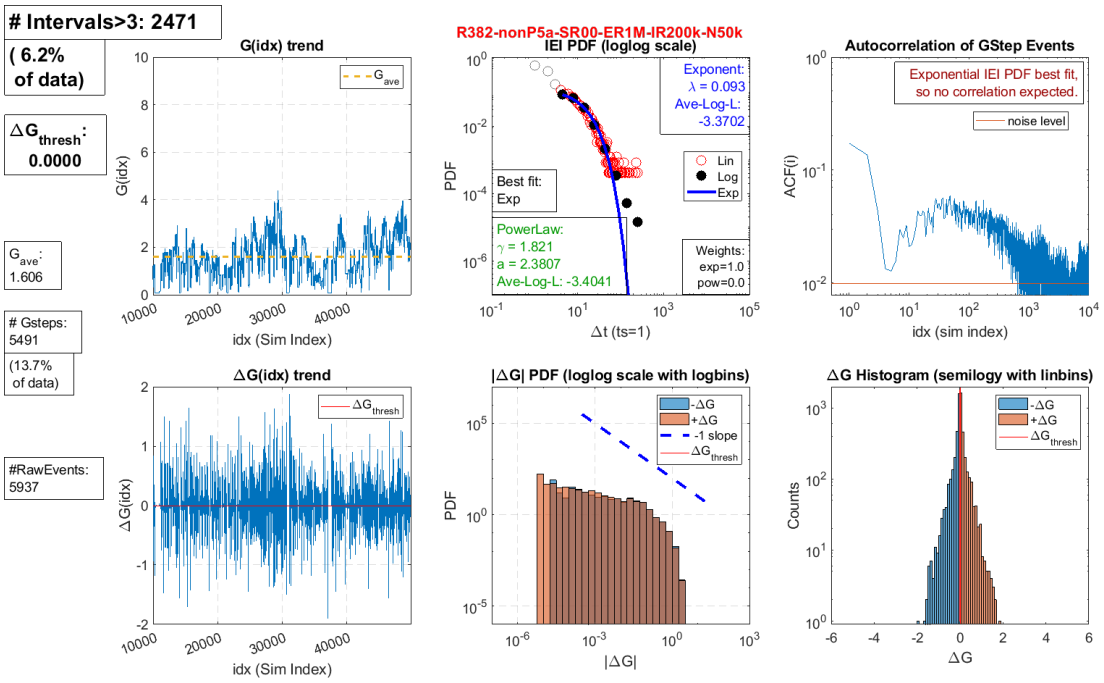

Figure 4.10 Here the E_R parameter is lower than for the simulation with results shown in Figure 4.9. Note that the result is an increased conductance. This is due to E_R inhibiting switching up events - lowering E_R results in more switching up events. It also worth noting that this combination of parameters has produced a G trend that is rising above the minimum, and an IEI PDF that is best fit with an exponential law model rather than with a power law model.

inhibits switching up events, so decreasing E_R allows the switching junctions to transition from the low conductance state to the high conductance state in fewer time-steps. This results in a higher total network conductance. As with increasing I_R, this increase in conductance appears to reach a new equilibrium: the higher conductance results in more current, which in turn encourages switching down events, thus counteracting the higher conductance. Overall, decreasing E_R tends to result in an increase in the number of events that occur during a simulation.

Note that the IEI-PDF in the top-middle subplot of Figure 4.10 shows that the best fitting model found in that case was the exponential law, rather than the power law. When this result is compared to Figures 4.8 and 4.9, it can be concluded that the choice of E_R and I_R can 'tune' the behaviour of the system through different regimes of behaviour. It has been observed that the regime most similar to the experimental results has a conductance trend briefly spiking upward from the minimum conductance, as seen in the results shown in Figure 4.8, rather than a conductance trend rising fully up from the minimum conductance level as shown in the example in Figure 4.10.

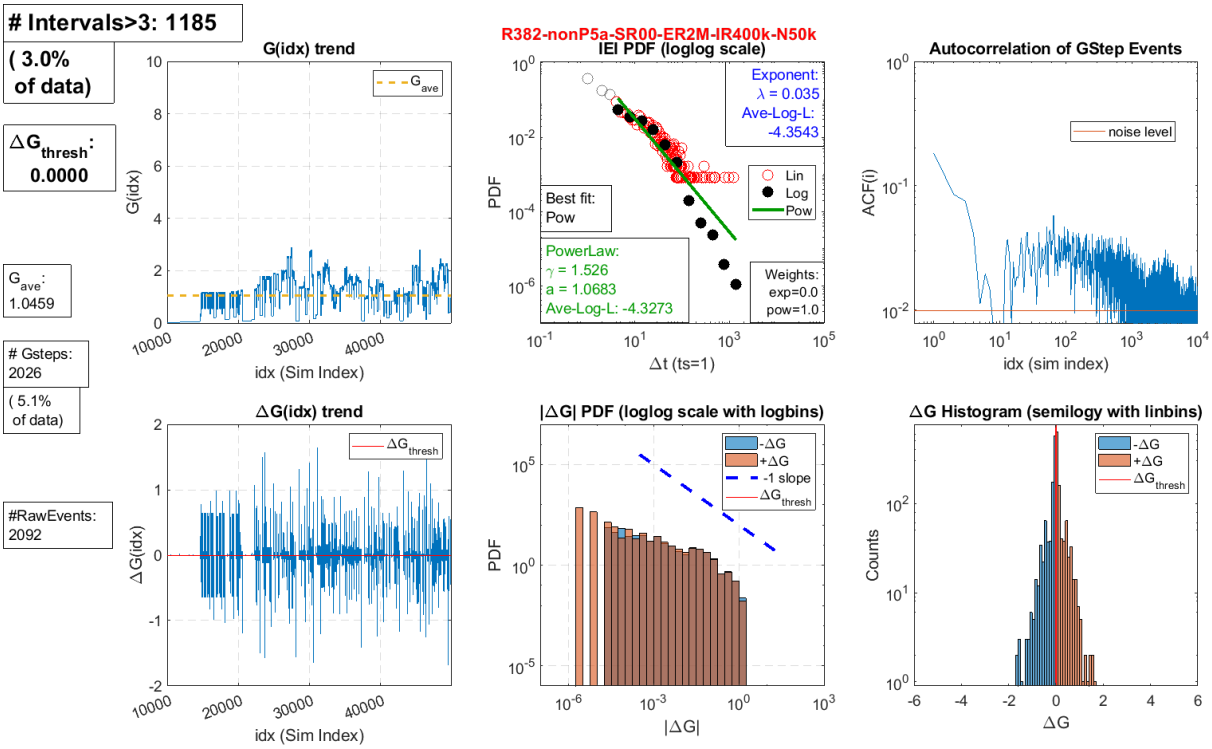

Figure 4.11 Here the E_R and I_R parameters are twice that of the simulation with results shown in Figure 4.10. The result is a mostly unchanged conductance trend, with a different time-scale. This is due to E_R and I_R both inhibiting switching events, resulting in all switching processes taking twice as many time-steps.

The previous examples showed the effect of changing just the E_R parameter or the I_R parameter. It is possible to change both the E_R and I_R parameters together. As shown in Figure 4.11, particularly when compared with Figure 4.10, scaling E_R and I_R together results in a time-scaling effect - the time between all events has been

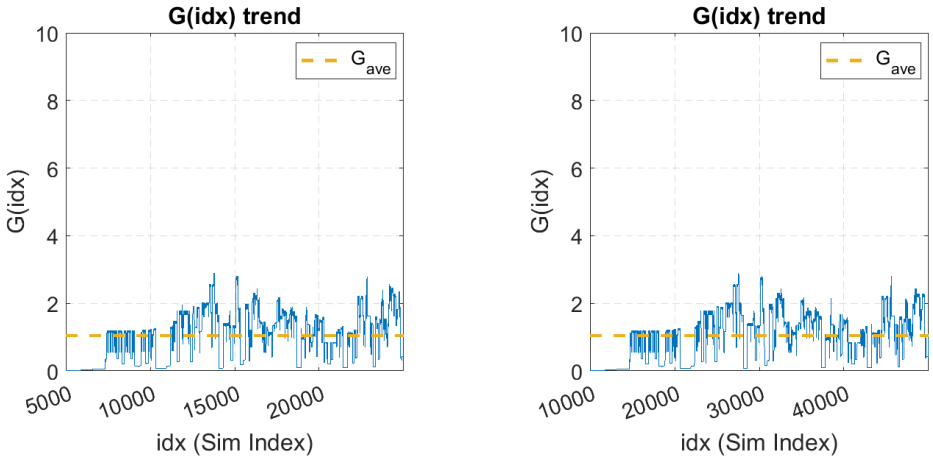

(a) Conductance trend for the fast case.

(b) Conductance trend for the slow case.

Figure 4.12 Fast and slow equivalents of a single series of events in two equivalent deterministic simulations. For the fast case in (a), the parameters used were E_R 1 M and I_R 200 k, for a time window from time-step 5000 to time-step 25 000. For the slow case in (b), the parameters used were E_R 2 M and I_R 400 k, for a time window from time-step 10 000 to time-step 50 000. All other parameters were the same for the two simulations. Comparing (a) and (b) shows that scaling E_R and I_R equally will result in an almost identical series of events, with the time between events scaled by the same factor. The parameters are scaled by a factor of two, and simulation time is effectively scaled by a factor of two. It is not quite identical because simultaneous events can be separated by slowing down activity, and their separation can lead to slight deviations in the series of events.

doubled. This is because doubling E_R causes switching up processes to take twice as many time-steps, and doubling I_R has the same effect on switching down effects.

Equally scaling E_R and I_R ensures that all of the events occur in the same sequence, with the exception that simultaneous switching events may separate into events on distinct time-steps. This can be seen clearly by comparing equivalent simulation time windows, such as from 5000 to 25 000 and from 10 000 to 50 000 in Figure 4.12. The two conductance trends appear to be identical despite one showing conductance data for twice as many time-steps. Careful inspection reveals subtle differences in the two plots, caused by small changes in the deterministic pattern of events as a consequence of time-scaling the simulation and resolving the events in discrete steps of simulation time. For example, if one switching process takes 2.5 time-steps and another takes 3 time-steps, the two switching junctions will both take 3 time-steps to switch, appearing to be simultaneous. If E_R and I_R are doubled, then those two switching junctions will take 5 and 6 time-steps, respectively.

4.4.2 Results – creeping conductance

This section briefly discusses the behaviour of the deterministic model when using creeping conductance, which causes switching junction conductance to change gradually between switching events. The implementation details of creeping conductance are discussed above in Section 4.3. For convenience, the conductance model without creeping conductance is referred to in this subsection as **simple conductance**.

In this subsection, analysis results of data from a creeping conductance deterministic simulation (shown in Figure 4.13), is compared with the analysis results of data from an equivalent simple conductance deterministic simulation, repeated from Figure 4.8. The two sets of results to be compared were both generated using E_R of 2 M and I_R of 33.33 k - the same dependence values used for the simple conductance deterministic result that best matched the experimental results, shown earlier in Figure 4.8. The plots, grouped in a different manner to aid the comparison, are presented in Figures 4.14 and 4.15 for convenience.

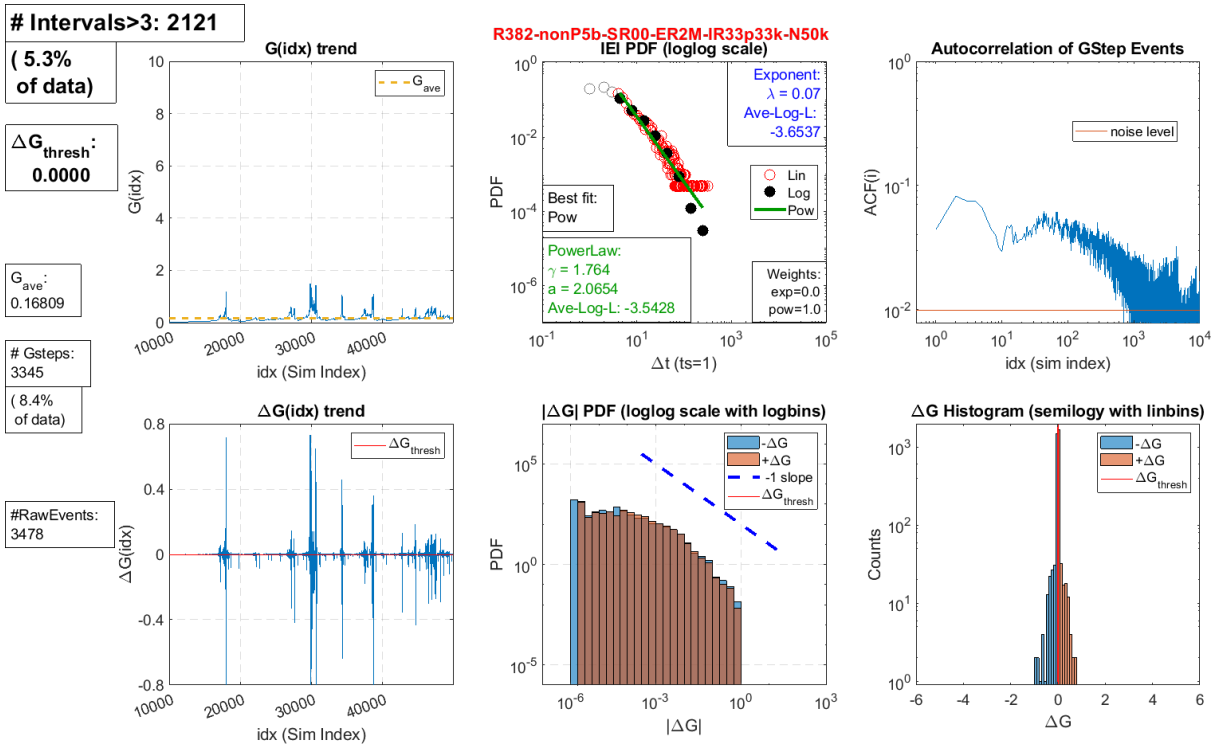

Figure 4.13 A six-panel plot showing analysis results of the deterministic model simulation, with creeping conductance, for the same parameter values used for the example in Figure 4.8. The relevant parameter values were: E_R 2M, I_R 33.33k, and random seed 382.

The G(idx), IEI, and ACF plots are compared in Figure 4.14. The G(idx) plot of the creeping result shown in Figure 4.14a demonstrates the expected behaviour of gradual increases in conductance before sharp increases, or 'spikes'. There are fewer 'spikes' shown in the creeping case, compared to the simple case shown in Figure 4.14d. The IEI plot of the creeping result shown in Figure 4.14b shows a distribution of intervals with

a linear appearance, like the simple case shown in Figure 4.14e. Qualitatively speaking, the two IEI plots are quite similar. Both sets of IEI data are better fit with a power law model than with an exponential law model. The autocorrelation trend has dropped and become more jagged in the creeping conductance model case, shown in Figure 4.14c, compared to the simple conductance model case, shown in Figure 4.14f. The creeping conductance model does not appear to produce long term correlation of the event times, i.e., the ACF trend does *not* appear linear over several decades, whereas for the simple case it does.

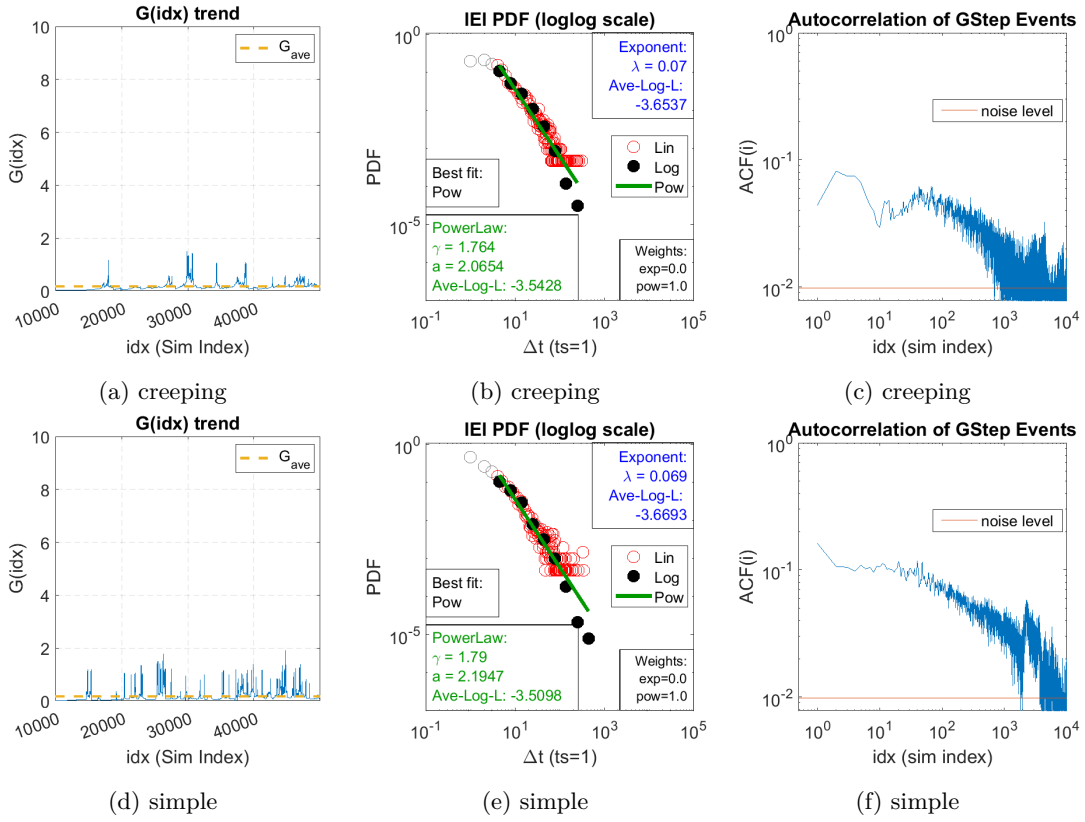

(a) creeping (b) creeping (c) creeping

(d) simple (e) simple (f) simple

Figure 4.14 Comparison of G, IEI, and ACF behaviour of simple conductance and creeping conductance deterministic models. As noted in the subfigure captions, the first row shows the behaviour for data from a simulation using the creeping conductance model while the second row shows the behaviour for data from a simulation using the simple conductance model. Both simulations used the set of parameters for the best matching result shown earlier in Figure 4.8 - E_R of 2 M and I_R of 33.33 k for seed 382.

The three types of ΔG plots are compared in Figure 4.15. The ΔG(idx) plot in Figure 4.15a, for the creeping conductance model, shows different grouping of change magnitudes compared to the ΔG(idx) for the simple model in Figure 4.15d. In the creeping case there are many fewer changes exceeding 0.5 in magnitude, and the changes appear to be grouped together. There is some similar grouping in the simple model case, but the changes are often larger in magnitude than in the creeping case. The histograms of $\|\Delta G\|$ and ΔG in Figures 4.15b, 4.15c, 4.15e and 4.15f are qualitatively similar, and are included for completeness.

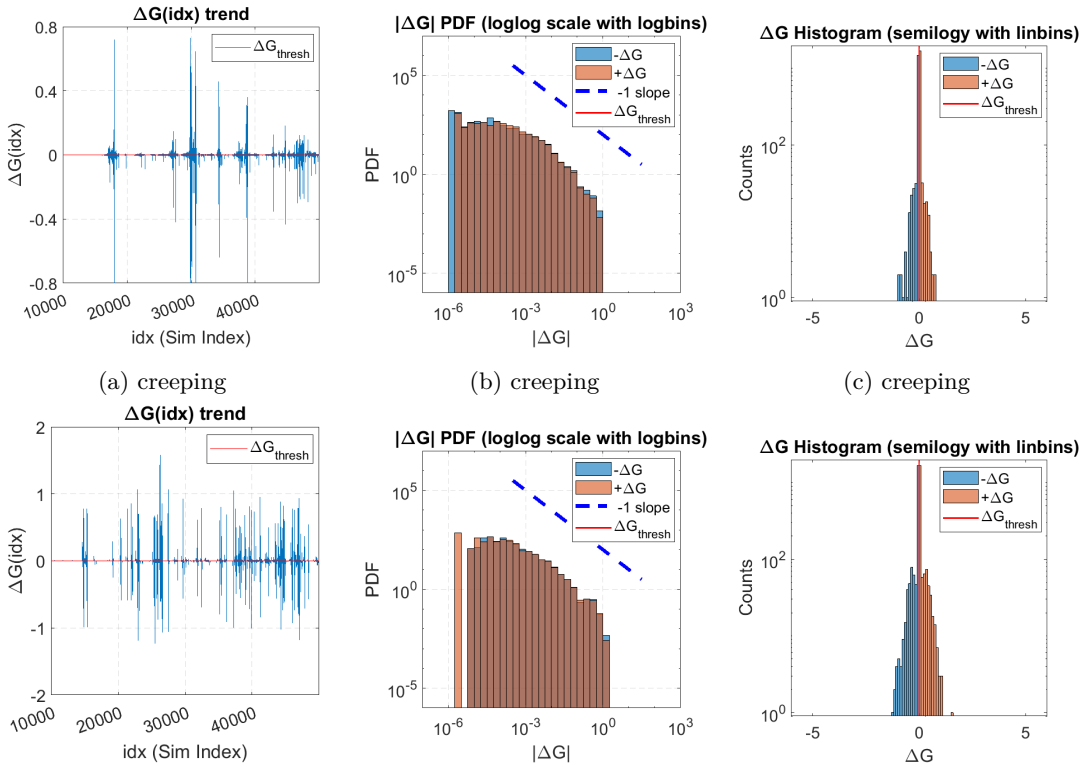

(a) creeping (b) creeping (c) creeping

(d) simple (e) simple (f) simple

Figure 4.15 Comparison of ΔG behaviour of simple conductance and creeping conductance deterministic models. As noted in the subfigure captions, the first row shows the behaviour for data from a simulation using the creeping conductance model while the second row shows the behaviour for data from a simulation using the simple conductance model. Both simulations used the set of parameters for the best matching result shown earlier in Figure 4.8 - E_R of 2 M and I_R of 33.33 k for seed 382.

The results shown here demonstrate that the creeping conductance deterministic model performs as expected in terms of its G(idx) behaviour. The G(idx) plots of the creeping conductance model show gradual changes, consistent with the observations for experimental data. Producing autocorrelation of switching event times that decays slowly over several decades (as observed in the experimental device behaviour) was a significant achievement of the deterministic model. The creeping conductance deterministic model shows lower autocorrelation than the simple conductance equivalent. This was considered reason enough to focus further investigation on the behaviour of the simple conductance deterministic model, despite some relative improvement in the appearance of the G(idx) and ΔG(idx) behaviour for the creeping conductance. Changes to the creeping conductance model that may produce better results are discussed as a topic of potential future work (Section 6.3), but are not explored further in the thesis.

4.5 LENGTH-DEPENDENT FILAMENT CHARACTERISTICS

In simulations with the deterministic model, high frequency switching behaviour was observed in some cases. The cause of this was discovered to be the existence of very small gaps. These junctions tended to transition between states much faster than other switching junctions. The rapid repetitive switching is present in the simulations shown in Figures 4.12a and 4.12b, but is more obvious when a specific example is focused on with a much expanded timescale, as shown in Figure 4.16.

This section discusses the issue, and explores a variant of the deterministic model that tested the use of length dependence in breaking filaments to mitigate it. The variant reduces the rate of filament thinning for short filaments. The implementation of this length dependent thinning rate is discussed in Section 4.5.2. This variant had the desired effect of slowing down the high frequency switching without greatly affecting the other components, but it produced undesirable IEI statistics and lowered autocorrelation. A single example is presented in Section 4.5.3 to illustrate this.

4.5.1 Motivation for introducing length dependence

In the deterministic model, the number of time-steps required for a switching junction to transition between the tunnel gap and filament states depends on the condition of the switching junction, as described in the discussion on implementing the deterministic model (Section 4.3). It is possible for a given switching junction in the tunnel gap state to have a strong electric field, and therefore transition to the filament state in a small number of time-steps. It is also possible that once in the filament state, that switching junction may immediately have a high current, and would therefore transition back to the tunnel gap state in a small number of time-steps. In this scenario, that switching junction would oscillate periodically between the tunnel gap and filament states. If this

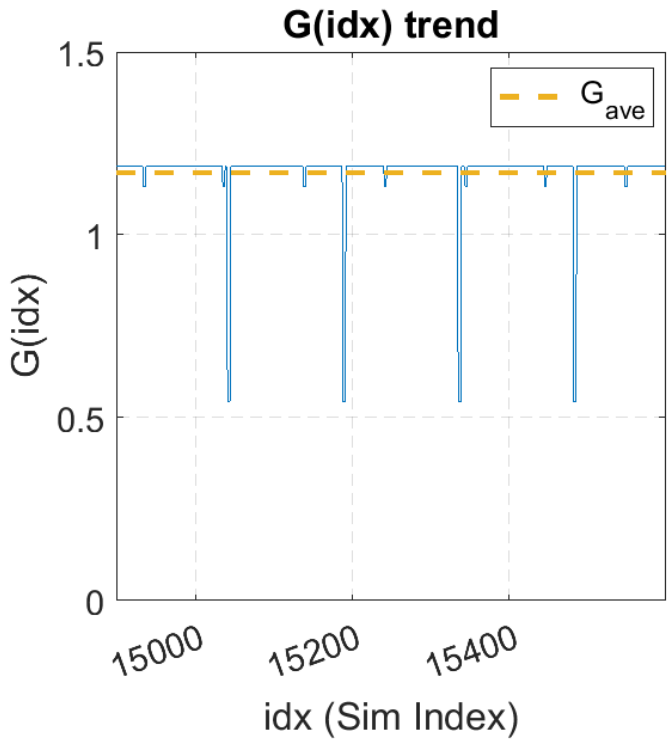

Figure 4.16 Zoomed in view of part the G(idx) for the deterministic simulation data shown in Figure 4.12b. Note that two periodic switching cycles are apparent here, resulting in a range of IEIs, but primarily short IEIs due to the brief down-then-up switching pattern.

oscillation was much faster than the activity of the other junctions in the network, then it would be visible in the G(idx) trend as periodic spikes.

An example of this behaviour is shown in the zoomed-in view of an example G(idx) in Figure 4.16. In this case, there are two cyclic switching processes visible, producing periodic spikes with different amplitudes and periods. The two periods of spikes produce a range of inter-event intervals between the up and down events. Note that the spikes are downward - the switching junctions are in the tunnel gap state for a short number of time-steps compared to the filament state, producing a consistent short interval between the down and up events. This is typical of observations of rapid cyclic switching in the deterministic model, and can produce outliers in the IEI plots. Examples of switching junctions producing this behaviour were investigated, and found to be among the smallest of all switching junctions in their networks in terms of gap length.

Switching junctions with small gap lengths tend to have high strength electric fields when in the tunnel gap state - a voltage across a small gap creates a strong electric field. A tunnel gap with a strong electric field will grow a filament quickly in terms of length grown per time-step. This quick growth combined with a small gap results in the complete growth of a filament in as little as one time-step. This explains why switching junctions with small gap lengths produce downward spiking cyclic switching.

This rapid cyclic switching of a small number of switching junctions is undesirable

because it makes it difficult to discern complex interactions between larger numbers of switching junctions in the network. One approach to dealing with rapid cyclic switching of small gaps is to inhibit the switching of small gaps in particular. This could be done by inhibiting the closing or the opening processes of switching junctions with small gap lengths.

4.5.2 Physical concepts and implementation details

The closing rate of a switching junction in the tunnel gap state in the deterministic model is dependent on the gap length of the switch for a given voltage - short gaps produce higher strength electric fields than long gaps. In contrast, the opening rate of a switching junction in the filament state in the deterministic model is independent of the filament - all filaments have the same conductance, so a given voltage will produce the same current and hence the same thinning rate in any switching junction that is in the filament state. Furthermore, all filaments start with the same width, so equal thinning rates lead to equal time-steps required to open the switching junction.

The switching junction opening process (as described in Section 4.3) lacks length dependence. In contrast, the closing process depends on electric field strength, so closing is accelerated in switching junctions with short gap lengths. Since closing already has length dependence, introducing length dependence into the opening process was explored as a method of inhibiting the cyclic switching observed in the deterministic model.

As has been discussed earlier (Section 4.2), research has shown that electromigration can cause filaments to constrict and then break at a single point [30, 31]. This mass transport is the basis of the filament thinning in the deterministic model.

Drift velocity due to electromigration increases with current density [36–39], and also increases with temperature [36–40]. For a given temperature and conductor geometry, there is a current density threshold below which no electromigration occurs [38]. This current density threshold decreases with increasing temperature [36, 39] and with increasing conductor length [36, 38]. It has also been shown that for fixed current density and temperature, there is a critical length of conductor below which electromigration will not occur at all [38, 41].

Electromigration is not the only process that may be driving mass transport in the filaments during thinning - thermal migration may also be acting in the material. Thermal migration is the diffusion of atoms on a negative temperature gradient. Both of these migration processes are driven by temperature and hence are affected by Joule heating [39].

From this information, it can be argued that a short filament will either not thin or will thin much slower than a long filament. A short filament will have a higher current density threshold than a long filament, will have less Joule heating due to lower

resistance, and will better conduct heat into the two clusters that the filament connects. In contrast, a long filament will have more Joule heating due to higher resistance and a lower current density threshold. The increased temperature due to Joule heating in a long filament will further decrease the current density threshold, cause thermal migration, and increase the drift velocity due to electromigration [39].

Temperature and a variable current density threshold are not considered in the deterministic model. Instead, the simulated filament thinning is driven by current with a fixed threshold. The addition of temperature and current density are areas for future work in further development of the simulation. It is clear from the above discussion that shorter filaments can be expected to thin slower than long filaments, so some form of length dependence is justified.

The following approach was used to implement length dependence. The filament width lost per time-step is scaled down according to the length of the filament, in such a way that the thinning of long filaments is unchanged while the thinning of short filaments is slowed. Equation (4.3) was modified to include the scaling factor $\left(\frac{Length}{d_{max}}\right)^n$, so the length dependent filament thinning per time-step was calculated using

$$\Delta w_i = \begin{cases} \left(\frac{Length}{d_{max}}\right)^n \left(\Delta w_{\max}\right)\left(\frac{I_i - I_T}{I_R}\right), & \text{if } I_T \leq I_i \leq (I_T + I_R) \\ \left(\frac{Length}{d_{max}}\right)^n w_{max}, & \text{if } I_i > (I_T + I_R) \\ 0, & \text{otherwise} \end{cases}, \tag{4.8}$$

where $Length$ is the characteristic length of the switching junction, d_{max} is the maximum length permitted in the simulation, and where the exponent n is defined as $\frac{S_R}{10}$ (reusing the multistep parameter S_R from Section 3.2.2 here as a tuning parameter to test different exponents).

In Equation (4.8), using the ratio of filament length ($Length$) and maximum filament length (d_{max}) as the base of $\left(\frac{Length}{d_{max}}\right)^n$ means that for long filaments (where $Length$ is close to d_{max}) the modifier will be close 1.0, and for short filaments (where length is close to 0) the modifier will be close to 0.0. The value of S_R controls the nature of the length dependence in terms of how sharply the rate modifier transitions from 1.0 to 0.0 with decreasing $Length$.

The length dependent thinning rate modification is designed to greatly reduce the filament width lost per time-step for very short filaments while not greatly affecting long filaments. The relationship of the scaling factor to the $\frac{Length}{d_{max}}$ ratio is demonstrated in Figure 4.17 for different values of S_R ranging from 1 to 50 (n from 0.1 to 5.0). The case of '$S_R = 1$' appears to be the most suitable value for producing the intended relationship: Figure 4.17 shows that $\left(\frac{Length}{d_{max}}\right)^{0.1}$ greatly reduces the filament width lost per time-step for very short filaments while not greatly affecting long filaments.

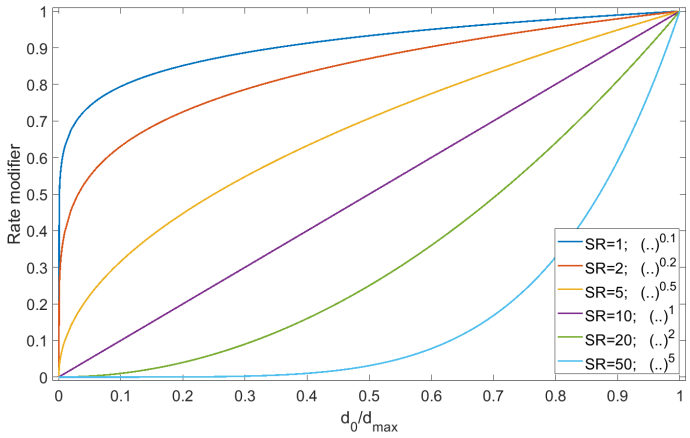

Figure 4.17 Relationship of thinning rate modifier to $\frac{Length}{d_{max}}$, for different exponents. Note that exponent values close to 0 result in sharp reduction of thinning rate for very short filaments ($\frac{Length}{d_{max}}$ close to 0.0) while not inhibiting long filaments much ($\frac{Length}{d_{max}}$ close to 1.0).

4.5.3 Results

The behaviour of the deterministic model with length-dependent filament characteristics was investigated for $S_R = 1$. This was expected to increase the number of time-steps required for short filaments to break while not changing the behaviour of the longer filaments.

It was found that the short filaments thinned less per time-step, as expected. Analysis results of a simulation using $S_R = 1$ are shown in Figure 4.18. A comparison of G(idx) trends of simulations using $S_R = 0$ and $S_R = 1$, shown in Figures 4.19a and 4.19c respectively, shows that introducing length dependence of filaments does not greatly affect the overall behaviour. This indicates that long filaments are not greatly affected, as intended. In contrast, a comparison of zoomed-in views of those G(idx) trends, shown in Figures 4.19b and 4.19d, shows that the rapid cyclic switching can be slowed by as much as half the rate seen without length dependence.

It was found that the filament length dependence had adverse effects on the IEI statistics and the autocorrelation. A comparison of the IEI plots of the example simulations using $S_R = 0$ and $S_R = 1$, shown in Figures 4.20a and 4.20c respectively, shows that introducing the length dependence changed the slope of part of the IEI trend. This produced a trend that was better fit with an exponential law model than with a power law model. This change makes the behaviour less like that of the experimental device.

A comparison of the autocorrelation plots for $S_R = 0$ and $S_R = 1$, shown in Figures 4.20b and 4.20d respectively, shows that introducing the length dependence lowered part of the autocorrelation. This change makes the behaviour less like that of the experimental device.

The modification to the deterministic model was successful in partially inhibiting the

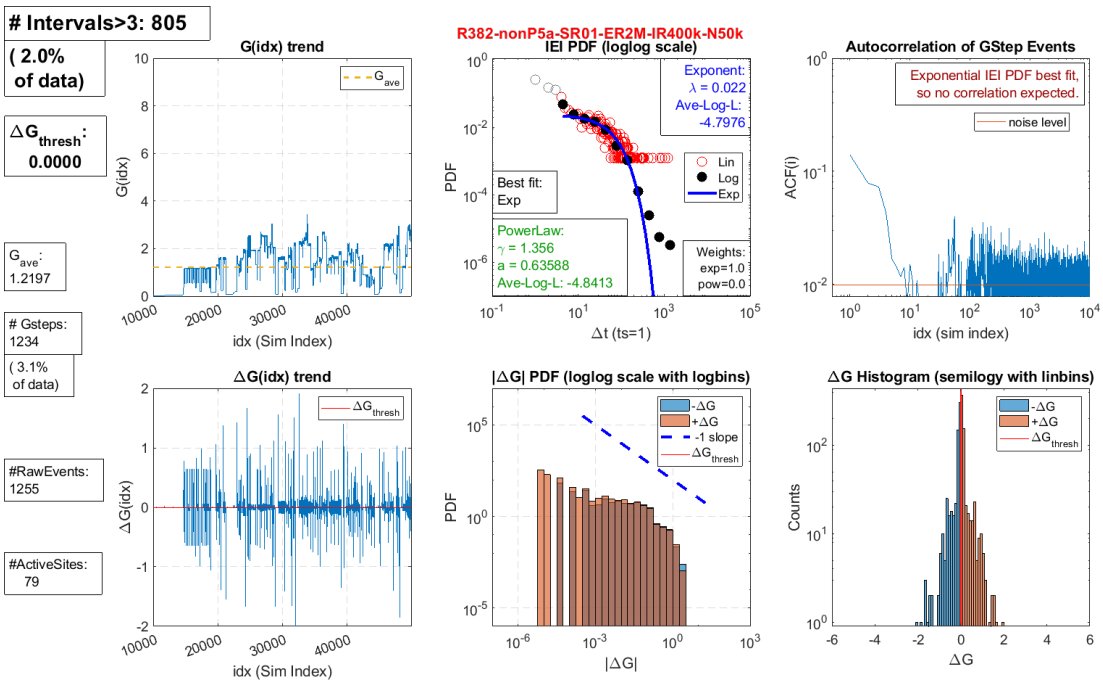

Figure 4.18 This example shows the 6-panel analysis results of a deterministic simulation with length dependence parameter S_R set to 1. The deterministic simulation parameters are E_R 2 M I_R 400 k, for seed 382. This is the same as the simulation that produced the results shown in Figure 4.11, apart from the length dependence.

cyclic switching as intended, as shown in Figure 4.19. However, it produced an adverse effect on the IEI behaviour and autocorrelation, as shown in Figure 4.20. The adverse effect means this modification needs further development in order to be appropriate for use. Other ideas for future development of the filament thinning aspect of the deterministic model are discussed in the 'future work' portion of the conclusion of the thesis (Section 6.3).

4.6 CHAPTER SUMMARY

The deterministic switching model was designed to implement switching activity that was deterministically driven by the conditions in the simulation network. In the model, closing of a switching junction depends on its electric field and opening depends on its current. Unlike the previous models, the deterministic model does not rely on probability to trigger switching events. Results demonstrated that the model works as intended and, for some parameter values, the deterministic model demonstrated switching behaviour similar to the experimentally observed device behaviour.

The physical process of filament growth and filament thinning is understood to cause small observable changes in conductance. The experimental device has demonstrated examples of small gradual changes in conductance that are consistent with this understanding. The deterministic model does not include gradual changes in

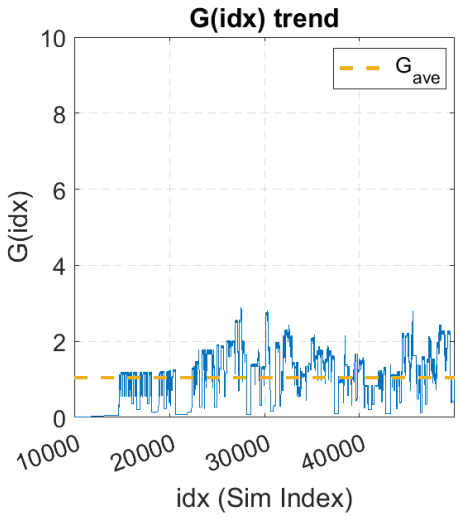

(a) G(idx) for no filament length dependence ($S_R = 0$).

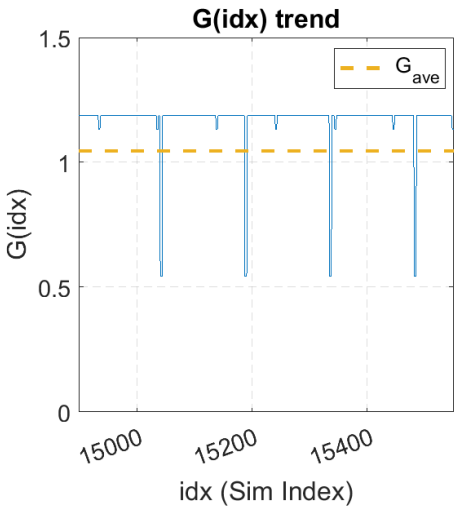

(b) Zoomed-in view of G(idx) for no filament length dependence ($S_R = 0$).

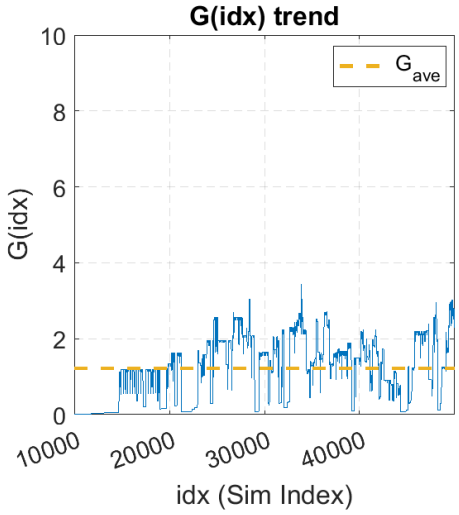

(c) G(idx) for filament length dependence ($S_R = 1$).

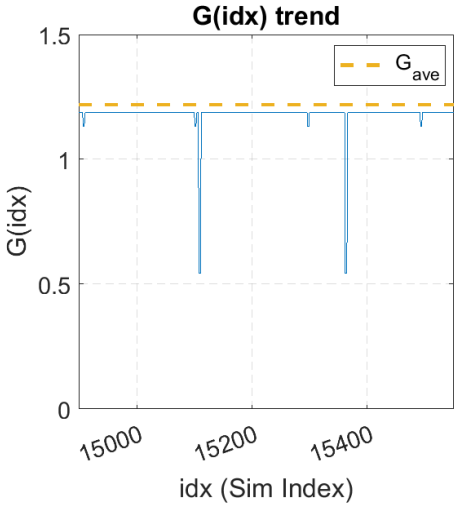

(d) Zoomed-in view of G(idx) for filament length dependence ($S_R = 1$).

Figure 4.19 A comparison of full views of G(idx) from results of equivalent simulations (a) without length dependence and (c) with length dependence, and again for zoomed-in views in (b) and (d). The deterministic simulation parameters were E_R 2 M and I_R 400 k, for seed 382. The zoomed-in views, shown in (b) and (d), show a section of changes in G(idx) that are known to be caused by cyclic switching in short filaments, and this activity is slowed down in the length dependent case, (d). The overall G(idx) behaviour with length dependence shown in (c) is not significantly different to the behaviour without it shown in (a).

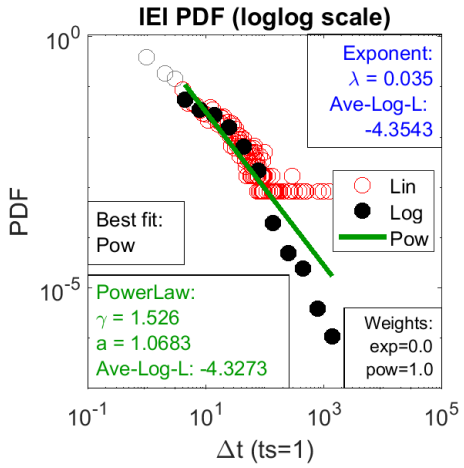

(a) IEI plot for no filament length dependence ($S_R = 0$).

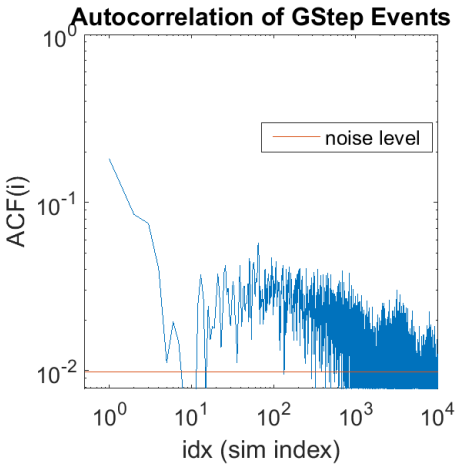

(b) Autocorrelation plot for no filament length dependence ($S_R = 0$).

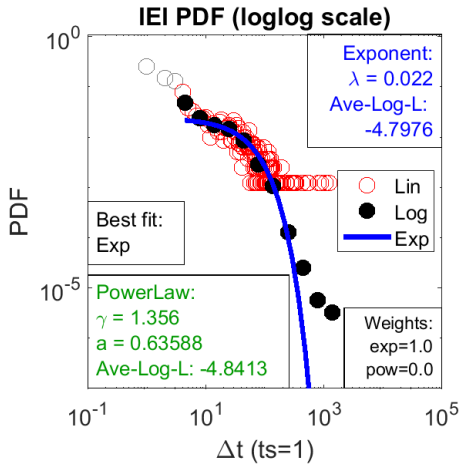

(c) IEI plot for filament length dependence ($S_R = 1$).

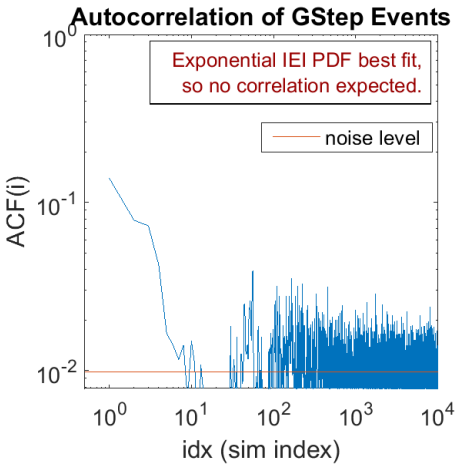

(d) Autocorrelation plot for filament length dependence ($S_R = 1$).

Figure 4.20 A comparison of IEI and autocorrelation plots (left and right columns) for simulations without and with filament length dependence (top and bottom rows). This comparison shows that the effect of the filament length dependence on the IEI statistics and the autocorrelation. The autocorrelation is lower and the IEI distribution is less like a power-law when length dependence is included ((c) and (d) compared to (b) and (a)). This is clear evidence that the filament length dependence modification to the deterministic model can have adverse effects on the IEI statistics and autocorrelation. The deterministic simulation parameters were E_R 2 M and I_R 400 k, for seed 382.

conductance. Including these gradual changes, referred to as creeping conductance, was explored and found to make the IEI statistics and autocorrelation of simulations using the deterministic model less similar to that of the experimental device. Since creeping conductance had this negative effect on the behaviour, it was not included during the majority of investigations into the behaviour of the deterministic model.

Rapid cyclic changes in conductance were observed in the deterministic model, and the cause was discovered to be small filaments. This rapid cyclic switching was believed to have a detrimental effect on the IEI statistics, and caused outlier values in some instances. A modification to the deterministic model was developed to mitigate this, by introducing length dependent filament characteristics to slow down the thinning and breaking of these small filaments. This modification successfully reduced the rate of this cyclic switching, but had a negative effect on the IEI statistics and autocorrelation of the deterministic model behaviour, so the modification was not considered useful in the deterministic model without further future development.

Overall, the deterministic model was successful in producing behaviour similar to that of the experimental device, depending on the parameters used. The results of the deterministic model that best matched the behaviour of the experimental device were produced while the model was not including creeping conductance or length-dependent filament characteristics. These results better matched the experimental behaviour than any results generated using the probabilistic switching models, so the goal of improving the simulation switching model can be considered achieved. Since the deterministic model performed best without creeping conductance or length-dependent filament characteristics, it is the focus for further investigation in this thesis.

The behaviour of the deterministic model depends on the choice of parameter values when configuring the simulation. The effects of these parameters are investigated thoroughly in Chapter 5.

Chapter 5

EXPLORING THE PARAMETER SPACE OF THE DETERMINISTIC SIMULATION

The deterministic model shows promising results if the E_R and I_R parameters are set such that the board remains in a predominantly low conductance state, with sporadic switch up events. In this chapter the parameter space around this particular set is explored. The goal is to learn the extent of this "good region" that produces promising results, and to know more about the effects each of the parameters have on the simulation behaviour.

The choice of values for the E_R and I_R parameters affects the behaviour of the simulation, as shown by the results of the deterministic model (Section 4.4). Further to this, the choices made for V, E_T, I_T and other parameters also affect the behaviour. The effects for each parameter are described and explained in Section 5.1, and a method of presenting results from a large number of simulations is briefly described in Section 5.2. In Section 5.3, plots summarising large numbers of simulations for ranges of values of each parameter are presented, showing the mean behaviour for multiple random seeds. The results of exploring the plane of parameter space for E_R and I_R are shown in Section 5.4, and these findings are compared with the observations made in Section 4.4. The chapter is concluded in Section 5.5.

5.1 KNOWN PARAMETER EFFECTS

The simulation parameters V, E_R, I_R, E_T, and I_T, are discussed here in terms of their understood effects on individual switching junctions and their expected impact on overall simulation behaviour when using the deterministic model. The applied voltage, V, directly affects the strength of electric fields and current in switching junctions of the simulation network. Because scaling voltage scales both electric field and current, increasing V leads to more switching junctions with $E > E_T$ and $I > I_T$, and also results in greater Δd and Δw. The overall effect is a greater number of active switching junctions, faster switching, and a higher mean value of the G(idx) data.

E_R and I_R have similarities: E_R inversely controls the rate of switching up, and I_R

inversely controls the rate of switching down. Increasing E_R tends to result in lower average network conductance and fewer events, while increasing I_R tends to result in higher conductance and fewer events. The relative values of E_R and I_R are also quite important for the behaviour of the simulation - scaling the two together demonstrates a time-scaling effect, and their relative values influence the shape of the G(idx) trend.

E_T and I_T also have similarities: increasing E_T results in fewer switching junctions closing, and increasing I_T results in fewer closed switching junctions opening again. E_T strongly affects the minimum voltage required for switching activity to occur, and since E depends on the length of gaps, E_T also influences the likelihood of long gaps activating. I_T strongly affects the maximum stable conductance, as it sets the maximum current a closed switching junction can conduct before beginning to open.

5.2 GATHERING AND PRESENTING DATA THROUGHOUT PARAMETER SPACE

The 6-panel plotting tool (Section 2.2) calculates several metrics in the process of producing the plots. These include mean conductance, the overall density of conductance step change events in the data, the number of switching junctions active, the model best fitting the IEI distribution, and the area under part of the ACF trend. These metrics can be used to compare the behaviour of simulations for different parameter choices. A tool was developed to automate plotting of these metrics for large sets of simulations. The resulting plots are referred to here as 'metaplots', as they are plots showing the change in the 6-panel plots. The use of these metaplots in the upcoming sections is summarised here.

The metaplots are featured in Section 5.3 to demonstrate the effect of parameter values on the simulation behaviour, varying single parameters over wide ranges of values for multiple random seeds. The metrics considered are:

- mean conductance – the mean of G(idx) for the simulation time window considered (time-steps 10 000 to 50 000 for these results).
- event density – the event density describes what percentage of time-steps considered had step changes in G(idx). For example, a simulation with 10 000 distinct step changes in 40 000 time-steps has an event density of 25%.
- number of active switches – the number of unique switching junctions that changed state at least once during a simulation.

In Section 5.4, metaplots are used to produce 2D maps of parameter space for ranges of values of E_R and I_R. These maps show metrics for simulations with the applied voltage set such that the event density is between 3% and 12%. The metrics plotted for each parameter space coordinate filled are:

- Voltage – as E_R and I_R are changed, the rate of up and down event occurrence changes. To compensate, the number of events can be tuned by adjusting the applied voltage.

- IEI fit names – whether the IEI distribution is best fit by power or exponential models, or neither, is shown with coloured areas in a 2D map. In the case of neither, the fit is labelled 'bad'.

- Rounded ACF Area – the area under the ACF trend and above the noise level, up to a correlation lag of 1000 time-steps. This area is indicated in Figure 5.1, and is rounded to the nearest 5 when shown in a 2D map. If the IEI fit is known to be poor, the result is marked 'bad' to separate it.

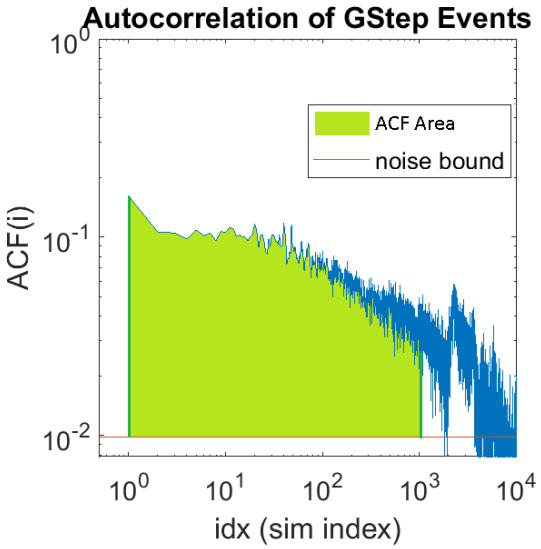

Figure 5.1 An example ACF plot result. The green area under the curve gives the metric 'ACF Area' used to quantify evidence of correlation between simulated switching events.

5.3 FINDINGS FOR SINGLE PARAMETERS

For parameters V, E_R, I_R, E_T, I_T, the effects of parameter changes were explored for a large set of simulations over multiple random seeds, varying one parameter at a time from a common starting simulation parameter set. The starting point simulation used $V = 3$, $E_R = 2 \times 10^6$, $I_R = 31.62 \times 10^3$, $E_T = 10$, and $I_T = 0.01$. The seeds used were 022, 162, 262, 382, 412, and 422. The other parameters used were the default values listed in Table 3.1 and are not known to be critical. The average conductance, the observed event density, and the number of switching junctions active during each simulation, were plotted for all values of each parameter varied, averaged over the set of seeds simulated.

5.3.1 Effects of varying voltage, V

The voltage was varied over a range, for simulations of multiple random seeds to show the mean effect across a variety of simulated network configurations. Figure 5.2 shows the trends in average conductance, event density, and number of active switches, resulting from changing the applied voltage.

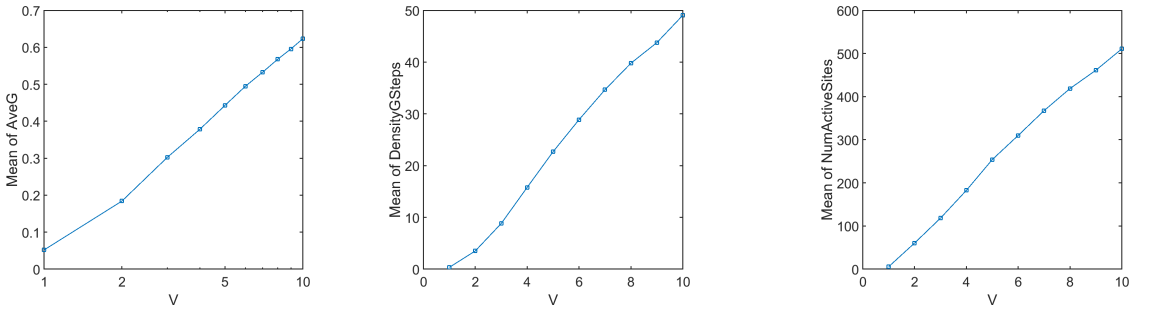

(a) Mean of G(idx) vs log(V) (b) Event density % vs V (c) Number of active switches vs V

Figure 5.2 Effects of applied DC voltage (V) on deterministic simulation behaviour, averaged over 6 different seeds for a range of values of V.

The mean conductance ('AveG', Figure 5.2a) during a simulation increases with increasing applied voltage. Note that the mean conductance appears approximately linear with log(V), but the significance of this is not known. The percentage of time-steps showing conductance changes ('DensityGSteps', Figure 5.2b) observed during a simulation increases with increasing applied voltage. The relationship appears to be approximately linear, which is consistent with the understanding that the rate of filament growing and breaking is linearly dependent on voltage (via current and electric field strength). The number of switches that were active during each simulation ('NumActiveSites', Figure 5.2c) observed during a simulation increases with increasing applied voltage. The relationship appears to be approximately linear, but the significance of this is not known. These results are consistent with expectations, as it is known that increasing V increases both the number of switching junctions that can close and also the rate of closing, leading to higher conductance overall.

5.3.2 Effects of varying E_R

The electric field dependence parameter, E_R, was varied over a range, for simulations of multiple random seeds, to show the mean effect across a variety of simulated network configurations. Figure 5.3 shows the trends in average conductance, event density, and number of active switches, resulting from changing E_R.

The mean conductance ('AveG', Figure 5.3a) during a simulation decreases with increasing E_R. The percentage of time-steps showing conductance changes ('DensityGSteps', Figure 5.3b) observed during a simulation decreases with increasing E_R. The number of switches that were active during each simulation ('NumActiveSites',

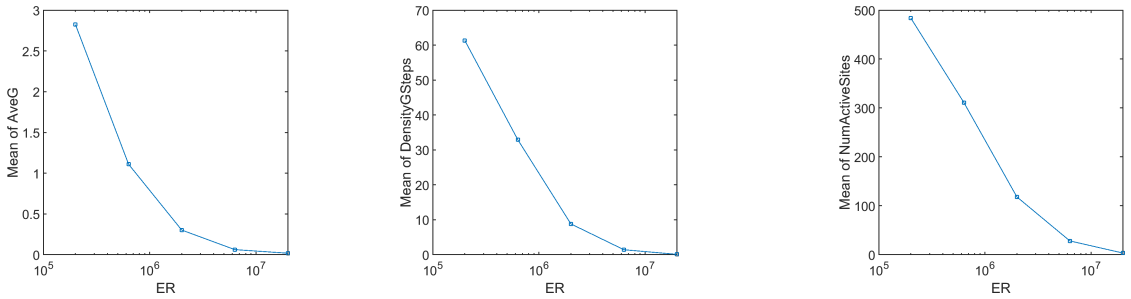

(a) Mean of G(idx) vs log(E_R) (b) Event density % vs log(E_R) (c) Number of active switches vs log(E_R)

Figure 5.3 Effects of electric field dependence parameter E_R on deterministic simulation behaviour, averaged over 6 different seeds for a range of values of E_R.

Figure 5.3c) observed during a simulation decreases with increasing E_R. These results are consistent with the understanding that E_R inversely controls the rate that switching junctions close. Increasing E_R leads to slower filament growth, while the rate of thinning remains the same. This leads to fewer switching junctions closed at any time (lower G(idx)), fewer events overall (lower data density), and fewer able to close (fewer active).

5.3.3 Effects of varying I_R

The current dependence parameter, I_R, was varied over a range, for simulations of multiple random seeds, to show the mean effect across a variety of simulated network configurations. Figure 5.4 shows the trends in average conductance, event density, and number of active switches, resulting from changing I_R.

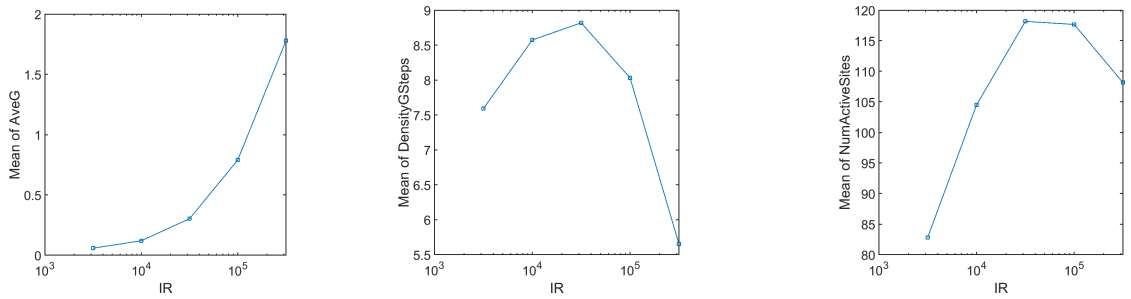

(a) Mean of G(idx) vs log(I_R) (b) Event density % vs log(I_R) (c) Number of active switches vs log(I_R)

Figure 5.4 Effects of current dependence parameter I_R on deterministic simulation behaviour, averaged over 6 different seeds for a range of values of I_R.

The mean conductance ('AveG', Figure 5.4a) during a simulation decreases with increasing I_R. The percentage of time-steps showing conductance changes ('DensityG-Steps', Figure 5.4b) observed during a simulation tends to increase and then decrease with increasing I_R. The number of switches that were active during each simulation ('NumActiveSites', Figure 5.4c), observed during a simulation tends to increase and then decrease with increasing I_R. These results are consistent with the understanding that I_R inversely controls the rate that switching junctions open. Increasing E_R leads to

slower filament thinning, while the rate of growth remains the same. This leads to closed switching junctions remaining closed for longer and more closed simultaneously (higher G(idx)). This results in more events overall but for very high I_R leads to saturation (higher and then lower data density). More closed switching junctions leads to higher electric field in some areas of the network (more active switches) but lower electric field in parallel to closed switches prevents parallel switches closing (causing fewer active switches for much higher I_R).

5.3.4 Effects of varying E_T

The electric field threshold parameter, E_T, was varied over a range, for simulations of multiple random seeds, to show the mean effect across a variety of simulated network configurations. Figure 5.5 shows the trends in average conductance, event density, and number of active switches, resulting from changing E_T.

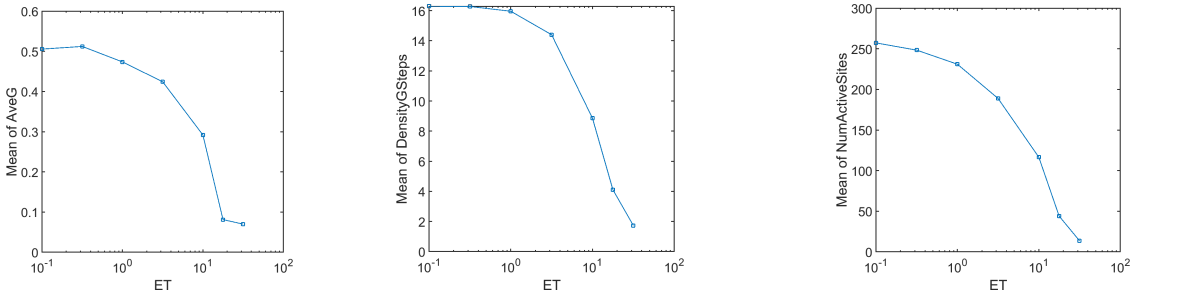

(a) Mean of G(idx) vs log(ET) (b) Event density % vs log(ET) (c) Number of active switches vs log(ET)

Figure 5.5 Effects of electric field threshold parameter E_T on deterministic simulation behaviour, averaged over 6 different seeds for a range of values of E_T.

The mean conductance ('AveG', Figure 5.5a) during a simulation decreases with increasing E_T. The percentage of time-steps showing conductance changes ('DensityG-Steps', Figure 5.5b) observed during a simulation tends to decrease with increasing E_T. The number of switches that were active during each simulation ('NumActiveSites', Figure 5.5c), observed during a simulation tends to decrease with increasing E_T. These results are consistent with the understanding that increasing E_T reduces the number of switching junctions that are able to begin closing. This has little effect for low values, as most switches have an electric field strength above E_T, but as E_T increases it begins to prevent filament growth in a greater percentage of the network, leading to reduction in the three metrics considered here.

5.3.5 Effects of varying I_T

The current threshold parameter, I_T, was varied over a range, for simulations of multiple random seeds, to show the mean effect across a variety of simulated network

configurations. Figure 5.6 shows the trends in average conductance, event density, and number of active switches, resulting from changing I_T.

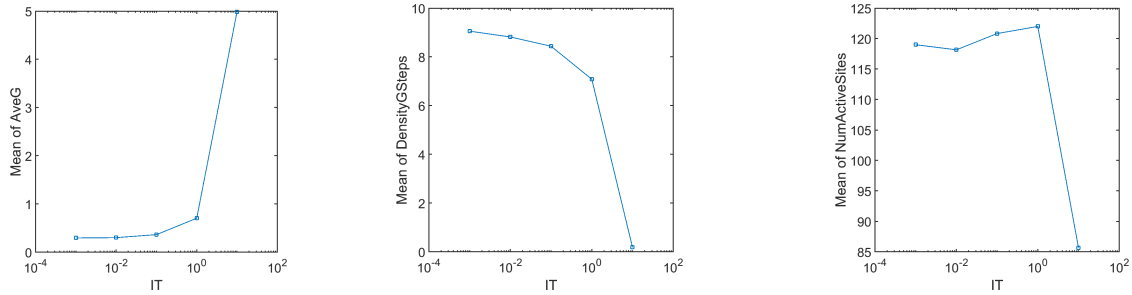

(a) Mean of G(idx) vs log(IT) (b) Event density % vs log(IT) (c) Number of active switches vs log(IT)

Figure 5.6 Effects of current threshold parameter I_T on deterministic simulation behaviour, averaged over 6 different seeds for a range of values of I_T.

The mean conductance ('AveG', Figure 5.6a) during a simulation increases with increasing I_T. The percentage of time-steps showing conductance changes ('DensityG-Steps', Figure 5.6b) observed during a simulation tends to decrease with increasing I_T. The number of switches that were active during each simulation ('NumActiveSites', Figure 5.6c), observed during a simulation tends to remain unchanged before sharply decreasing with increasing I_T. These results are consistent with the understanding that increasing I_T reduces the number of closed switching junctions that are able to begin opening. This has little effect for low values, as most closed switches do not have current above I_T, but as I_T increases it begins to prevent filament thinning in a greater percentage of the network. This leads to saturation of the network, and consequently a dramatic increase in the conductance, and decrease in the number of events and active switches (similar to very high values of I_R).

5.4 2D PARAMETER SPACE FINDINGS

The response of the simulation was recorded for changes in E_R and I_R in an area of two orders of magnitude in E_R and four orders of magnitude in I_R. The applied voltage was adjusted for each point simulated in this area of E_R-I_R parameter space, such that the resulting event density was between 3% and 12%. This ensured sufficient events to express the underlying statistical behaviour, without inhibiting the maximum IEI by crowding events.

The following metrics were plotted to create maps of E_R-I_R space, where a single point on each map corresponds to the same simulation in all maps:

- the applied voltage giving event density between 3% and 12%,
- the mean of the G(idx) data,
- the ACF area, rounded to nearest 5,

- the model best fitting the IEI distribution.

The voltage required to maintain event density in the range 3% to 12%, across the E_R-I_R plane, is shown in Figure 5.7. It appears to increase radially in contours. This is consistent with the understanding that increasing either E_R or I_R will decrease the event density, so the event density tends to decrease radially. Increasing the voltage increases the event density, so maintaining event density leads to voltage increasing radially on the E_R-I_R plane.

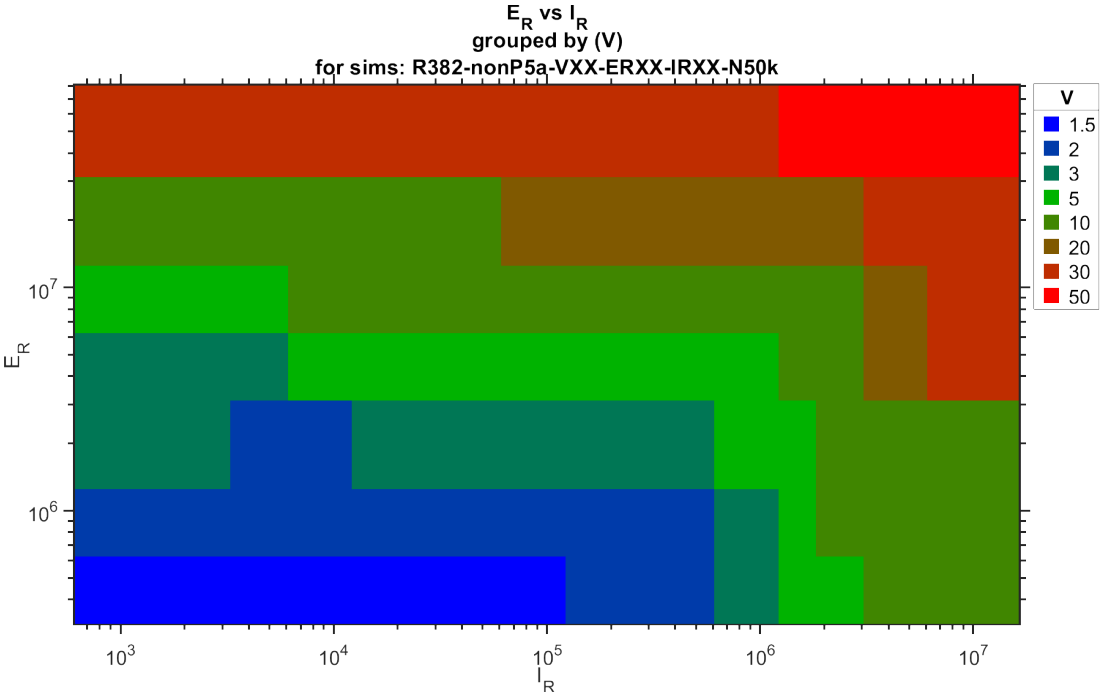

Figure 5.7 Parameter space map of E_R-I_R for voltage used. Note that voltage was adjusted for each coordinate in order to achieve an event density between 3% and 12% in the corresponding simulation.

The average G across the E_R-I_R plane is shown in Figure 5.8. It appears to follow an increasing gradient from a minimum in the top left, to a maximum in the bottom right. This is consistent with the understanding that the average conductance increases with I_R and decreases with E_R.

The rounded ACF area for each simulation across the E_R-I_R plane is shown in Figure 5.9. It is at a minimum in the bottom right (high I_R, low E_R), and at a maximum in a cluster of points around $E_R = 2 \times 10^6$ and $I_R = 3 \times 10^4$. There are some points marked as 'bad', these correspond to simulations where the conductance was very low (less than 0.5) and the majority of events came from a small number of switches with periodic switching, leading to strong periodic event correlation. This periodic event correlation produces a large ACF area, but is not the desired ACF behaviour, so it is marked as such to compensate for the shortcoming of using ACF area to indicate evidence of event correlation.

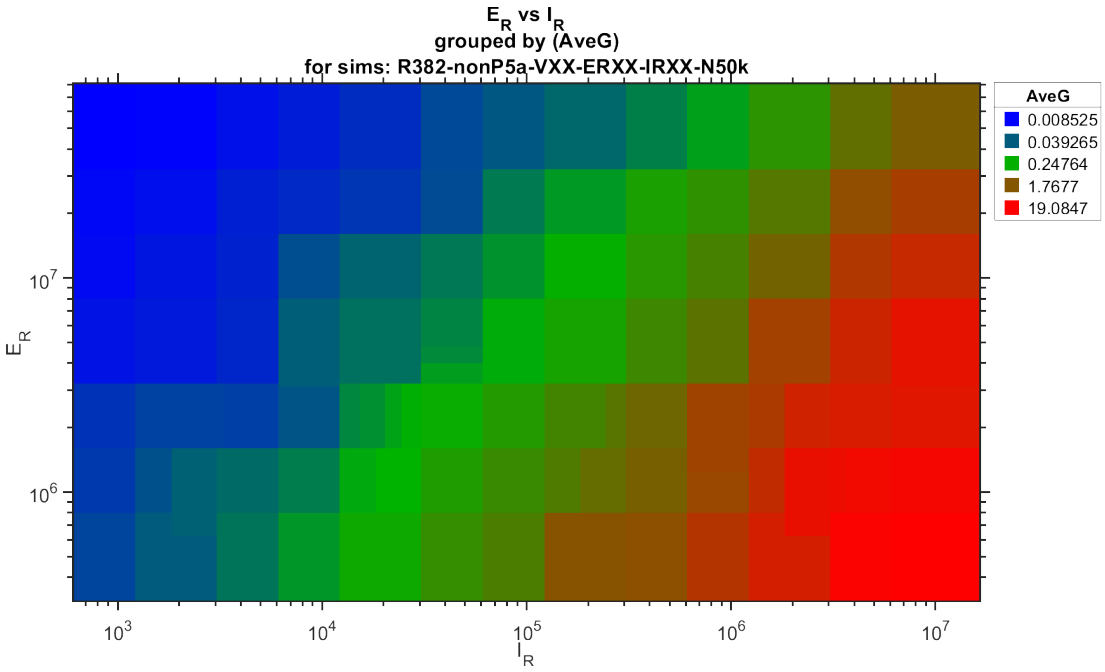

Figure 5.8 Parameter space map of E_R-I_R for average G. Note that it tends to be low in the upper left region, and tends to increase on a diagonal path to the lower right region.

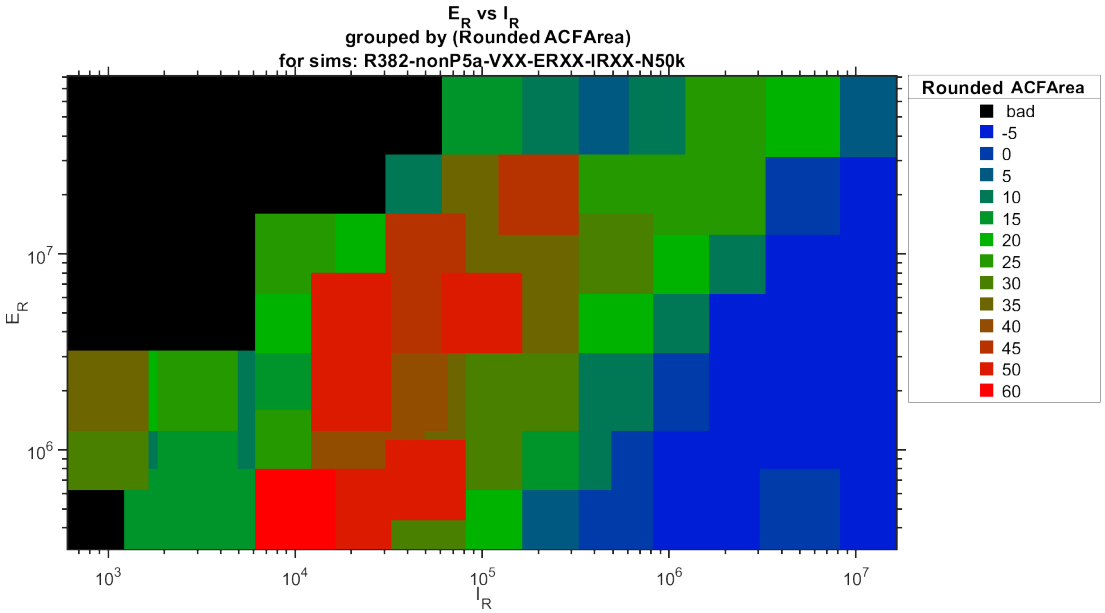

Figure 5.9 Parameter space map of E_R-I_R for the ACF area, rounded to nearest fives. Note that it appears to be at a maximum in a region around $E_R = 10^6$ and $I_R = 3 \times 10^4$. The area marked as 'bad' correspond to results that had very low conductance (indicating minimal network activity) and periodic switching that produced high ACF values (indicating activity due to a minority of switching sites).

The models best fitting the IEI distributions, varying across the E_R-I_R plane, are shown in Figure 5.10. It indicates power law IEI behaviour for a diagonal band from low E_R and I_R to high E_R and I_R. The diagonal band of points on the E_R-I_R plane

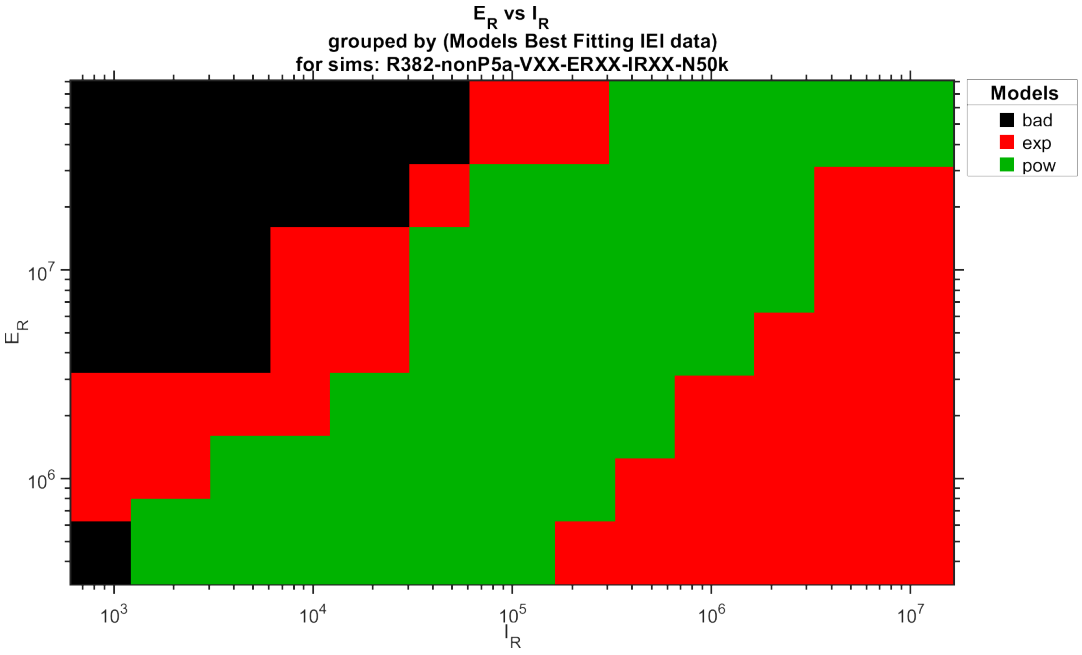

Figure 5.10 Parameter space map of E_R-I_R for the models best fitting the IEI distribution. 'pow' indicates that a power law model best fit the IEI distribution, 'exp' indicates exponential, and 'bad' indicates that the observed result was flagged due to low conductance and periodic switching events.

that produce power law behaviour and some correlation, suggests that there is a small range of E_R-I_R ratios that produce the desired behaviour.

5.5 CONCLUSION

The effects of the simulation parameters V, E_R, I_R, E_T, and I_T, were discussed and then shown by varying each and averaging the effect across six different random seeds. The effect on the behaviour observed in terms of the number of active switching junctions, the average conductance, and the event density during simulations, was generally consistent with expectations and understanding of the deterministic model.

The effects of the simulation parameters E_R and I_R were explored together by stepping throughout an area of the E_R-I_R parameter space plane. The behaviour for each simulation was recorded and plotted, creating maps showing how behaviour changes as E_R and I_R are changed. This mapping showed a diagonal band of points on the E_R-I_R plane that produce power law behaviour and some correlation, suggesting that there is a small range of E_R-I_R ratios that produce the desired behaviour. The insight gained from this mapping can be used to produce simulations that behave in a qualitatively similar fashion to the experimental device, which is a significant achievement.

Chapter 6

CONCLUSION & FUTURE WORK

6.1 KEY ACHIEVEMENTS, OBJECTIVES, & FINDINGS

The research group lead by Prof. Simon Brown has been researching and developing an experimental device with possibly computationally useful properties. Measurements of the device conductance have shown step change events with evidence of correlation between event times, which is a key requirement for some computing applications. A simulation of the device had so far been unsuccessful in reproducing evidence of event correlation. In order to make predictions of device behaviour, and to model its use in computing, the simulation must show correlation between events (consistent with observations in the device measurements).

The key achievement of this work is the development and testing of the new deterministic switching model (Chapter 4) and simulation parameters which produce behaviour with statistical properties similar to that of the experimental device. Three key statistical properties of the device are: ΔG measurements that range over several orders of magnitude; IEIs that follow a power law probability distribution; and IEIs producing slowly decaying ACFs of events times. Previous switching models could reproduce certain aspects of the devices, such as conductance measurements that show sudden step changes, but did not demonstrate correlation between the conductance events. The deterministic model presented in this thesis is capable of not only producing power-law distributed IEIs (a signature of correlated non-Poisson processes), but also shows slowly decaying ACFs of event times (further evidence of correlation between events).

The primary objective of the Master's project was to make improvements to the simulation, to close the gap between the real devices and the simulation by making the switching model more closely reflect real processes. It was expected that making the switching model replicate the internal device dynamics would allow experimentally observed properties to be demonstrated in simulations of the device. The original probabilistic switching model was briefly investigated (Section 3.1.1), and new probabilistic models were developed that included features intended to cause correlation between

events – 'multistep switching' (Section 3.2) and 'electric field and current dependent probability' (Section 3.3). The probabilistic models were not able to produce evidence of correlation, so probability was removed from the model and replaced with deterministic rules. Several versions of the deterministic model were developed and tested, each testing different models of physical processes, before successfully demonstrating the desired behaviour in simulations (Chapter 4).

The secondary objective was to develop tools to better comprehend simulation results. This was achieved by writing scripts to process results and produce plots, and by modifying the simulation to make accessing internal behaviour easier. A script written in MATLAB (Section 2.2) produces plots of experimental or simulation data, aiding comparison of different switching models with the device behaviour. Scripts written in Python produce visualisations of the simulated board that show the distribution of potentials, currents, and switching events (Section 2.3), while also showing the structure of the internal network. A new Python script collects the electric field strengths and currents of all switching junctions during switching events and produces histograms that depict the distribution of events relative to the range of electric field strengths and currents present on the board (Section 2.4). The simulation was modified to routinely record switching event information for every junction at every time-step (Section 2.5). This made it possible to easily collect data necessary for analysing the relationships between individual internal switching events and observed changes in external conductance. The storage required for these data was minimised by employing run-length encoding, taking advantage of the typically small number of switching events at each time-step.

The existing probabilistic models and the new probabilistic models investigated demonstrate ΔG measurements that range over several decades, but produce neither power-law distributed IEIs, nor slowly decaying ACFs of event times. The IEIs of the probabilistic models considered are consistent with exponential law probability distributions, and the ACFs of event times are indistinguishable from random noise. It is conjectured that this is due to the dependence of the models on probability – events with independent probability at each time-step of the simulation will not show correlation.

In contrast to previous models, the deterministic switching model does not use probability to generate switching events, and instead uses rules based on known physical phenomena (Section 4.2). It is known that metal filament growth can be induced by electric fields, and that stronger electric fields result in faster growth, so the deterministic model uses an electric field dependent rate of switch closure via filament growth. For opening switches, it uses current dependent filament thinning, inspired by electromigration. Switching progresses gradually, at rates dependent on the electric field strength and current in each individual switching element. Exploring the effects of the deterministic model electric field strength dependence and current dependence

parameters, E_R and I_R, showed that the statistical properties of the model behaviour depend on their values. These parameters independently affect the rates of switching up and switching down, respectively, so their relative values determine the overall shape of the conductance trend, G(idx). Increasing E_R tends to result in lower conductance due to fewer switch-up events, while increasing I_R tends to result in higher conductance due to fewer switch-down events (Section 5.3). When these parameters were chosen such that the G(idx) trend was briefly increasing above its minimum in bursts (similar to G(t) in experimental data), the IEIs produced were consistent with a power law distribution for more than one decade, and the ACF of event times showed a slowly decaying response that was above the noise. This result is a good match with experimental behaviour, which suggests that the simulation is now a good approximation of the physical system.

6.2 CRITIQUE

There were a number of simplifications made in the model that do not reflect what is known about the physical device. These are as follows:

- The device shows 'fatigue' – experimental measurements have shown that the switching elements in the device are not able to continue toggling indefinitely when higher voltages are applied. The device can continue operating normally for several months if the applied voltage is kept below 6 V, but the lifetime of the device is shortened by experiments with higher voltages (e.g., 10 V). The simulation has no mechanism which can cause a switching element to age or degrade.

- The models use a simplistic equation for tunnelling conductance that is not dependent on voltage, unlike some models in literature. Experimental measurements involving applying stepped voltage have shown that changing the applied voltage changes the device conductance without requiring switching events, suggesting that the device conductance is directly voltage dependent.

- There is no consideration of intragroup conductance – the models treat single particles and groups of overlapping particles as having zero resistance. While this is likely to be a valid approximation when there are a large number of switching junctions in series, it may not be when a group of particles spans a large fraction of a simulation board.

6.3 FUTURE WORK

Here several ideas and suggestions for future work are discussed, in no particular order:

- A heat map of the board for switching events would be useful for showing trends of switching event locations over time. The existing network and particles board viewer tools could be adapted to show the number of switching events in different locations by colouring the junctions or network connections based on how many times they switched or based on how many time-steps each switching element was in the filament state (on).

- A heat map of current flowing during the simulation would be useful as a different way to indicate primary current paths, and may be useful for showing properties of different network structures. The network currents board view shows the currents in the network at single time-steps. It may be useful to see a heat map version of this for ranges of time-steps. The colours of network edges could be set based on the integral of current, rather than instantaneous current.

- A new particle board view with switching junctions coloured based on gap length would give an impression of the spatial distribution of tunnelling gaps of different lengths. This would be useful, in conjunction with switching event location data, for seeing whether events are occurring more frequently in regions with smaller switching junctions.

- More electrodes could be added to the board. The existing simulated board has only two electrodes, on the left and right edges. The top and bottom edges are treated as unconnected. Additional electrodes could be implemented by partitioning the board perimeter into sections treated as either connected to an electrode or unconnected. After the 'deposition' phase of board generation, any particles positioned in contact with an electrode section would be added to that electrode group – much like how the existing algorithm treats any in contact with the left or right edges as part of the input or output groups respectively. This would allow simulation of multiple electrode devices.

- More variations of deterministic dependence should be explored. The deterministic model uses a simplistic dependence on current and electric field, in that the dependence of both is linear. In particular, the effect of using a squared current dependence should be explored, in line with treating power dissipation as the primary cause of filament destruction (and therefore depending on I^2R).

- Reversible filament growth and/or thinning could be added to the deterministic model. It has been suggested that partially grown filaments may be gradually reabsorbed if the electric field strength in a switching junction drops sufficiently. The deterministic model presented here does not include any reversal of filament growth or thinning, only monotonic growth and thinning. The effect of reversible switching progress should be explored.

- The deterministic thinning process could be converted from current dependence to current density dependence. This should be explored because current density is reported as the driving quantity in electromigration. An important consequence of this is that for a given current, as the filament thins the current density will increase. The increased current density will lead to more electromigration and more thinning – a process with positive feedback, like electric fields increasing in shortening gaps during filament growth. Introducing this symmetry between growth and thinning would be a significant change to the deterministic switching model, and so it is expected to affect the IEI and ACF behaviour of the model.

Appendix A

MODEL PARAMETERS

A comprehensive list of the parameters used to configure the simulation, and their purpose.

A.1 GENERAL

- V0 - (V)the DC voltage applied
- ET - (E_T) the electric field threshold. Any given switch that is in its low state must have an electric field equal to or above this value in order to be able to switch up to its high state.
- IT - (I_T) the current threshold. Any given switch that is in its high state must have a current equal to or above this value in order to be able to switch down to its low state.
- XY - (also labelled 'size') the dimensions of the board in width and length, in units of particle diameters. This determines the board area. The aspect ratio is usually 1:1 but X and Y can be set independently if necessary.
- G_{on} - the nominal conductance of a switch in its high state. Some switch models may modify this per switch.
- A - Alpha; the nominal tunnel gap conductance. Most switch models use this in Equation (1.1) to calculate the conductance of a switch in its low state.
- β - beta; the distance dependence exponent for tunnel gap conductance. Most switch models use this in Equation (1.1) to calculate the conductance of a switch in its low state.
- seed - the random seed for random number generation. This allows the user to repeat simulations for particular random results.
- coverage - the fraction of the board that is covered in particles.

- d_{max} - the maximum distance of any gap between particles for which the simulation will construct a switching junction. This limits the construction of negligible conductance junctions.
- Timespan - (also labelled 'N') the number of time steps that the simulation will run until.
- Initial ON % - the percentage of switches that will be set to their high state at the beginning of the simulation.

A.2 BASE MODEL

- P_{up} - the probability that a switch in its low state (tunnel gap) will switch up to the high state (filament), given that the switch has an electric field above the threshold.
- P_{down} - the probability that a switch in its high state (filament) will switch down to the low state (tunnel gap), given that the switch has a current above the threshold.

A.3 MULTISTEP AND EI-DEPENDENT PROBABILITY

- SR - (S_R) the number of steps for a switch to complete its transition.
- ER - (E_R) the transition range of E above E_T in which $P_{up}(E)$ increases linearly to a maximum of 0.5.
- IR - (I_R) the transition range of I above I_T in which $P_{down}(E)$ increases linearly to a maximum of 0.5.

A.4 DETERMINISTIC

- SR - (S_R) part of the exponent used to non-linearly scale down switch-down rates according to the length of filaments: $\frac{S_R}{10}$
- ER - (E_R) the transition range of E above E_T in which the growth in length per step of filaments increases linearly, to a maximum of d_{MAX} (at which point even the longest allowable gap would close in a single step).
- IR - (I_R) the transition range of I above I_T in which the decay in width of filaments increases linearly to a maximum of 1.0 (at which point any filament would decay to open in a single step).

Appendix B

ADDITIONAL RESULTS

B.1 EI-DEPENDENT PROBABILITY MODEL

Here are some results omitted from Section 3.3.3. They are the full 6-panel plots of the simulations presented in comparison to the best match representative results of the model.

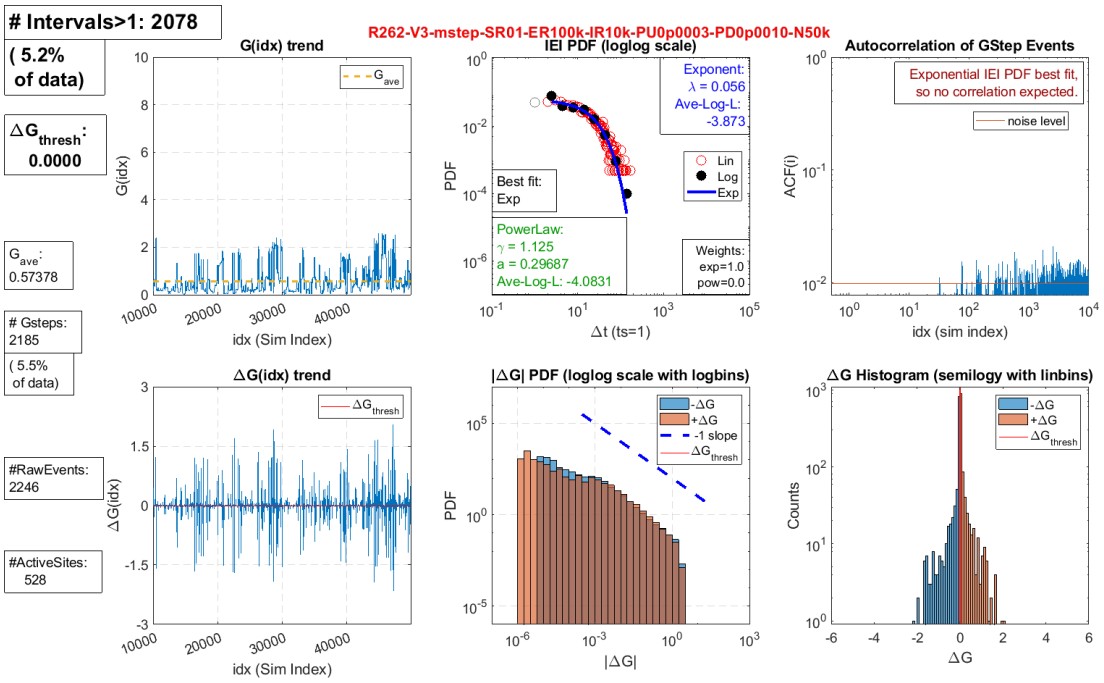

Figure B.1 A six-panel plot showing the analysis results of the best match EI-Dependent P simulation. These results were produced using lower switching probabilities than in the best match base model results, and using weak dependence parameters in the electric field and current dependent probability model. This is a repeat of Figure 3.18.

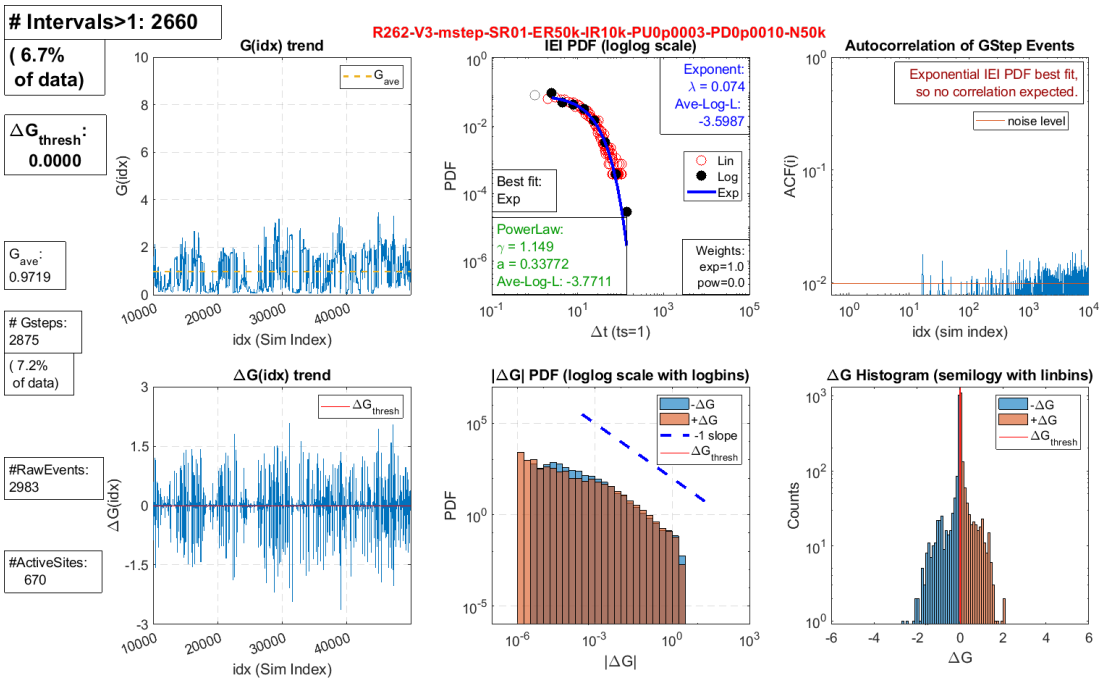

Figure B.2 A six-panel plot showing the analysis results of the electric field and current dependent probability model, when using using E_R set to half of that used in the EI-Dependent P best match results (shown in Figure B.1). Halving E_R led to an increase in overall conductance, as expected, due to more switching up events occurring.

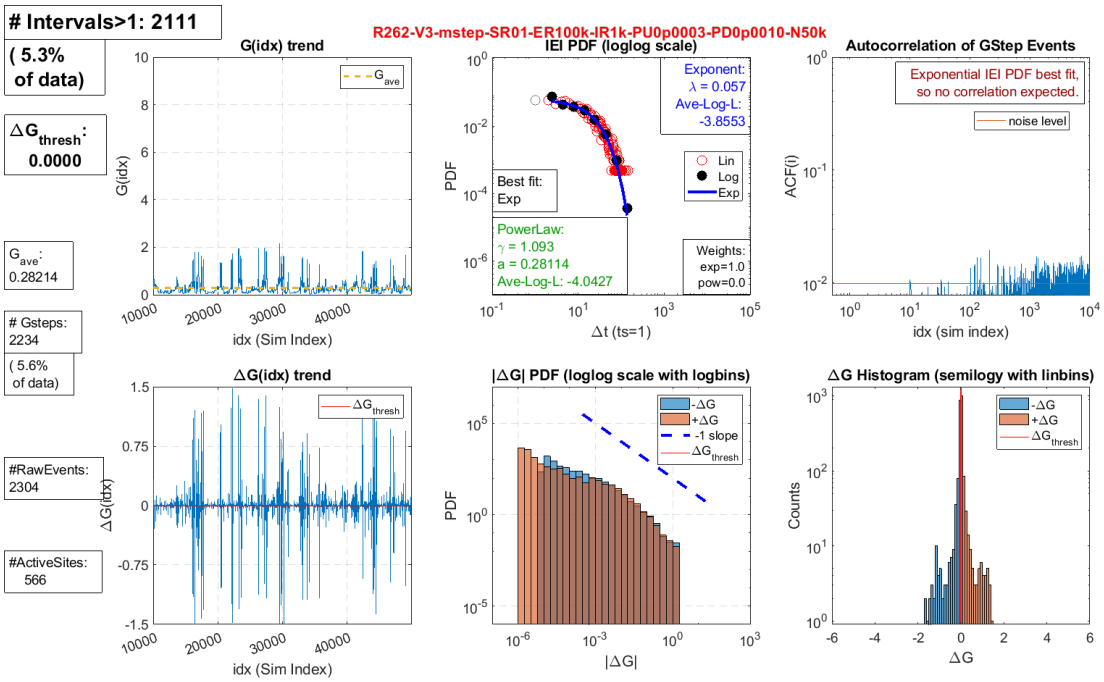

Figure B.3 A six-panel plot showing the analysis results of the electric field and current dependent probability model, when using I_R set to one tenth of that used in the EI-Dependent P best match results (shown in Figure B.1). Using this I_R resulted in a decrease in overall conductance, as expected, due to more switching down events occurring.

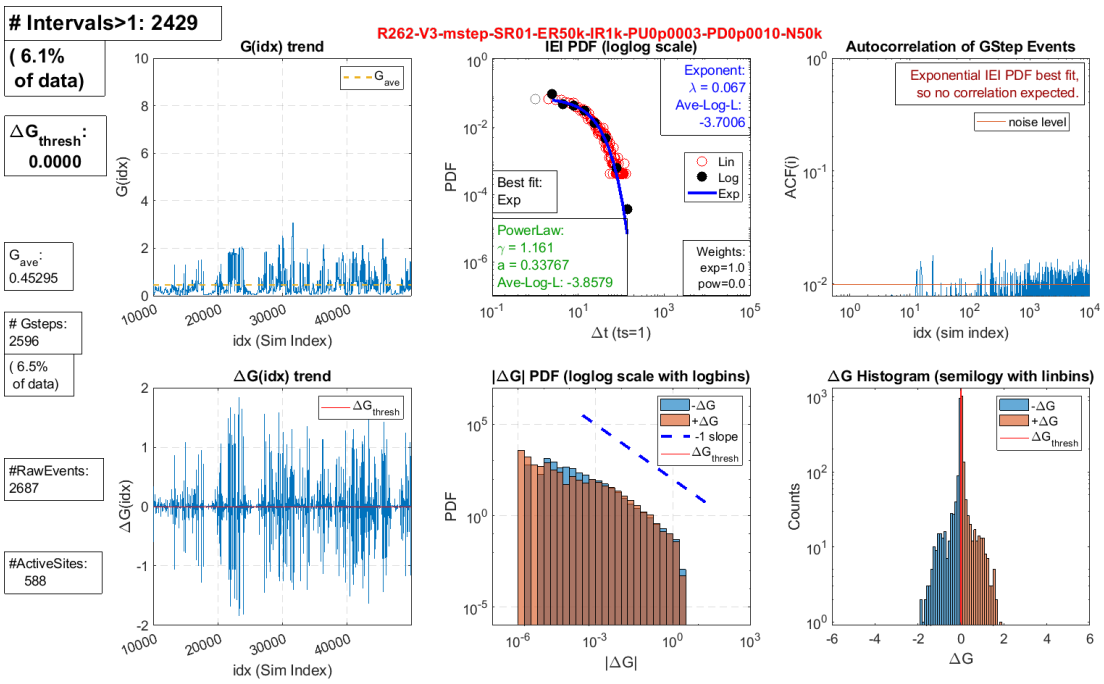

Figure B.4 A six-panel plot showing the analysis results of the electric field and current dependent probability model, when using E_R and I_R respectively set to half and a tenth of the corresponding values of the EI-Dependent P best match results (shown in Figure B.1). Using these E_R and I_R values resulted in more switching events as expected, and approximately unchanged conductance (due to counteracting conductance changes of the up and down events balancing in this case).

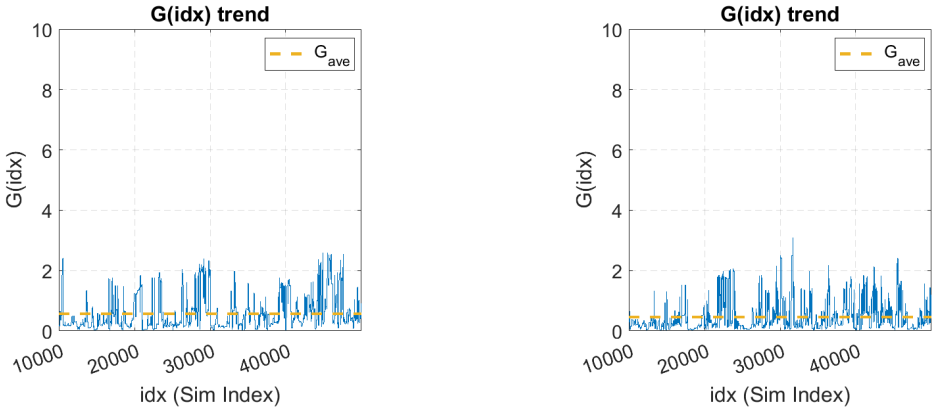

(a) Result best matching experiment.

(b) Result when both E_R is reduced to a half, and I_R is reduced to a tenth.

Figure B.5 Comparison of the G(idx) trend plots for the best match EI-dependent probability model results with results when using E_R reduced by half, and I_R reduced to one tenth. The mean conductance decreased from 0.57 to 0.45, while the number of step changes in G increased from 2185 to 2596. The maximum G(idx) increased from ∼2.5 to ∼3.0.

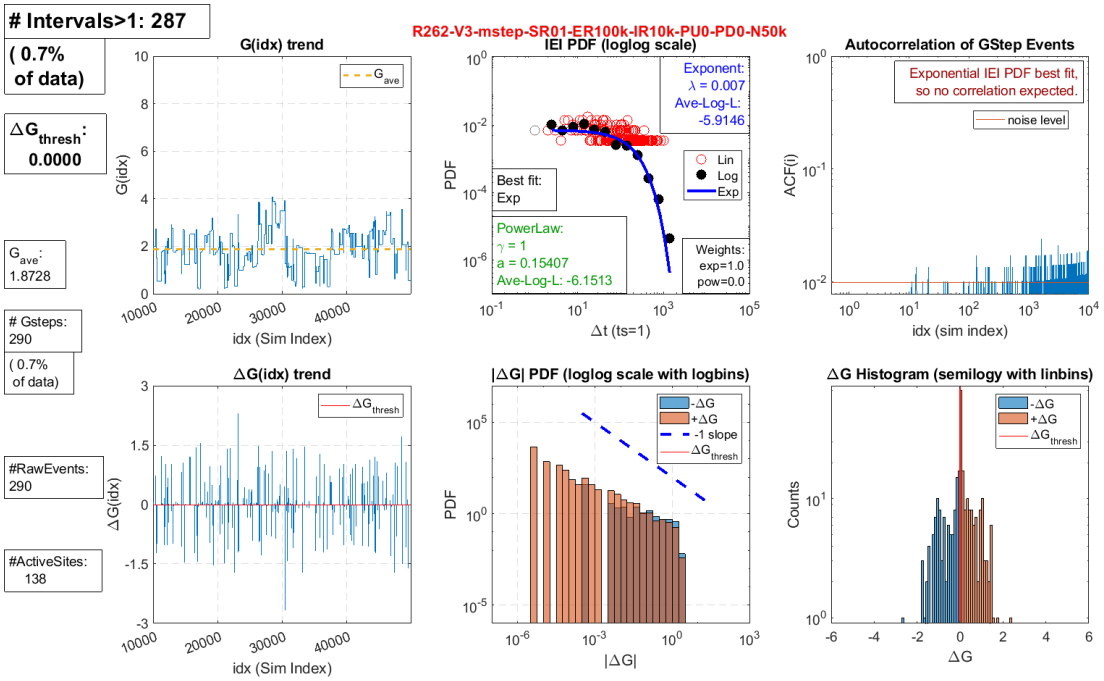

Figure B.6 Six-panel plot results of the EI-dependent P model, with base switching probabilities set to zero. E_R and I_R were set to the same values as for the EI-Dependent P best match results (shown in Figure 3.18). This plot shows that the EI-dependent P model does result in an increase in switching probabilities above the chosen base probabilities.

BIBLIOGRAPHY

[1] D. Silver, A. Huang, C. J. Maddison, A. Guez, L. Sifre, G. Van Den Driessche, J. Schrittwieser, I. Antonoglou, V. Panneershelvam, M. Lanctot, S. Dieleman, D. Grewe, J. Nham, N. Kalchbrenner, I. Sutskever, T. Lillicrap, M. Leach, K. Kavukcuoglu, T. Graepel, and D. Hassabis, "Mastering the game of Go with deep neural networks and tree search," *Nature*, vol. 529, no. 7587, pp. 484–489, Jan. 2016, ISSN: 14764687. DOI: 10.1038/nature16961. [Online]. Available: https://www.nature.com/articles/nature16961#supplementary-information.

[2] H. Markram, "THE HUMAN BRAIN PROJECT," *Scientific American*, vol. 306, no. 6, pp. 50–55, 2012, ISSN: 00368733, 19467087. [Online]. Available: http://www.jstor.org/stable/26014516.

[3] M. Le Page, "Knowledge means power," *New Scientist*, vol. 240, no. 3199, pp. 22–23, 2018, ISSN: 02624079. DOI: 10.1016/s0262-4079(18)31841-4. [Online]. Available: http://www.sciencedirect.com/science/article/pii/S0262407918318414.

[4] G. Tanaka, T. Yamane, J. B. Héroux, R. Nakane, N. Kanazawa, S. Takeda, H. Numata, D. Nakano, and A. Hirose, "Recent advances in physical reservoir computing: A review," *Neural Networks*, vol. 115, pp. 100–123, 2019, ISSN: 18792782. DOI: 10.1016/j.neunet.2019.03.005.

[5] D. Monroe, "Neuromorphic computing gets ready for the (really) big time," *Communications of the ACM*, vol. 57, no. 6, pp. 13–15, Jun. 2014, ISSN: 00010782. DOI: 10.1145/2601069. [Online]. Available: http://dl.acm.org/citation.cfm?doid=2602695.2601069.

[6] D. Stauffer and A. Aharony, *Introduction to Percolation Theory*, 2nd. London, UK: Taylor & Francis, Jul. 2003, p. 192, ISBN: 9781135747831. [Online]. Available: https://www.taylorfrancis.com/books/9781135747831.

[7] H. Kesten, "What is ... percolation?" *Notices of the American Mathematical Society*, vol. 53, no. 5, pp. 572–573, 2006. [Online]. Available: https://www.ams.org/notices/200605/what-is-kesten.pdf.

[8] S. Fostner and S. A. Brown, "Neuromorphic behavior in percolating nanoparticle films," *Physical Review E - Statistical, Nonlinear, and Soft Matter Physics*, vol. 92, no. 5, p. 052 134, Nov. 2015, ISSN: 15502376. DOI: 10.1103/PhysRevE.92.052134. [Online]. Available: https://link.aps.org/doi/10.1103/PhysRevE.92.052134.

[9] J. Mallinson, "Percolating Sn Nanoparticle Networks for Neuromorphic Applications," PhD thesis, University of Canterbury, 2016.

[10] A. Sattar, S. Fostner, and S. A. Brown, "Quantized conductance and switching in percolating nanoparticle films," *Physical Review Letters*, vol. 111, no. 13, p. 136 808, Sep. 2013, ISSN: 0031-9007. DOI: 10.1103/PhysRevLett.111.136808. [Online]. Available: https://link.aps.org/doi/10.1103/PhysRevLett.111.136808.

[11] S. K. Bose, J. B. Mallinson, R. M. Gazoni, and S. A. Brown, "Stable self-assembled atomic-switch networks for neuromorphic applications," *IEEE Transactions on Electron Devices*, vol. 64, no. 12, pp. 5194–5201, 2017, ISSN: 00189383. DOI: 10.1109/TED.2017.2766063.

[12] R. Reichel, J. G. Partridge, A. D. Dunbar, S. A. Brown, O. Caughley, and A. Ayesh, "Construction and application of a UHV compatible cluster deposition system," *Journal of Nanoparticle Research*, vol. 8, no. 3-4, pp. 405–416, 2006, ISSN: 13880764. DOI: 10.1007/s11051-005-9021-1.

[13] S. K. Bose, S. Shirai, J. B. Mallinson, and S. A. Brown, "Synaptic dynamics in complex self-assembled nanoparticle networks," *Faraday Discussions*, vol. 213, pp. 471–485, 2019, ISSN: 1359-6640. DOI: 10.1039/C8FD00109J. [Online]. Available: http://xlink.rsc.org/?DOI=C8FD00109J.

[14] Y. Yang, P. Gao, S. Gaba, T. Chang, X. Pan, and W. Lu, "Observation of conducting filament growth in nanoscale resistive memories," *Nature Communications*, vol. 3, pp. 732–738, 2012, ISSN: 20411723. DOI: 10.1038/ncomms1737. [Online]. Available: http://dx.doi.org/10.1038/ncomms1737.

[15] S. T. Thornton and A. F. Rex, *Modern physics for scientists and engineers*. Cengage Learning, 2013, p. 6, ISBN: 1133103723.

[16] A. Stockdill, "Neuromorphic Computing with Reservoir Neural Networks on Memristive Hardware," PhD thesis, University of Canterbury, 2016.

[17] K. Terabe, T. Hasegawa, T. Nakayama, and M. Aono, "Quantized conductance atomic switch," *Nature*, vol. 433, no. 7021, pp. 47–50, Jan. 2005, ISSN: 0028-0836. DOI: 10.1038/nature03190. [Online]. Available: https://doi.org/10.1038/nature03190.

[18] S. Shirai, S. K. Acharya, S. K. Bose, J. B. Mallinson, E. Galli, M. D. Pike, M. D. Arnold, and S. A. Brown, "Long-range temporal correlations in scale-free neuromorphic networks," *Submitted Manuscript*, vol. submitted, 2019.

[19] J. B. Mallinson, S. Shirai, S. K. Acharya, S. K. Bose, E. Galli, and S. A. Brown, "Avalanches and criticality in self-organized nanoscale networks," *Science Advances*, vol. 5, no. 11, Nov. 2019, ISSN: 2375-2548. DOI: 10.1126/sciadv.aaw8438. [Online]. Available: http://advances.sciencemag.org/lookup/doi/10.1126/sciadv.aaw8438.

[20] Z. Deng and Y. Zhang, "Collective behavior of a small-world recurrent neural system with scale-free distribution," *IEEE Transactions on Neural Networks*, vol. 18, no. 5, pp. 1364–1375, Sep. 2007, ISSN: 1045-9227. DOI: 10.1109/TNN.2007.894082. [Online]. Available: http://ieeexplore.ieee.org/document/4298110/.

[21] M. Karsai, K. Kaski, A.-L. Barabási, and J. Kertész, "Universal features of correlated bursty behaviour," *Scientific Reports*, vol. 2, p. 397, Dec. 2012, ISSN: 2045-2322. DOI: 10.1038/srep00397. [Online]. Available: http://www.nature.com/articles/srep00397.

[22] S. B. Lowen and M. C. Teich, "Fractal renewal processes generate 1/f noise," *Physical Review E*, vol. 47, no. 2, pp. 992–1001, 1993, ISSN: 1063651X. DOI: 10.1103/PhysRevE.47.992.

[23] J. M. Palva, A. Zhigalov, J. Hirvonen, O. Korhonen, K. Linkenkaer-Hansen, and S. Palva, "Neuronal long-range temporal correlations and avalanche dynamics are correlated with behavioral scaling laws," *Proceedings of the National Academy of Sciences*, vol. 110, no. 9, pp. 3585–3590, Feb. 2013, ISSN: 0027-8424. DOI: 10.1073/pnas.1216855110. [Online]. Available: http://www.pnas.org/lookup/doi/10.1073/pnas.1216855110.

[24] S. Fostner, R. Brown, J. Carr, and S. A. Brown, "Continuum percolation with tunneling," *Physical Review B*, vol. 89, no. 7, p. 075 402, Feb. 2014, ISSN: 1098-0121. DOI: 10.1103/PhysRevB.89.075402. [Online]. Available: https://link.aps.org/doi/10.1103/PhysRevB.89.075402.

[25] H. Sun, Q. Liu, C. Li, S. Long, H. Lv, C. Bi, Z. Huo, L. Li, and M. Liu, "Memory Switching: Direct Observation of Conversion Between Threshold Switching and Memory Switching Induced by Conductive Filament Morphology (Adv. Funct. Mater. 36/2014)," *Advanced Functional Materials*, vol. 24, no. 36, p. 5772, 2014, ISSN: 16163028. DOI: 10.1002/adfm.201470243.

[26] C. Minnai, A. Bellacicca, S. A. Brown, and P. Milani, "Facile fabrication of complex networks of memristive devices," *Scientific Reports*, vol. 7, no. 1, p. 7955, 2017, ISSN: 2045-2322. DOI: 10.1038/s41598-017-08244-y. [Online]. Available: https://doi.org/10.1038/s41598-017-08244-y.

[27] A. Stockdill, Private communication, Feb. 2018.

[28] E.-J. Wagenmakers and S. Farrell, "AIC model selection using Akaike weights," *Psychonomic Bulletin & Review*, vol. 11, no. 1, pp. 192–196, Feb. 2004, ISSN: 1069-9384.

[29] L. Arzubiaga, F. Golmar, R. Llopis, F. Casanova, and L. E. Hueso, "In situ electrical characterization of palladium-based single electron transistors made by electromigration technique," *AIP Advances*, vol. 4, no. 11, p. 117 126, Nov. 2014, ISSN: 21583226. DOI: 10.1063/1.4902170. [Online]. Available: http://aip.scitation.org/doi/10.1063/1.4902170.

[30] S. L. Johnson, A. Sundararajan, D. P. Hunley, and D. R. Strachan, "Memristive switching of single-component metallic nanowires," *Nanotechnology*, vol. 21, no. 12, p. 125 204, Mar. 2010, ISSN: 09574484. DOI: 10.1088/0957-4484/21/12/125204. [Online]. Available: http://www.ncbi.nlm.nih.gov/pubmed/20203360.

[31] C. Xiang, J. Y. Kim, and R. M. Penner, "Reconnectable sub-5 nm nanogaps in ultralong gold nanowires," *Nano Letters*, vol. 9, no. 5, pp. 2133–2138, 2009, ISSN: 15306984. DOI: 10.1021/nl900698s.

[32] C. Untiedt, M. J. Caturla, M. R. Calvo, J. J. Palacios, R. C. Segers, and J. M. Van Ruitenbeek, "Formation of a metallic contact: Jump to contact revisited," *Physical Review Letters*, vol. 98, no. 20, pp. 1–4, 2007, ISSN: 00319007. DOI: 10.1103/PhysRevLett.98.206801.

[33] D. R. Strachan, D. E. Smith, D. E. Johnston, T. H. Park, M. J. Therien, D. A. Bonnell, and A. T. Johnson, "Controlled fabrication of nanogaps in ambient environment for molecular electronics 043109," *Applied Physics Letters*, vol. 86, no. 4, 2005, ISSN: 00036951. DOI: 10.1063/1.1857095.

[34] M. Olsen, M. Hummelgård, and H. Olin, "Surface modifications by field induced diffusion," *PLoS ONE*, vol. 7, no. 1, 2012, ISSN: 19326203. DOI: 10.1371/journal.pone.0030106.

[35] T. T. Tsong, *Effects of an electric field in atomic manipulations*, 1991. DOI: 10.1103/PhysRevB.44.13703.

[36] H. C. Yu, S. H. Liu, and C. Chen, "Study of electromigration in thin tin film using edge displacement method," *Journal of Applied Physics*, vol. 98, no. 1, p. 013 540, Jul. 2005, ISSN: 0021-8979. DOI: 10.1063/1.1954871. [Online]. Available: http://aip.scitation.org/doi/10.1063/1.1954871.

[37] J. Black, "Electromigration - A brief survey and some recent results," *Electron Devices, IEEE Transactions on*, vol. 16, no. 4, pp. 338–347, 1969, ISSN: 0018-9383. DOI: 10.1109/T-ED.1969.16754. [Online]. Available: https://ieeexplore.ieee.org/stamp/stamp.jsp?arnumber=1475796.

[38] I. A. Blech, "Electromigration in thin aluminum films on titanium nitride," *Journal of Applied Physics*, vol. 47, no. 4, pp. 1203–1208, Apr. 1976, ISSN: 0021-8979. DOI: 10.1063/1.322842. [Online]. Available: http://aip.scitation.org/doi/10.1063/1.322842.

[39] J. Lienig and M. Thiele, "Fundamentals of Electromigration," in *Fundamentals of Electromigration-Aware Integrated Circuit Design*, Cham: Springer International Publishing, 2018, pp. 13–60, ISBN: 978-3-319-73558-0. DOI: 10.1007/978-3-319-73558-0_2. [Online]. Available: https://doi.org/10.1007/978-3-319-73558-0_2.

[40] M. Nathan, E. Glickman, M. Khenner, A. Averbuch, and M. Israeli, "Electromigration drift velocity in Cu interconnects modeled with the level set method," *Applied Physics Letters*, vol. 77, no. 21, pp. 3355–3357, Nov. 2000, ISSN: 0003-6951. DOI: 10.1063/1.1327274. [Online]. Available: http://aip.scitation.org/doi/10.1063/1.1327274.

[41] I. Blech, "Diffusional back flows during electromigration," *Acta Materialia*, vol. 46, no. 11, pp. 3717–3723, Jul. 1998, ISSN: 1359-6454. DOI: 10.1016/S1359-6454(97)00446-1. [Online]. Available: https://www.sciencedirect.com/science/article/pii/S1359645497004461.